



Movement at the nanoscale:
Catalytically and light driven micromotors

Juliane Simmchen

Doctoral Thesis

Material Science

Supervised by Dr. Daniel Ruiz Molina,
Dr. Alejandro Baeza García,
and tutor Dr. Jordi Hernando Campos

Departament de Química

Facultat de Ciències

2014

Memòria presentada per aspirar al Grau de Doctor per Juliane Simmchen

Vist i plau

Dr. Alejandro Baeza García

Dr. Daniel Ruiz Molina

Dr. Jordi Hernando Campos

Acknowledgements

This thesis would not have been accomplished without the help, the support and the encouragement of many people.

First of all I acknowledge my thesis director Dr. Daniel Ruiz for this amazing project that you had in the drawer, thanks for giving it to me and for granting me all the freedom with my research. Furthermore I highly value the possibilities to go on several shorter research stays to acquire different knowledge with other research groups and your way of being "the boss" that definitely created an enjoyable work surrounding in the Nanosfun group.

I would like to express my gratitude to Dr. Alejandro Baeza for all the time you spent tutoring and teaching me about all the small details in the lab, discussing new ideas or outlines for this thesis, and for all the funny and philosophical anecdotes I heard over the years. You were very encouraging and your enthusiasm for research was always very inspiring.

Jordi Hernando thank you for officially tutoring this thesis, as well as for many critical comments on the chemistry and the help with the calculations on the FRET measurements.

I also acknowledge the CSIC for the funding I obtained for this thesis within the call JAE Pre.

I should also mention all of the students in Nanosfun that made my work in Barcelona enjoyable and worthwhile. Second to none is Nuria who basically helped me with everything, from political correctness to orthography and even though our topics were very different, without you I wouldn't have finished this thesis. Special thanks goes to Mireia and Pablo who were great and faithful company for 11 o'clock coffee, but also always up for fruitful scientific discussions. Bea, thanks for sharing sore muscles after capoeira classes, Elena for being an inspiration as a friend and a scientist and Gemma for the initial help with the silica particles. Not to mention Claudio for much advice and amazing Italian food, Marta and Jon for lots and lots of laughs, Fabi for all the 'mayordomo' sessions in NMR, Carolina for incredible lab performances, and all the others who joined Nanosfun for research stays and shared memorable moments.

I owe my gratitude to Maria Jose Esplandiu for the initial scientific support and later for being an example that will hopefully guide me on my future paths. Josep Sedó, for many discussions on both science and philosophy that many times opened my eyes (and often quite shocked me), and that were usually followed by some link sent around to enlarge Nanosfun's general knowledge.

Further acknowledgement is due to Prof. Maria Vallet for the possibility to stay several times in her group and learn from Alejandro, and thanks to all the Postdocs (Chico, Marina, Gonzalo and Miguel) and PhDs (especially Edu, Marina and Shruti) in her group for all the help during long lab hours and many beers afterwards.

Whenever I found some problem that seemed impossible to solve I could count on Dr. Samuel Sanchez and his teams in Dresden and Stuttgart. I learnt a lot in this collaboration. Special thanks goes to Veronika, who was a great collaborator and became a dear friend, Lluís, who hopefully one day will have to leave science in order to become the president of Catalunya, Jaideep for convincing my Dad that vegetables deserve some space on the barbecue, Carolina, for simply being herself, Simon and all the other people from Dresden that are not named here.

Apart from that I want to thank several people from UAB and ICN2, I really appreciate all the help and useful discussions, firstly Marcos for teaching me basically everything I learned about SEM, without you there would be no Nanozoo. All the things I learned about TEM were thanks to Pablo, Emma and Belén. I am also very grateful to all the other people in the organic chemistry labs and the rest of ICN2. I should mention Mireia and Angela from administration who always helped with paper work and Toni for patiently answering all my questions. I hugely appreciate all the scientists, especially the groups of V. Puntès, D. MasPOCH and A. Merkoci who patiently shared their chemicals and lab devices with me and to Isaac who taught me a lot during my second year of this PhD.

Special thanks goes to my friends and roommates that made Barcelona so enjoyable while sharing the culture, beach and food. Without all of you, Nuria, MJ, Teresa, Pablo, Giovanna, Brian, Abraham, Ray, Omer and many more, I would not have enjoyed the time half as much!

Also to my friends back in Germany (Gregor, Ulrike, Stephan, Inga, Rabea, Lara and many more) who probably did not get as much attention as they deserved but still keep inviting me for coffee and kept in touch.

Der größte Dank gebührt natürlich meiner Familie, meinen Eltern, meiner Schwester, ihrem frischgebackenen Ehemann, meinen Großeltern und Josè. Ihr alle habt die ganze Zeit meine Entscheidungen mitgetragen und geduldig alle Geschichten und Beschwerden angehört. Ich danke Euch für die Unterstützung, die Zeit, die Ermutigungen und die Besuche wo immer ich gerade war, nur um ein paar Tage gemeinsam verbringen zu können. All das hat mir viel geholfen und noch mehr bedeutet, danke!

Table of content

<u>Chapter 1</u>	<u>General Introduction</u>	1
1.1	Nano- and Micromotors	2
1.1.1	History	2
1.1.2	Physical fundamentals	2
1.1.3	Natural motors	4
1.1.4	Synthetic motors	5
1.1.4.1	Early motors	5
1.1.4.2	Electrocatalytic motors	6
1.1.4.3	Gradient driven motors	7
1.1.4.4	Biocatalytic propulsion	8
1.1.4.5	Self-propelled devices by bubble propulsion mechanism	8
1.1.5	Alternative fuelling	9
1.1.5.1	Chemical alternatives	9
1.1.5.2	Magnetically powered devices	10
1.1.5.3	Other approaches for external powering	11
1.1.6	Applications	11
1.2	Introduction to silica particles	12
1.2.1	Chemical properties	12
1.2.2	Janus particles	13
1.3	Enzymes	15
1.3.1	Historical milestones	15
1.3.2	Catalase	15
1.3.3	Immobilization of enzymes	16
1.4	Platinum as catalyst	18
1.5	Literature	18
<u>Chapter 2</u>	<u>Objectives</u>	23
<u>Chapter 3</u>	<u>Experimental</u>	25
3.1	Abbreviations	26
3.2	Chemicals	28
3.3	Material	30
3.4	Detailed description of synthetic methods	31
3.4.1	Silica particles and enzyme - based micromotors	31
3.4.1.1	Particle synthesis	31
3.4.1.2	Particle functionalization	31
3.4.1.3	Grafting of biomolecules	33
3.4.1.4	Motor experiments	34
3.4.2	Enzyme encapsulation for micromotors with prolonged lifetime	36

3.4.2.1 Enzyme encapsulation	36
3.4.2.2 Silica motors	37
3.4.2.3 Polystyrene particle motors	38
3.4.2.4 Janus motors	39
3.4.2.5 Other enzymes	39
3.4.3 Platinum driven micromotors	40
3.4.3.1 Fabrication	40
3.4.3.2 Speed experiments	41
3.4.3.3 Effects of soap on particle-/ tube- movements	41
3.4.3.3 Effects of thiols on particle-/ tube- movements	42
3.4.4 AgCl -light driven micromotors	42
3.4.3.1 Synthesis of AgCl microstars	42
3.4.3.2 Degradation of organic molecules	43
3.4.3.3 Bactericide effects	44
3.5 Analytical techniques	44
3.6 Detailed description of analytical methods	45
3.6.1 Enzyme activity catalase	45
3.6.2 Enzyme activity GOx	46
3.6.3 BCA assay	47
3.6.4 Fmoc assay for amino quantification	48
3.6.5 Fluorescamine assay for amino determination in proteins	48
3.7 Literature	49
<u>Chapter 4 Results and discussion</u>	51
<u>4.1 Silica particles and enzyme-based nanomotors</u>	53
4.1.1 Motion based DNA sensor	54
4.1.1.1 Introduction to DNA	54
4.1.1.2 DNA nanodetection devices	55
4.1.1.3 Motion based sensors	56
4.1.1.4 Particle tandem based micromotor for DNA analysis	57
4.1.2. Synthesis of silica particles	57
4.1.3 Asymmetrization and surface functionalization	58
4.1.4 Enzyme attachment	62
4.1.5 DNA micromotor	63
4.1.5.1 DNA grafting	63
4.1.5.2 DNA recognition and motion	63
4.1.5.3 FRET-experiments	65
4.1.6 Directionality of the movement	68
4.1.6.1 Attempts to introduce directionality using magnetic fields	69
4.1.6.2 Asymmetrization	70
4.1.7 Summary	72

4.1.8 Literature	73
<u>4.2 Enzyme encapsulation for micromotors with prolonged lifetime</u>	75
4.2.1 Enzyme encapsulation	76
4.2.1.1 Enzyme encapsulation using acrylate-type monomers	76
4.2.1.2 Encapsulation of catalase	78
4.2.1.3 Activity evaluation for encapsulated catalase	79
4.2.2 Micromotors powered by encapsulated catalase	80
4.2.2.1 Silica motors	80
4.2.2.2 Comparative evaluation of enzymatic activity	82
4.2.2.3 Motion experiments	83
4.2.2.4 Polystyrene motors	84
4.2.3 Janus motors	85
4.2.4 Other enzymes	87
4.2.5 Summary	88
4.2.6 Literature	89
<u>4.3 Platinum driven micromotors</u>	91
4.3.1 Conferring directionality to micromotors using Janus motors	92
4.3.1.1 Introducing magnetism	92
4.3.1.2 Replacing the catalase by Pt catalysts	92
4.3.1.3 Mechanism of motion	93
4.3.1.4 Role of surfactants in bubble driven motion	94
4.3.2 "out-of-plane magnetized" Janus particles as micromotors	95
4.3.2.1 Fabrication	95
4.3.2.2 Directing motion	97
4.3.4 Studies of micromotor motion	97
4.3.4.1 Particles vs. tubes in diluted peroxide solutions	99
4.3.4.2 Particles vs. tubes in presence of surfactants	100
4.3.4.3 Comparison particles vs. tubes	102
4.3.5 Movement of thiol modified particles vs. tubes	103
4.3.6 Summary	104
4.3.7 Literature	105
<u>4.4 Light driven micromotors</u>	107
4.4.1 State of the art - light driven micromotors	108
4.4.2 State of the art - environmental applications of micromotors	109
4.4.3 Properties of AgCl	109
4.4.3.1 Degradation of pollutants	109
4.4.3.2 Antibacterial properties	110
4.4.4 Branched AgCl structures	110

4.4.4.1 Synthesis	110
4.4.4.2 Tuning of experimental parameters	111
4.4.4.3 Characterization of the chemical composition	112
4.4.4.4 Hexapod formation	113
4.4.5 Tuning octapod morphology	114
4.4.6 Light induced movement	115
4.4.7 Decomposition of organic molecules	117
4.4.8 Antibacterial activity	118
4.4.9 Conclusions	121
4.4.10 Literature	122
<u>Chapter 5 Conclusion and future perspectives</u>	123
5.1 Conclusion	125
5.2 Outlook	126

General Introduction

1

This chapter contains a general overview of the field of micromotors, starting with its brief history spanning the last two decades, its main physical fundamentals and finally natural machines carrying out motion in living cells or organisms. With this background, the principle types of modern micromachines are introduced, classified and a first outlook on the applications is given. In the second part silica beads and enzymes, as the material that is used throughout the thesis is presented so that the reader is familiar with its basic characteristics.

1.1 Nano- and Micromotors

1.1.1 History

Movement has been an important part of life since ancient times. Approximately 6000 years ago, when the wheel was invented, the revolution of human movement started ¹. Initially the efforts were to transport heavier objects with minimal work input and the focus gradually shifted to building vehicles for human transport. What started with inventions like the bicycle led to a world where we



Fig. 1.1 Comic of a prehistoric man with wheel, image from www.peppitext.de

have conquered the medium of land, sea and air. In the field of engineering immense knowledge about movement has been accumulated and implemented. After the middle ages science prospered and in the late 16th century the first microscope was constructed in the Netherlands, opening the eyes of scientists to an entirely new world that exists on the smaller scales. Bacteria, cells and many kind of microorganisms were discovered and structure started to be associated with their properties. So, a general understanding of the microscale progressed and as early as in 1930 W. Ludwig recognized that movement in the microscale does not work the way it does at the

macroscale ². Observing microorganisms as bacteria and cilia he realized that inertia does not exist at this scale and he described and analyzed detailed observations of a different mechanism for self-propulsion ². Further investigation concerning the swimming of microorganisms were presented around 20 years later by G. Taylor ³ who developed a model explaining how flagellated cells move forward in a force free way. 1960 Richard Feynman gave his famous speech 'There is plenty of room at the bottom' about the limits of nanotechnology where he suggested creating cars for mites and swallow-able surgeons ⁴. Perhaps, this speech inspired the film "the fantastic voyage" which told the story of a team of scientists that was shrunk below the microscale to treat a secret service agent who was about to die from an coagulation in his artery. And not long after, in 1977 a paper from Purcell was published that treated the theoretical background of movement at the nanoscale ⁵. Later popular writings of Drexler and Freitas praised the benefits of nano- and micromachines. In the nineteen nineties first publications on molecular motors were reported and in 2002 Whiteside's ground breaking article on Pt catalysing peroxide degradation to propel millimetre-sized disks paved the way for an amazing new field of research with several examples being described in the following parts of the introduction. However to remind the reader of some physical laws that determine the circumstances at the microscale this overview shall be initiated explaining some basics in physics.

1.1.2 Physical fundamentals

One key factor that led to the discovery of movement at the microscale was Brownian motion, i.e. the random motion of objects suspended in fluid. It was discovered by Robert Brown in 1827 while observing pollen suspended in water under an optical microscope. Although he observed that the

pollen was in constant movement, as if jostled by something, he could not determine the source of this motion. Only in 1905 did Albert Einstein publish an explanation that collisions with water molecules might be "pushing particles around". A few years later Jean Perrin confirmed this theory experimentally and therefore gave the proof that materials consisted of more than pure energy - namely molecules and atoms. Brownian motion was further described by the Stokes-Einstein equation that can be interpreted as the dependence of the Brownian motion on particle size (influencing the drag force, i.e. the force acting opposite to the relative motion of the particle respective to the surrounding fluid) and the temperature.

$$D = kT / 6\pi\mu r \quad (1.1)$$

with D being the Diffusion constant, k the Boltzmann constant, T the temperature, μ the dynamic viscosity and r the radius of a sphere. If self-propelled motion of objects needs to overcome size dependent Brownian motion or if the non-directed motion of self-propelling objects can itself be considered a kind of Brownian motion was analyzed theoretically by B. ten Hagen *et al.* ⁶. Solving the Brownian dynamics they concluded that particle movement shows some rotational Brownian dynamics, but for a complete characterization more details on mechanism and hydrodynamic interactions need to be investigated ⁶. Howse *et al.* used polystyrene beads half-covered by a catalytic platinum layer to study their trajectories at different peroxide concentrations and see whether their behaviour can be categorized as Brownian. It was found that in any case the velocity depended on the fuel concentration. Furthermore they differentiated two cases: at short times the motion had a substantial component of directed motion and an average direction was found. Observing longer intervals the motion randomizes due to rotational diffusion of the bead. The fuelling caused larger diffusion coefficients than standard Brownian diffusion ⁷. Being a natural process that is present in all particles to some extent nowadays it became a challenge for relatively small synthetic micromotors to overcome Brownian motion.

Another parameter with high impact at the small scale is the Reynolds number (Re), a dimensionless quantity which qualitatively captures the characteristics of the flow regime and therefore helps scientists to evaluate the circumstances concerning a certain particle size and viscosity conditions in the fluid. It is capable to predict similar flow patterns in different fluid flow situations. The concept was introduced by George Gabriel Stokes in 1851 who physically obtained Re by solving the Navier–Stokes equation, even though it is named after Osborne Reynolds who popularized its use in 1883 to quantify the relative importance of laminar or turbulent flow.

$$Re = f_{inertia} / f_{viscous} = \rho UL / \mu \quad (1.2)$$

with ρ being the fluid density, L the length, U the velocity, and μ the dynamic viscosity. Due to the small dimensions of microscale objects their Re is very small. Re is defined as the ratio of inertial forces to viscous forces and therefore in a low Reynolds number regime the forces come primarily from viscous drag. The drag refers to forces acting opposite to the relative motion of any solid moving in a fluid and it is generated by the difference in velocity between both, which implies that drag forces depend on velocity ⁸. To have a deeper look at the effects of the different Reynolds numbers on swimming objects on the macro- and microscale, we firstly have to define a 'swimmer'. A tentative definition was given by Lauga and Powers as "a creature or object that moves by deforming its body in a periodic way" ⁹. There are however, many examples using other propulsion mechanisms. Swimming at the macroscale usually works by imparting momentum to the fluid that will cause some coasting movement, as for example in paddling or human swimming. At high Reynolds number the drag force is equal to the inertial force and proportional to the product of

viscosity, square speed and square length, causing that a human swimmer can coast in water for a couple of meters:

$$f_{\text{drag}} = f_{\text{inertia}} \sim \rho U^2 L^2 \quad (1.3)$$

At the low Reynolds numbers ruling at the microscale the coast movement is foiled by the large viscous damping, caused by the fact that the drag force has the viscous scaling:

$$f_{\text{drag}} = f_{\text{viscous}} \sim \mu UL \quad (1.4)$$

Movement of microscale objects was studied extensively by E.M. Purcell in 1977. In his paper he observed that a scallop cannot move by opening and closing its shell periodically, independent of the rate of this movement⁵. At low-Reynolds numbers, a swimmer cannot move if the movement is time reversible, i.e. the sequence of shapes displayed by a swimmer is identical seen either "forwards" or "backwards". This puts a strong geometrical constraint on the type of deformation it needs to generate non-zero forces on average to cause effective motion. A related principle is the rate independence, which means that if a body moves by changing between different surface configurations the motion does not depend on the rate at which the surface deformation occurs but only on its geometry. Another example of a time reversible deformation is a dumbbell - two solid spheres with a time dependent longer or shorter distance. No absolute movement is obtained by this periodical movement, as it only possesses a single degree of freedom and its deformations occur in a reciprocal way. It can be concluded that asymmetry or drag anisotropy is fundamental for generating directional force at zero Reynolds number.

Hydrodynamics: Generally conditions at low Reynolds numbers can be imagined as extremely slow movements in a very viscous fluid, with huge importance of even distant walls. Those conditions are mathematically described through the Navier-Stokes equation, which basically assumes that a viscous flow consists of a viscous term and a pressure term. In the special case of Stokes flow the inertia terms are zero, strictly accurate for $Re=0$ but the Stokes equation is accepted for $Re \ll 1$.

$$-\nabla p + \mu \nabla^2 u = 0 \quad (1.5)$$

As the inertia term is omitted there is no time dependence (except through boundary conditions) and movements are assumed to be instantaneous and time reversible. There is no more transition to turbulence, so all flow is laminar flow and the presence of any wall becomes highly important so that a wall many body lengths away can affect the swimming of a micromotor¹⁰. The Stokes equation describes fluid dynamics of linear flow as proportional to the force applied to it, i.e.

$$f_{\text{thrust}} = f_{\text{drag}} \quad (1.6)$$

therefore the driving force of a microsphere depends linear on its velocity calculated through Stokes drag law

$$f_{\text{drag}} = 6\pi\mu r\vartheta \quad (1.7)$$

with μ being the dynamic viscosity, r the radius of the sphere and ϑ the particle velocity. For other shapes than spheres the drag coefficient must consider the asymmetry, as well as changed orientation.

1.1.3 Natural motors

Movement is essential for most forms of life - and in many cases achieved by multi protein complexes in their function as nanomotors with important tasks in cells and organisms: kinesin motor, myosin motor, polymerase and F1-adenosine triphosphate synthase. It is astonishing how

many processes can be drawn back to this kind of nanomotors, e.g. myosin II is responsible for muscle contraction while it moves along bundles of actin filaments. Each type has its particular functions: kinesin transports cellular cargo for several processes to the edges of the cell along microtubules, it moves at an average velocity of 100 steps of 8 nm each per second¹¹ towards the plus end of the tubules. Dynein instead moves along the same filaments but in opposite direction¹². Common to all the natural motors listed here is their high efficiency in converting chemical energy into mechanical work. The fuel is ATP that is hydrolysed to ADP and one phosphate with an efficiency of approx. 50% for kinesin and even more for F1-adenosine triphosphate synthase¹³. Generally those motors perform their tasks continuously, as long as energy is provided. An excellent review giving a very detailed outlook on natural motors has been recently published¹⁴.

Microorganisms as spermatozoa, algae, bacteria and cilia need to move freely in their environment and they cannot count on lanes as protein based nanomotors do. Therefore they had to develop their own mechanisms to move in the microworld at low Reynolds numbers and in the course of evolution they turned into highly specialized microsized motors. The mechanisms they use to create motion are typically either a flexible oar or corkscrew movement to overcome viscous drag forces, and some even exploit the drag. Most systems in nature that perform swimming motion on the microscale use one or more appendages for propulsion, mostly either a stiff helix moved by a rotor or a flexible filament moved by many dynein motors along the filament. Examples for those swimmers are eukaryotic flagella, cilia and bacterial flagella. Between them exist mainly differences in size and shape, but also the variety of beat patterns has to be considered. Many other forms are also found as flagella in-between the inner and outer cell wall, or swimming via propagation of pairs of kinks along the length of the body as used by *Spiroplasma*⁹.

In general the main disadvantage of the use of natural motors in nanotechnology lies in the specific conditions they need to perform their function, which limits *in vitro* lifetime and makes their implementation in experimental platforms extremely difficult. In spite of these obstacles natural motors have been an inspiration and study objects for scientists, and some have even been used as 'motors' for hybrid devices. Probably the first successful combination of a biological motor with synthetic devices was the prominent nanopropeller created by R.K. Soong in Montemagno's group¹⁵ by coupling the rotary motor F1-adenosine triphosphate synthase to nanopropeller structures. Later Weibel *et al.* moved polystyrene beads through phototroph algae and released them photochemically¹⁶. The 'phi29 nanomachine' of Guo and coworkers should be listed as another example, inspired by the packaging of DNA in preformed procapsid by some viruses^{17, 18} and Magdanz *et al.* used sperms to propel microtubes¹⁹.

1.1.4 Synthetic motors

1.1.4.1 Early motors

The earliest publications in this field from the early years of this millennium are molecular machines which are defined by Alberto Credi as assemblies of a discrete number of molecular compounds that perform a function through mechanical movement of its components induced by an appropriate external stimulus²⁰. Several early contributions on stimuli-responsive systems come from the Stoddart group²¹ and light-powered devices were generated in Feringa's lab mainly through photoisomerization²²⁻²⁴. In those examples conformational changes or displacements in supramolecular assemblies of organic molecules induce macroscopic changes of material properties.

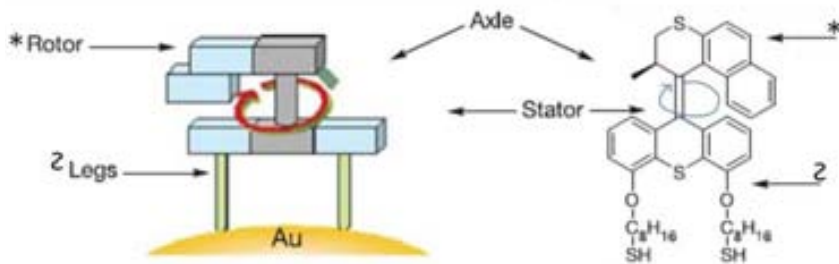


Fig. 1.2 Scheme of Feringa's unidirectional molecular motor, adapted from reference 24

Strongly inspired by natural motion are the DNA machines presented in recent years. Many of these works are based on hybridization and dehybridization between complementary strands and so the control of the conformation of DNA strands that enable researchers to obtain movement as 'walkers'. The movement of larger assemblies (i.e. 10^{-4} – 10^{-9} m) requires however significantly bigger amounts of energy. Therefore several approaches are implied, as the usage of the high power density stored in some materials as chemical energy or the energy stored in external fields (see figure 1.2).

The first example of a self-propelled device larger than molecular scale used the chemical energy stored in peroxide to obtain propulsion: Whitesides' group created tiny boats from PDMS-discs equipped with catalytic platinum strips to catalyze the decomposition of the fuel ²⁵. Those boats floated at the air-liquid interface and a thrust of oxygen bubbles created at the platinum caused motion through a jet-like mechanism. This approach was followed by a microscale rotating catalytic gear presented in 2005 by Catchmark *et al.* ²⁶. From here the number of micromotors reported has increased over the years. A recompilation of such work is described next.

1.1.4.2 Electrocatalytic motors

Early self-propelled micromotors were in most cases rod shaped objects that contained Pt or similar catalytically active metals to decompose peroxide and propel motion. Pioneering in this field have been two teams, Paxton, Mallouk and Sen in Pennsylvania ²⁷ and Ozin's group in Toronto ²⁸. Both groups used bimetal nanowires in hydrogen peroxide solution transforming chemical energy into autonomous motion, an approach that was followed by several more publications ²⁹⁻³⁴.

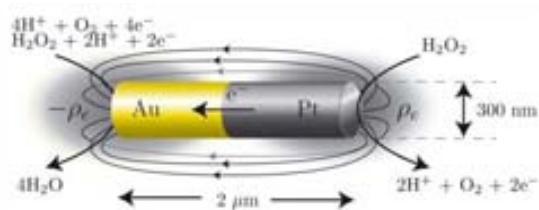
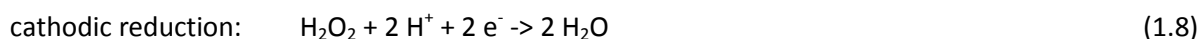


Fig. 1.3 Scheme of a catalytic Au-Pt rod propelled towards the right as a micromotor in hydrogen peroxide, indicated are typical dimensions, electrochemical reactions, charges and approximate electric field lines. Extracted from reference 29.

Fabrication of those bi-segmental nanorods commonly employs template-directed electro deposition within the uniform nanopores in a porous membrane, followed by template removal ^{27, 28, 30}. Basic nanowires consist of a gold part connected to a catalytic segment of either Pt or Ni (see figure 1.3). This method allows free choice of size and aspect ratio and as additional segments can add additional capabilities, and rod composition can be also varied. Examples are for example magnetic direction that can be achieved by introduction of a ferromagnetic segment ³⁰, an increase of catalytic activity was obtained by adding carbon nanotubes to the Pt-segment or by replacing the gold segment by an

alloy^{32,33}. The electrophoretic mechanism of motion is described as electrocatalytic decomposition of the peroxide on the poles of the rods³¹:



The two segments should be considered as an interconnected electrochemical cell - electrons are generated in the wire and protons at the interface around it. Those protons migrate from the Pt segment to the cathode where they are consumed in the reduction. This proton gradient causes fluid motion in the same direction and the wire moves towards the anode, usually the Pt end.

1.1.4.3 Gradient driven motors

Self-diffusiophoresis involving self-generated local gradients is mainly found in the movement of spherical particles that present some asymmetry^{7, 35, 36}. Those so called Janus particles were first used as micromotors by Howse *et al.*⁷ using a fabrication protocol to evaporate Pt on a half sphere developed by Whitesides' group³⁷. In this pioneering article the movement is described as random movement similar to Brownian with a higher diffusion coefficient considering long time scales, while in short intervals the movement seems to be directional due to a missing influence of the rotational diffusion that causes randomization. Since then sputtering of Pt on the particle surface has been established as most common way of preparation of Janus motors but promising alternatives as electrochemical deposition were presented recently³⁸. In most publications Pt capped particle shaped motors move through bubble free gradient dependent propulsion as showed in several publications of Baraban *et al.*, Howse *et al.* and others^{7, 39-44}. The gradient in most cases refers to concentration of oxygen caused by the degradation of peroxide and leads to self-diffusiophoresis. However some influence of more complex mechanisms like ionic self-diffusiophoresis probably have to be considered. Very recently even a version of electrophoretic motion enabled through non homogeneous thickness of evaporated Pt has been controversially reported^{43, 45}. DeBuyl *et al.* suggested a theoretical mechanism of how self-propulsion should be possible through symmetry breaking in small particles; this however still needs practical demonstration³⁵. Sanchez *et al.* were the first to implement catalytic micromotors into microchannels for directed transport of microparticles⁴¹ and showed their chemotactic activity⁴⁰. They also achieved precise magnetic directionality through evaporation of selected magnetic material under the catalytic Pt-layer⁴¹. Wu *et al.* added multi-functionality to spherical particles by preparing a capsule motor instead of using solid particles. Therefore they used a template-assisted layer by layer self-assembly based on silica particles as template and covered them with several polymer layers combined with a microcontact printing method to attach Pt nanoparticles on the surface. After HF dissolution of the silica core result capsules, asymmetrically covered with Pt particles, that catalyze peroxide degradation and propel the capsules as motor⁴⁶.

A completely different type of gradient to obtain self-propulsion was also implemented into the spherical system: Baraban *et al.* deposited a permalloy layer resulting in vortice magnetization on silica particles and applied an alternating magnetic field to heat the magnetic caps of particles to achieve thermophoresis. As this vortex is magnetically saturated everywhere except at the centre it is suited for directing the particles applying a static magnetic field⁴⁷.

1.1.4.4 Biocatalytic propulsion

Ensembles of one or more enzymes used to propel microscale objects are categorized as biocatalytic propulsion. The big variety of enzymes available in nature should lead to an increase in available methods for motor propulsion, which is observed in a few examples that even obviate the peroxide fuel^{48,49}. For instance in the work of Feringa *et al.* on functionalized nanotubes bearing an enzymatic tandem of catalase and glucose oxidase (GOx): this tandem is able to produce small concentrations of peroxide as by-product of the conversion of glucose to gluconolactone. The peroxide is degraded by the catalase to water and oxygen which produces bubbles that generate a jet force moving the nanotube. The second example using a similar enzymatic tandem approach was presented by Mano and Heller in 2005. They functionalized carbon fibres with redox polymer and the enzymes glucose oxidase and bilirubin oxidase. The glucose fuelled reaction leads to a proton flux that empowers a self-electrophoresis mechanism for the movement of the conducting microfiber.

The use of enzymes to catalyze chemical reactions to empower motion brings several advantages: probably the main advantage is the re-emplacment of toxic peroxide by more biocompatible fuels as glucose solution. Furthermore the specificity of enzymes is superior to most inorganic catalysts which avoids undesired side-reactions and their biodegradability will cause less waste problems if it comes to industrial production one day.

Nowadays the grafting of catalase by activation of COOH-surface groups and their coupling to enzyme amino groups can be seen as an established method. This was shown by Sanchez *et al.* and later by Gao *et al.* on gold microjets functionalized with alkanethiols and subsequent activation of their acid groups by the previously described method^{50,51}. The use of the same method for other enzymes is more critical as activity lost at lower activity levels is more severe and might affect the utility of the micromotor. Feringa's team presented a highly active manganese complex as mimic for catalase anchored on irregular SiO₂ particles that perform translational and rotational movement.

1.1.4.5 Self-propelled devices by bubble propulsion mechanism

The first example of hollow structures with the catalytic surface on their inside, namely microtubes, was presented in 2008 by Y. Mei *et al.*⁵². The group from Dresden used roll-up fabrication to create tubes, a mechanism that is based on intrinsic strain gradients that create tension and leads to bending of the material that rolls up and forms a tube. These tubes typically possess a catalytic Pt inner layer, mostly a magnetic middle layer that enables directed motion and an inert outer layer. Additionally some titanium or gold might be sputtered to improve attachment and rolling process. In recent years it was shown that rolled up tubes can be fabricated using several different materials as graphene oxide⁵³, GaAs⁵⁴, SiO/SiO₂⁵⁵. Wang's group developed an alternative production method: membrane template electro deposition similar to rod production. It offers a simplified low cost approach that enables the use of further materials such as polymers^{51,56}.

Generally the propulsion of microtubes is associated to a bubble-driven jet mechanism: movement is attributed to a continuous thrust producing a force that moves the tube in the opposite direction of bubble expulsion. Thereby size and frequency of bubbles are defining factors in the movement dynamics⁵⁷ and other forms as helical movement are caused by asymmetric tube form, followed by a tilted release of bubbles⁵⁴. For this type of micromotors first potential applications have recently been presented with several approaches for water cleaning or as DNA sensors⁵⁸⁻⁶⁰.

In the field of spherical motors few examples for bubble propelled motion can be found, both presented by Zhao's group^{61,62}. In 2009 no reason was given why bubble formation is favoured compared to other systems⁶¹ (see figure 1.4 a-b) while in a later publication larger particles were used and their motion was analyzed and found related to the competition between bubble growth and burst processes. In this article Manjare *et al.* suggest detailed physical models for their description⁶³. Later the same group presented an approach based on vapour deposition followed by particle etching that resulted in catalytically active hollow capsules (see figure 1.4 c). The concave motor design facilitates bubble formation and those motors are therefore much faster than traditional Janus motors⁶⁴. Those systems present interesting elements to study in order to compare tube and particle motors. Wilson *et al.* presented bowl shaped supramolecular polymer vesicles with Pt-particles entrapped in the cavity⁶⁵. The cavity opening provided good conditions for exchange of peroxide and the catalytic motors moved depending on the fuel concentration either producing bubbles or by a phoretic mechanism⁶⁶, the scheme of bubble propelled motion is depicted in figure 1.4 d.

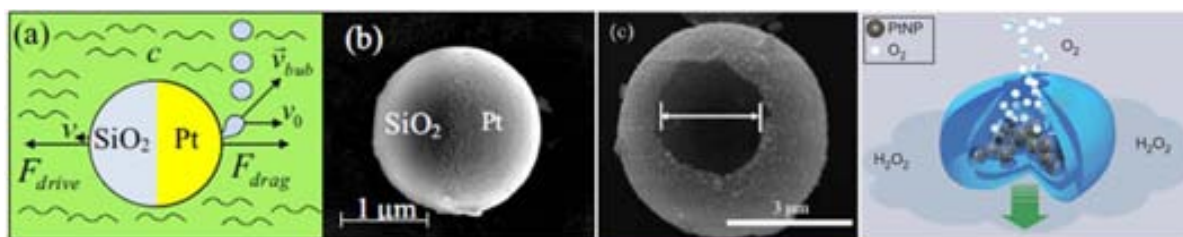


Fig 1.4 Samples of bubble driven motors a) force and velocity schematic of a Pt-covered microsphere in diluted hydrogen peroxide, b) SEM images from reference 61 c) nanoshell motor with a diameter of approx. 5 μm and an opening of approx. 2.7 μm , from reference 64 d) Autonomous movement of stomatocyte-like vesicle in peroxide through entrapping of catalytically active Pt nanoparticles, from reference 65,66.

1.1.5 Alternative fuelling

1.1.5.1 Chemical alternatives

So far most described motors were fuelled by hydrogen peroxide, which might present an inhibition for many applications. Peroxide needs to be strictly avoided in all *in vivo* applications, especially in clinical approaches and diagnostics where it might cause alterations in the sample. Therefore many groups try to find alternative routes or new innovative fuels are explored nowadays and some attempts will be briefly listed here. Wang's group reported several examples of movement based on water decomposition^{67,68}. The water splitting reactions occur either on Ag/Ga or on Mg catalysts. Currently the main drawback is the consumption of the catalyst that limits the lifetime of micromotors to few minutes. To obtain polymerization induced motion Pavlick *et al.* utilized ring-opening metathesis polymerization of norbornene using a Grubbs' catalyst anchored covalently on a

chemically modified silica side of ca. 1 μm gold capped SiO_2 microparticle. Placing this assembly into norbornene, the propelled particles show increased diffusion and exhibit chemotaxis in a monomer gradient ⁶⁹. In a very recent publication active motion is obtained due to the local demixing of a critical binary liquid mixture that be easily tuned by illumination ⁷⁰. Another solvent based strategy is the exploitation of the Marangoni effect or the mass transfer at the interface of two fluids. A solvent is asymmetrically released causing a gradient and at the same time a difference in surface tension that moves small objects like particles. Zhao *et al.* released dimethylformamide from the motor-capsule pushing the object towards higher surface tension side ⁷¹. Sharma *et al.* released ethanol from a hydrogel, a process that makes the motor rise to the air-water interface and generates a surface tension gradient that leads to motion ⁷². Once more Wang's team used the release of a surfactant molecule to propel micromachines by the Marangoni effect and while dispensing laccase as enzymatic remediation agent to degrade organic pollutants ⁷³. Very recently the same group reported Janus particles that rely on an iridium catalyst to gain energy from the decomposition of hydrazine in connection to SiO_2 . The concentration that was necessary to move was reported to be an impressively low 0.001% and reached speeds of approximately 20 body length per second. So even though hydrazine is highly toxic the low required concentrations make this a promising candidate for future applications ⁷⁴.

1.1.5.2 magnetically powered devices

Motors powered by a magnetic field have been divided into three types: helical, flexible swimmers and surface walkers, wherein last type relies on a surface to break symmetry and escapes from basic physical rules that normally have to be considered in this field ⁷⁵. Therefore this type shall not be considered here. In a recent review Nelson *et al.* listed two main methods to wirelessly transmit power to the device: first is the transmission of electrical energy through magnetic fields, based on Faraday's law. However this approach is limited to mesoscale devices as circuits are required and the increase of the magnetic field underlies some safety regulation ¹⁰. The second alternative is to cause motion through application of forces and torques directly to magnetic materials. The helical swimmers are divided in subcategories by their shape, the most obvious is the helix structure, characterized by a slender filament with a void centre, while the screw has a solid centre and the third shape is similar to a ribbon twisted around its own axis ⁷⁶. The most common method to generate magnetic fields are coils, but even rotating permanent magnets can be used due to the relatively small size of the material compared to the spatial changes of magnetic field, so it can be considered uniform across the microrobot ⁷⁶. It was shown that the materials to produce magnetic swimmers can be either permanent-magnetic ^{77, 78} or soft magnetic ^{79, 80}. In most cases the swimmers used are rigid propellers, meaning that by reversing the rotational direction of the magnetic field the direction of motion can be switched between pushing and pulling the object.

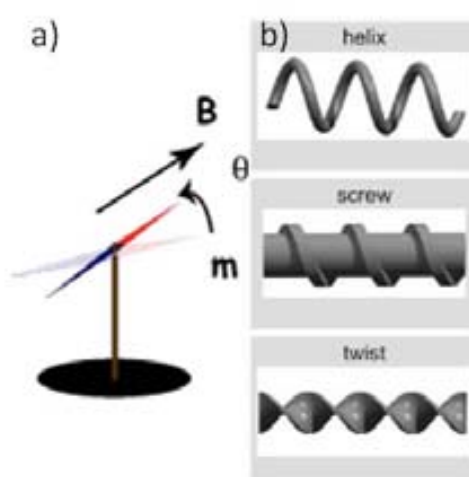


Fig. 1.5 a) Scheme of magnetic alignment by the torque, from www.magician.ucsd.edu b) basic shapes of magnetic components that are able to translate rotary to translation motion, extracted from reference 76.

To obtain motion, power must be applied by a transducer: the magnetic torque acts to align the magnetization axis with the orientation of the magnetic field ⁷⁶ resulting in rotation of the object (see scheme in fig. 1.5 a). To obtain further rotation of the object, once the axis and the field are aligned the magnetic field itself has to be rotated. This causes the rotation frequency of the magnetic field to be the main parameter to control micromotor movement. In case of very small swimmers as 2 μm silicon dioxide structures produced by glancing angle deposition in Fischer's group the effect of Brownian motion tends to dominate the effects of the magnetic field. Therefore Gosh *et al.* calculated the thermal effects on the movement and considered that the effects of the magnetic field on the colloid must be stronger than thermal motion.

$$\mu * B \gg k * T \quad (1.11)$$

B being the magnetic field strength, μ the permanent magnetic moment, k the Boltzmann constant and T the temperature ⁷⁸.

A very early example demonstrates the movement of flexible swimmers: Dreyfus *et al.* attached colloidal magnetic particles linked by DNA that can act as a flexible artificial flagellum to a red blood cell ⁸¹ and studied their movement. This kind of propulsion was later investigated by Behan *et al.*, finding that travelling waves provide an effective means of propulsion at low Re and are even more efficient than helical propellers ⁸². Anyway flexible flagella are more difficult to obtain at the microscale and so few works have been published on this mechanism. Another approach that has not found many applications until now is wireless pulling through the use of field gradients, but this approach has certain limitations due to the small dimensions of the swimmers ¹⁰.

1.1.5.3 Other approaches for external powering

As already described above, certain particles can be propelled by thermophoresis. Apart from Baraban's magnetically induced temperature gradient ⁴⁷ Jiang *et al.* used Au capped particles in defocused laser ⁸³ and Yang *et al.* presented a thermophoretically working microgear ⁸⁴. Several examples in the groups of Wang and Mallouk used ultrasound to create pressure gradient in the media, leading to self-acustophoresis ^{85,86} or to degradation of on-board fuel, resulting in a propelling force ⁸⁷. Electrical fields are used in the approach of electrically driven minidiodes - that was presented in 2007 by Chang *et al.*, placing minidiodes in an electric field (AC) where they converted electrical energy into movement. This strategy was miniaturized by Wang's group in 2009 by using multisegment diode nanowires ⁸⁸.

The use of light energy to propel motors is not very developed yet. Some works come from Sen's group but they mostly consider swarming effects, not single particle movement ⁸⁹. This can be considered a promising topic for further investigations.

1.1.6 Applications

Once shown the feasibility self-propelling nanoscale motors, scientists started dreaming about their practical applications. A few examples are just beginning to emerge. Probably inspired by the

fantastic voyage, Wang's group presented the use of nanoshuttles for transport and release of biodegradable drug-loaded particles in a controlled way⁹⁰. Later the same group presented more biomedically inspired applications of their catalytic microtubes by the capture and transport of cancer cells⁹¹. And with a more biosensing oriented approach they isolated and detected nucleic acids from microliter biologic samples as saliva, blood or urine⁶⁰. When the drawbacks of peroxide use for fuelling micromotors got more widely known the target applications focused on detection. Kagan *et al.* presented a new approach for analysis of trace silver ions based on the significant speed increase of Au-Pt nanowires³⁴ and using the same motor design. Wang's team described a quantitative motion-based method for DNA detection that relates the DNA concentration with the speed changes of Au-Pt nanowires⁹². The on board carrying of catalytically active substances introduces the use of micromotors for waste water cleaning as shown by Soler *et al.* benefitting from the Fenton effect of a catalytic Iron layer on the outside of microtubes⁵⁸. Guix *et al.* presented an approach to use microtubes covered by an organic layer to remove oil from water samples⁵⁹. The importance of this new environmental line is reflected in recent reviews^{93, 94}. One intensively discussed proposal for micromotor applications was the use of magnetic microtubes to trap and guide spermatozoa in order to enhance in vitro fertilization¹⁹. At an even more advanced state is the research of Nelson's group to use magnetically driven micromotors for surgery and other medical applications^{10, 95-97}.

Another phenomenon that will not be extensively discussed in this thesis is swarming behaviour of micromotors. When individual motors in a swarm receive stimuli from their surroundings their behaviour might change, causing collective behaviour. Several researchers have been studying self-organization and cooperative action in nano- and micromotors in order to contribute to an understanding of swarming actions found in nature (for more detailed information see⁸⁹).

1.2 Introduction to silica particles

1.2.1 Chemical properties

In the field of particle shaped motors until now not much attention has been paid to the materials of particles, but nonetheless silica has been used quite often due to its ease of surface modification, the hydrophilic properties which are good for enzyme anchorage and due to the fact that no swelling is observed that would cause peeling off of metal layers. When this thesis was started in late 2010 few examples of silica based micromotors were published. Probably the first publication on motile silica particles was published by Vicario *et al.* using SiO₂ with sizes ranging from 40 to 80 µm driven by an artificial catalase mimic⁹⁸. Few years later researchers around Howse *et al.* moved to smaller particles by degradation of peroxide using Pt as inorganic catalyst and even started to characterize the motion⁷. In parallel L. Baraban started to experiment with motile particles during her PhD thesis, but no publications resulted from this early work³⁹, so most of the publications came from Zhao's group^{61, 99}. This early work has been summarized in a review by Howse and Ebbens¹⁰⁰. Due to promising applications, especially in the biomedical field, this thesis was centred in silica based micromotors.

Silica represents a family of silicon dioxide materials that is very abundant in nature and has been known since ancient times. About 10% of the earth's crust is composed of silica and its processing mostly occurs by processing quartz. Several different chemical methods as pyrogenic or precipitation

strategies can be used, but the most common ways to produce silica in the laboratory start from silanolesters, either by thermal degradation or through the hydrolysis of esters, giving mostly colloidal silicon dioxide. The reaction is based in following decomposition:



Numerous methods are used to obtain colloidal silica. One of the first and best known methods was published by Stoeber *et al.* in 1968¹⁰¹. It is based on a fast nucleation and subsequent growth through monomer addition, leading to a homogeneous size distribution. Later modifications of the same method led to different properties as hollow particles^{102, 103} or the formation of surfactant micelles in solution previous to nucleation resulted in porous particles¹⁰⁴⁻¹⁰⁶. Porous particles have unique properties as a higher surface area and the low specific weight that open possibilities for a broad range of applications from catalysis¹⁰⁷ to separation technology or drug delivery¹⁰⁸⁻¹¹⁰. All of those functionalities might also be beneficial in motor systems and open doors for future applications. Synthetically in the first step solvents and surfactants are mixed to allow micelle formation and their arrangement in liquid crystals. In the second step the TEOS is added and

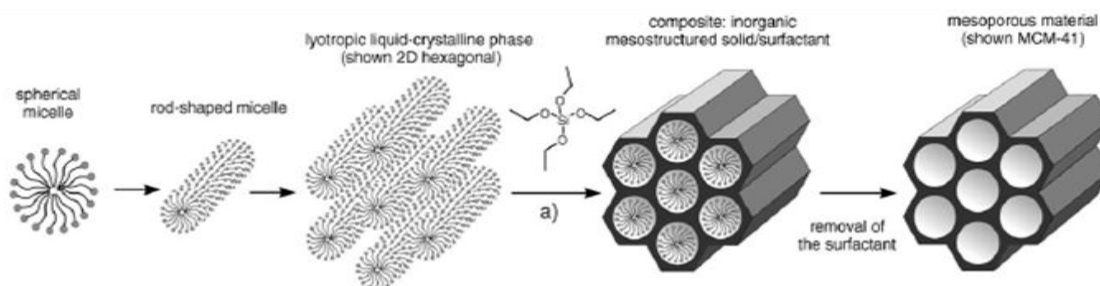


Fig 1.6 Formation of mesoporous structures by use of surfactants as structure directing agents (image from reference 115)

condensates around the surfactant structures the TEOS to form patterned silicon dioxide structures (see figure 1.6). In a further step the surfactant is removed (typically by extraction or calcination) and the mesoporous structure is left behind. Silica particles are produced in a wide size range from 20 to 2000 nm and due to their manifold properties their applications range from analytical use in chromatography to highly advanced drug delivery devices, filling material in polymer composites or as moisture absorbents¹¹¹⁻¹¹⁵. It is easy to functionalize and its hydrophilic surface properties bear an additional advantage for enzyme immobilization, and therefore it was chosen as basic material for our nano- and micromotors.

1.2.2. Janus particles

Among all different kinds of particles the ones with probably most fascinating properties are Janus particles, named after the Greek two-faced god Janus, who stands for beginnings, transitions and endings, as well as patron of doors and gates. Janus particles typically have two faces, as the statue of Janus does and therefore they bear anisotropy and the possibility to unite different properties in one particle. Yet achieved particle architectures reach from simple spherical particles with different hemispheres to dumbbell shapes, cylinders or disks. The anisotropy can be of very different origin: it can arise in the full particle core (core-compartmentalized), from the shape, just at the surface (surface-compartmentalized), or the full particle with surface and core can be compartmentalized¹¹⁶.

The team around J. Lahann divides anisotropic particles in four groups (see figure 1.7 right). The first approach to generate anisotropy is the creation of asymmetric shapes or the coupling of several shapes into complex architectures ¹¹⁷. Nowadays almost all shapes are accessible, many through microfluidic approaches or crystallization. This however will not be discussed in detail in this thesis. Janus particles are mainly found in both remaining groups: "patchy" particles and anisotropically compartmentalized structures (see figure 1.7).

The first group is named "patchy" particles because the anisotropy is introduced through formation of surface patterns on the colloidal structures, mostly particles. Therefore all kind of surface modifications have been used, such as chemical functionalization, use of elastomeric stamps, sputtering or evaporation among others. In many of the early approaches the low yield is a major problem as 2D assemblies were necessary to selectively manipulate the accessible hemisphere.

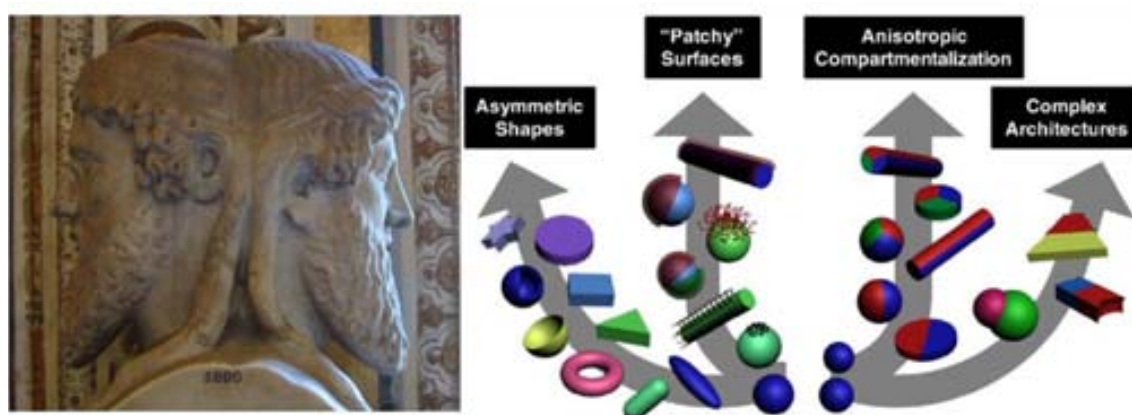


Fig. 1.7 Statue of the Roman god Janus and categories of anisotropic particles by Lahann *et al.* from reference 117.

Solutions were offered by new masking techniques that use 3D surfaces of microfibers and Pickering emulsions ¹¹⁸⁻¹²². Especially the use of Pickering emulsions makes higher particle yields possible, but the multiphase equilibria are not universal and therefore very sensitive to modifications in the composition. Apart from that in a recent review many other techniques have been discussed, including metal sputtering, photodeposition or printing techniques ¹¹⁷.

Different from the previously described surface modifications, anisotropic compartmentalization offers not only surface anisotropy but also confers this property to the whole material which improves properties such as swelling or degradability ¹¹⁷. Fabrication of such anisotropic objects is predominated by microfluidic approaches or electrodynamic cojetting, both methods that offer the possibility to combine different materials, entrap dyes or nanoparticles and obtain special particle shapes as rods, discs, cylinders, ovals and obviously spheres. Here the anisotropy is not just limited to Janus structures (2 compartments) but the number of compartments can be increased up to 6 or more compartments (e.g. ¹²³) and additional manipulations might be conducted. As different as the approaches to obtain anisotropy in Janus particles are the synthetic strategies to make them. Lattuada and Hatton divided the main classification into self-assembly techniques, phase separation and masking techniques, and new papers are constantly published on different methods ¹²⁴.

Experts in the field see possible applications of Janus and other anisotropic particles in several fields, as drug delivery, molecular imaging, self-assembly as particulate surfactants or use in modulated, optical (bio)sensors ^{116, 117, 120, 124}. However A. Müller points out that all applications need to be evaluated concerning the increased effort and cost that Janus particle production requires ¹¹⁶. However in the field of self-propelling beads the broken symmetry provides a unique approach to

design spatially confined catalysis. This reaches far beyond the possibilities of homogeneous particles and Janus particles already became firmly established in the field ^{7, 40-42, 47, 61, 125}.

1.3 Enzymes

Enzymes are large biomolecules that catalyze many important reactions for life, increasing either rate, specificity or both. Most enzymes are proteins even though few enzymes are also known to consist of RNA, the so called ribozymes. The smallest known enzyme only consists of 62 amino acids, being a tautomerase, while the largest structures may contain up to 2500 amino acids ¹²⁶. Their function depends largely on their structure and the folding of the amino acid chains ¹²⁷. Over 4000 biochemical reactions are known to be enzyme catalyzed - a fact that shows the high flexibility of enzymatic structures. The highly specific reactions catalyzed by enzymes avoid side reactions and undesired side products in chemical processes and are therefore used in several processes in modern laboratories, from biotechnology to organic catalysis. There the use of enzymes is highly beneficial, not only because separations of side products can be spared but also less heavy metal catalysts such as Pt or Mn need to be discharged or recovered. This makes the use of enzymes not only cheaper, but also more environmentally friendly. Generally trends in industry are observed to replace conventional chemical methods by enzyme-based strategies to improve efficiency, quicker performance and multifarious use.

1.3.1 Historical milestones and overview

In 1833 Payen, a French chemist discovered with diastase the first enzyme. Later during the 19th century Luis Pasteur studied fermentation and concluded that some vital force needs to be responsible for the observed transformations, a theory that was widely accepted at this time. This changed with the discovery of E. Buchner in 1897 that only yeast extract without living yeast fermented sugar to alcohol ¹²⁸. He recognized that not a complex living organism is responsible for fermentation but a more simple soluble substance to which he already associated protein nature. Having understood the nature of enzymes, the beginning of the 20th century was dedicated to their structural crystallization. The protein structure was not established at this time and only in 1926 was the first enzyme crystallized by J.B. Sumner and its purely protenic structure was proven. 1937 he isolated catalase and this work was awarded a Nobel Prize in 1946, together with his colleagues Northrop and Stanley for the conclusion that pure proteins can be enzymes.

1.3.2. Catalase ¹²⁹

Catalase is one of the oldest known enzymes, present in many types of cells to protect them from the harmful effects of peroxide by decomposing it. Amongst all known enzymes, catalase is one of the most efficient. Its turn over numbers approach about 200.000 catalytic events per second and subunit, a number that comes close to the diffusion-controlled limit. Decomposing a very reactive energy rich substrate into water and oxygen makes

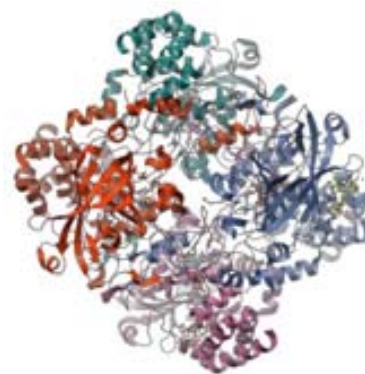


Fig 1.8 Structure of a catalase tetramer (upload.wikimedia.org/wikipedia/commons/7/71/Catalase_Structure.png).

catalase an ideal candidate to propel micromotors. Pioneering work was done by Sanchez *et al.* moving tubes with catalase⁵⁰ but further examples followed soon^{51, 130}. Catalase is formed by a tetramer of four identical polypeptide chains that form a dumbbell-shaped structure of 220-350 kDa. The bovine catalase which is used here has a molecular weight of 240 kDa and is characteristic of certain species. Each subunit contains a tightly bound NADP unit to protect the enzyme from oxidation by its substrate. One bovine catalase monomer shown in figure 1.8 consists of 506 amino acids plus one heme group plus one NADH molecule.

1.3.4 Immobilization of enzymes

The report of the first immobilization method was published in 1916: Nelson and Griffin discovered that invertase on $Al(OH)_3$ was still active. However this discovery was not used until the 1950s¹³¹. Initially mainly physical absorption methods were used, but good results meant that soon research on covalent immobilization followed up. From there scientists and industry started to recognize that the immobilization of enzymes might be highly advantageous and the topic began to be widely investigated¹³¹.

The use of supported enzymes present several advantages such as catalyst reuse because the immobilization facilitates the separation of the catalyst from products. Immobilization often enhances the stability of the enzymes and choosing a proper method might have positive effects on activity and selectivity¹³¹. Concerning the engineering details of production it can facilitate the operation of reactors and open additional possibilities in the choice of reactors¹³². However, its utilization also bears some limitations as inappropriate methods can cause loss or reduction in activity, when anchoring enzymes on bigger substrates limits the diffusion and by additional processing the cost might be increased¹³².

An immobilized enzyme is defined as an enzyme attached to an inert, insoluble material, through several techniques for enzyme immobilizations^{131, 133}, though in most of them chemical treatment is necessary. Ideally immobilization methods should be based on mild chemical procedures as many enzymes are unstable in harsh conditions. They should involve a regio-specific linkage to control the

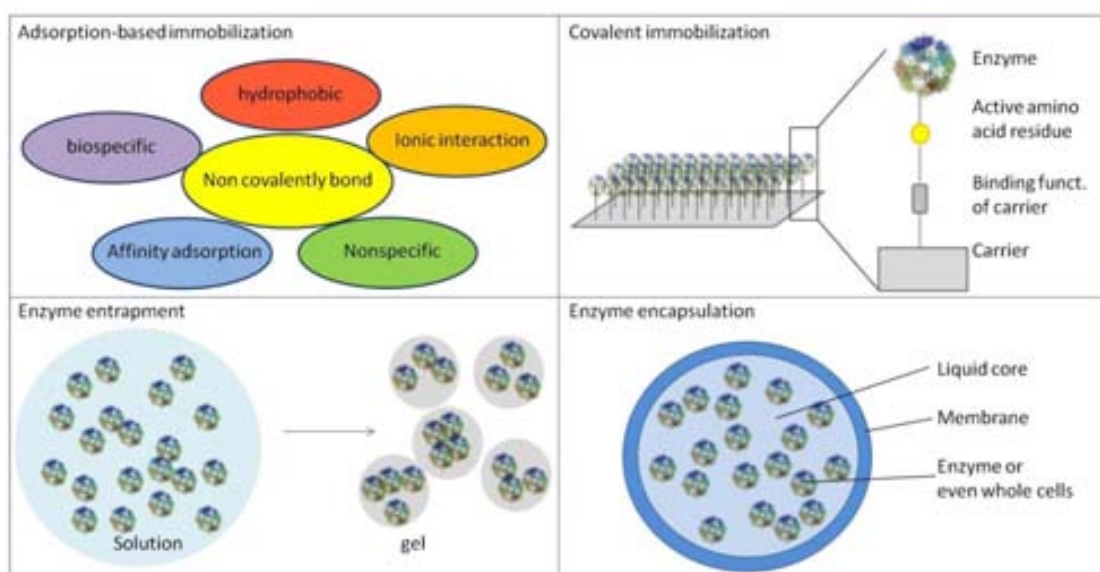


Fig 1.8 Scheme of different immobilization methods for the immobilization of an enzyme on a surface, inspired by reference 131.

enzyme's orientation without blocking or chemically modify the binding sites. Researchers have developed a variety of methods that can be classified as adsorption-based immobilization, covalent enzyme immobilization, enzyme entrapment, enzyme encapsulation and further unconventional strategies¹³¹. In the following paragraphs all methods shall be quickly introduced.

Adsorption-based immobilization was the first and probably the most simple method used by scientists, offering very mild conditions and reusability of both, enzymes and the carrier. As the adsorption results mainly from hydrophobic and salt linkages¹³³, the biggest drawback is leakage of the enzyme because no covalent bond between the enzyme and the support is formed. Anyway modern approaches as crosslinking of enzymes, the use of spacers or interaction as affinity, bio specific bonding or electrostatic interactions have diminished the disadvantages and managed to improve the results obtained by this method¹³¹.

Covalent immobilization is used since the late 1950s. Considering that a covalent bond is a very strong chemical linkage, this method does not bear a high risk of leakage. Generally it is based on a chemical reaction of activated carrier and either some reactive amino acid residue located on the enzyme surface or different group as phenol, imidazole etc. This chemical modification might affect enzyme activity strongly. Chemically one of the most used connectors is glutaraldehyde, being widely employed due to its synthetically simple strategy. However glutaraldehyde forms reversible imine structures with reactive amine groups, so that toxic glutaraldehyde is released. In order to diminish health problems caused by glutaraldehyde this method is now commonly replaced by other bifunctional linkers as carbodiimides or methods based on cyanogen bromide, that led to the development of several commercially available isothiocyanates¹³⁴. It was however found that not only chemical binding but also the nature of the carrier has important influence on the enzyme performance. Characteristics as carrier morphology, pore size, pH and hydrophobicity can both, stabilize or destabilize the immobilized enzyme and need to be considered before choosing a scaffold^{131, 134}.

Entrapped enzymes can be defined as those confined in a matrix, mostly a gel or a fibre. Therein the entrapment can include purely physical caging or involve the formation of covalent bindings. The production is normally a two-step process starting with an initial solution or dispersion of enzyme and a physical process to obtain solidification of the solvent in a second step. This can occur by several methods as crosslinking or gelation. A reversed approach is the entrapment of enzymes into ready-made matrices as sepharose or sephadex beads followed by chemical crosslinking to avoid leaching. In any case the matrix needs to be permeable to substrate molecules as the enzyme locked inside but the matrix shape can be tuned flexibly. Entrapment often stabilizes the enzyme through confinement effects and so does encapsulation¹³¹. Critically seen, it is quite difficult to delimit both methods and define them. Generally the dimension of the surrounding medium is the criterion.

Encapsulated enzymes have a membrane-like physical barrier surrounding the enzyme. Several processes to create capsules have been developed, where many are based on interfacial phenomena or phase inversion. Furthermore it is possible to encapsulate more than one enzyme in a capsule, either by chance or by engineering complexes of enzymes and subsequent encapsulation as shown by Liu *et al.*¹³⁵.

1.4 Platinum as catalyst

The metal itself is a rare element in the earth crust and in the periodic table of elements it is located in group 10, together with palladium and nickel. The groups 8 to 10 are often referred to as platinum group. Metallic palladium and platinum normally present face centred cubic structures, both are ductile materials and form active catalysts. The catalytic properties of a surface depend on the bonding properties of the potential reactant, if it is too strongly adsorbed, it will be bonded too tightly to react with other species. For too weakly bonded substances, the energy required to displace them is so low that they are desorbed very quickly and have no time to react¹³⁶. Even today few industrial catalysts would work without platinum and a huge part of the world's Pt production is used in catalysts. Platinum group metals are resistant to most acidic or basic solutions, only under oxidizing conditions in concentrated acids some oxidation of Pt may be observed.

In the initial state of this thesis Pt had already been intensively used as catalyst to propel microrods and even the use in microtubes and Janus particles was becoming more widespread^{33, 56, 137, 138}.

1.5 Literature

1. Anthony, D. A., *The horse, the wheel, and language: how Bronze-Age riders from the Eurasian steppes shaped the modern world*. Princeton University Press: Princeton, 2007.
2. Ludwig, W. Z. *f. vergl. Physiologie* **1930**, 13, (3), 397-504.
3. Taylor, G. *Proceedings of the Royal Society of London. Series A. Mathematical and Physical Sciences* **1951**, 209, (1099), 447-461.
4. Feynman, R. P. *Caltech Engineering and Science* **1960**, 23, (5), 22-36.
5. Purcell, E. M. *American Journal of Physics* **1977**, 45, (1), 3-11.
6. ten Hagen, B.; van Teeffelen, S.; Löwen, H. *Journal of Physics: Condensed Matter* **2011**, 23, (19), 194119.
7. Howse, J. R.; Jones, R. A. L.; Ryan, A. J.; Gough, T.; Vafabakhsh, R.; Golestanian, R. *Physical Review Letters* **2007**, 99, (4), 048102.
8. National-Aeronautics-and-Space-Administration What is drag? <http://www.grc.nasa.gov/WWW/k-12/airplane/drag1.html>
9. Lauga, E.; Powers, T. R. *Reports on Progress in Physics* **2009**, 72, (9), 096601.
10. Nelson, B.; Kaliakatsos, I.; Abbott, J. *Annual Review of Biomedical Engineering* **2010**, 12, 55-85.
11. Howard, J.; Hudspeth, A. J.; Vale, R. D. *Nature* **1989**, 342, (6246), 154.
12. Howard, J., Mechanics of motor proteins. In *Physics of bio-molecules and cells. Physique des biomolécules et des cellules*, Flyvbjerg, F.; Jülicher, F.; Ormos, P.; David, F., Eds. Springer Berlin Heidelberg: 2002; Vol. 75, pp 69-94.
13. Hess, H.; Bachand, G. D. *Materials Today* **2005**, 8, (12, Supplement 1), 22-29.
14. Guix, M.; Mayorga-Martinez, C. C.; Merkoçi, A. *Chemical Reviews* **2014**.
15. Soong, R. K.; Bachand, G. D.; Neves, H. P.; Olkhovets, A. G.; Craighead, H. G.; Montemagno, C. *D. Science* **2000**, 290, (5496), 1555-1558.
16. Weibel, D. B.; Garstecki, P.; Ryan, D.; DiLuzio, W. R.; Mayer, M.; Seto, J. E.; Whitesides, G. M. *PNAS* **2005**, 102, (34), 11963-11967.
17. Fang, H.; Jing, P.; Haque, F.; Guo, P. *Biophysical Journal* **2012**, 102, (1), 127-135.
18. Wendell, D.; Jing, P.; Geng, J.; Subramaniam, V.; Lee, T. J.; Montemagno, C.; Guo, P. *Nature Nanotechnology* **2009**, 4, (11), 765-772.
19. Magdanz, V.; Sanchez, S.; Schmidt, O. G. *Advanced Materials* **2013**, 25, (45), 6581-6588.
20. Credi, A. *Journal of Physics: Condensed Matter* **2006**, 18, (33), S1779.

21. Saha, S.; Stoddart, J. F. *Chemical Society Reviews* **2007**, 36, (1), 77-92.
22. Richard A. van Delden, M. K. J. t. W., Michael M. Pollard, Javier Vicario, Nagatoshi Koumura, Ben Feringa. *Nature* **2005**, 437, 1337-1340.
23. Rienk Eelkema, M. M. P.; Javier Vicario, N. K., Blanca; Serrano Ramon, C. W. M. B.; Dirk J. Broer, B. L. F. *Nature* **2006**, 440, 163.
24. van Delden, R. A.; Koumura, N.; Harada, N.; Feringa, B. L. *Proceedings of the National Academy of Sciences* **2002**, 99, (8), 4945-4949.
25. Ismagilov, R. F.; Schwartz, A.; Bowden, N.; Whitesides, G. M. *Angewandte Chemie International Edition* **2002**, 41, (4), 652-654.
26. Catchmark, J. M.; Subramanian, S.; Sen, A. *Small* **2005**, 1, (2), 202-206.
27. Paxton, W. F.; Kistler, K. C.; Olmeda, C. C.; Sen, A.; St. Angelo, S. K.; Cao, Y.; Mallouk, T. E.; Lammert, P. E.; Crespi, V. H. *Journal of the American Chemical Society* **2004**, 126, (41), 13424-13431.
28. Fournier-Bidoz, S.; Arsenault, A. C.; Manners, I.; Ozin, G. A. *Chemical Communications* **2005**, (4), 441-443.
29. Posner, J. D.; Moran, J. L.; Wang, J.; Wheat, P. In *Catalytic Nanomotor Function and Locomotion Physics*, Functional nanoscience, Bozen, 2011; Bozen.
30. Kline, T. R.; Paxton, W. F.; Mallouk, T. E.; Sen, A. *Angewandte Chemie International Edition* **2005**, 44, (5), 744-746.
31. Wang, Y.; Hernandez, R. M.; Bartlett, D. J.; Bingham, J. M.; Kline, T. R.; Sen, A.; Mallouk, T. E. *Langmuir* **2006**, 22, (25), 10451-10456.
32. Demirok, U. K.; Laocharoensuk, R.; Manesh, K. M.; Wang, J. *Angewandte Chemie International Edition* **2008**, 47, (48), 9349-9351.
33. Laocharoensuk, R.; Burdick, J.; Wang, J. *ACS Nano* **2008**, 2, (5), 1069-1075.
34. Kagan, D.; Calvo-Marzal, P.; Balasubramanian, S.; Sattayasamitsathit, S.; Manesh, K. M.; Flechsig, G.-U.; Wang, J. *Journal of the American Chemical Society* **2009**, 131, (34), 12082-12083.
35. de Buyl, P.; Kapral, R. *Nanoscale* **2013**, 5, (4), 1337-1344.
36. Golestanian, R.; Liverpool, T. B.; Ajdari, A. *New Journal of Physics* **2007**, 9, (5), 126.
37. Love, J. C.; Gates, B. D.; Wolfe, D. B.; Paul, K. E.; Whitesides, G. M. *Nano Letters* **2002**, 2, (8), 891-894.
38. Lodget, G.; Kuhn, A. *Nature Communications* **2011**, 2, 535.
39. Baraban, L. Capped Colloids as Model Systems

for Condensed Matter. University of Konstanz, Konstanz, 2008.

40. Baraban, L.; Harazim, S. M.; Sanchez, S.; Schmidt, O. G. *Angewandte Chemie International Edition* **2013**, 52, (21), 5552-5556.
41. Baraban, L.; Makarov, D.; Streubel, R.; Mönch, I.; Grimm, D.; Sanchez, S.; Schmidt, O. G. *ACS Nano* **2012**, 6, (4), 3383-3389.
42. Baraban, L.; Tasinkevych, M.; Popescu, M. N.; Sanchez, S.; Dietrich, S.; Schmidt, O. G. *Soft Matter* **2012**, 8, (1), 48-52.
43. Ebbens, S.; Gregory, D. A.; Dunderdale, G.; Howse, J. R.; Ibrahim, Y.; Liverpool, T. B.; Golestanian, R. *Soft condensed matter* **2013**, arXiv:1312.6250.
44. Ebbens, S. J.; Howse, J. R. *Langmuir* **2011**, 27, (20), 12293-12296.
45. Brown, A. T.; Poon, W. C. K. *Soft condensed matter* **2013**, arXiv:1312.4130.
46. Wu, Y.; Wu, Z.; Lin, X.; He, Q.; Li, J. *ACS Nano* **2012**, 6, (12), 10910-10916.
47. Baraban, L.; Streubel, R.; Makarov, D.; Han, L.; Karnaushenko, D.; Schmidt, O. G.; Cuniberti, G. *ACS Nano* **2012**, 7, (2), 1360-1367.
48. Pantarotto, D.; Browne, W. R.; Feringa, B. L. *Chemical Communications* **2008**, (13), 1533-1535.
49. Mano, N.; Heller, A. *Journal of the American Chemical Society* **2005**, 127, (33), 11574-11575.
50. Sanchez, S.; Solovev, A. A.; Mei, Y.; Schmidt, O. G. *Journal of the American Chemical Society* **2010**, 132, (38), 13144-13145.
51. Gao, W.; Sattayasamitsathit, S.; Uygun, A.; Pei, A.; Ponedal, A.; Wang, J. *Nanoscale* **2012**, 4, (7), 2447-2453.

52. Mei, Y.; Huang, G.; Solovev, A. A.; Ureña, E. B.; Mönch, I.; Ding, F.; Reindl, T.; Fu, R. K. Y.; Chu, P. K.; Schmidt, O. G. *Advanced Materials* **2008**, *20*, (21), 4085-4090.
53. Yao, K.; Manjare, M.; Barrett, C. A.; Yang, B.; Salguero, T. T.; Zhao, Y. *The Journal of Physical Chemistry Letters* **2012**, *3*, (16), 2204-2208.
54. Solovev, A. A.; Xi, W.; Gracias, D. H.; Harazim, S. M.; Deneke, C.; Sanchez, S.; Schmidt, O. G. *ACS Nano* **2012**, *6*, (2), 1751-1756.
55. Harazim, S. M.; Xi, W.; Schmidt, C. K.; Sanchez, S.; Schmidt, O. G. *Journal of Materials Chemistry* **2012**, *22*, (7), 2878-2884.
56. Manesh, K. M.; Cardona, M.; Yuan, R.; Clark, M.; Kagan, D.; Balasubramanian, S.; Wang, J. *ACS Nano* **2010**, *4*, (4), 1799-1804.
57. Li, J.; Huang, G.; Ye, M.; Li, M.; Liu, R.; Mei, Y. *Nanoscale* **2011**, *3*, (12), 5083-5089.
58. Soler, L.; Magdanz, V.; Fomin, V. M.; Sanchez, S.; Schmidt, O. G. *ACS Nano* **2013**, (10.1021/nn405075d).
59. Guix, M.; Orozco, J.; García, M.; Gao, W.; Sattayasamitsathit, S.; Merkoçi, A.; Escarpa, A.; Wang, J. *ACS Nano* **2012**, *6*, (5), 4445-4451.
60. Kagan, D.; Campuzano, S.; Balasubramanian, S.; Kuralay, F.; Flechsig, G.-U.; Wang, J. *Nano Letters* **2011**, *11*, (5), 2083-2087.
61. Gibbs, J. G.; Zhao, Y.-P. *Applied Physics Letters* **2009**, *94*, (16), 163104.
62. Manjare, M.; Yang, B.; Zhao, Y. P. *The Journal of Physical Chemistry C* **2013**, *117*, (9), 4657-4665.
63. Manjare, M.; Yang, B.; Zhao, Y. P. *Physical Review Letters* **2012**, *109*, (12), 128305.
64. Huang, W.; Manjare, M.; Zhao, Y. *The Journal of Physical Chemistry C* **2013**, *117*, (41), 21590-21596.
65. Wilson, D. A.; Nolte, R. J. M.; van Hest, J. C. M. *Nature Chemistry* **2012**, *4*, (4), 268-274.
66. Wilson, D. A.; de Nijs, B.; van Blaaderen, A.; Nolte, R. J. M.; van Hest, J. C. M. *Nanoscale* **2013**, *5*, (4), 1315-1318.
67. Gao, W.; Pei, A.; Wang, J. *ACS Nano* **2012**, *6*, (9), 8432-8438.
68. Gao, W.; Feng, X.; Pei, A.; Gu, Y.; Li, J.; Wang, J. *Nanoscale* **2013**, *5*, (11), 4696-4700.
69. Pavlick, R. A.; Sengupta, S.; McFadden, T.; Zhang, H.; Sen, A. *Angewandte Chemie International Edition* **2011**, *50*, (40), 9374-9377.
70. Volpe, G.; Buttinoni, I.; Vogt, D.; Kummerer, H.-J.; Bechinger, C. *Soft Matter* **2011**, *7*, (19), 8810-8815.
71. Zhao, G.; Seah, T. H.; Pumera, M. *Chemistry – A European Journal* **2011**, *17*, (43), 12020-12026.
72. Sharma, R.; Chang, S. T.; Velev, O. D. *Langmuir* **2012**, *28*, (26), 10128-10135.
73. Orozco, J.; Vilela, D.; Valdés-Ramírez, G.; Fedorak, Y.; Escarpa, A.; Vazquez-Duhalt, R.; Wang, J. *Chemistry – A European Journal* **2014**, *20*, (10), 2866-2871.
74. Gao, W.; Pei, A.; Dong, R.; Wang, J. *Journal of the American Chemical Society* **2014**, *136*, (6), 2276-2279.
75. Wang, J., *Micromachines*. Wiley: 2013.
76. Peyer, K. E.; Tottori, S.; Qiu, F.; Zhang, L.; Nelson, B. J. *Chemistry – A European Journal* **2013**, *19*, (1), 28-38.
77. Honda, T.; Arai, K.; Ishiyama, K. *IEEE Trans. Magn* **1996**, *32*, (5), 5085-5087.
78. Ghosh, A.; Fischer, P. *Nano Letters* **2009**, *9*, (6), 2243-2245.
79. Zhang, L.; Abbott, J. J.; Dong, L.; Peyer, K. E.; Kratochvil, B. E.; Zhang, H.; Bergeles, C.; Nelson, B. J. *Nano Letters* **2009**, *9*, (10), 3663-3667.
80. Zhang, L.; Peyer, K. E.; Nelson, B. J. *Lab on a Chip* **2010**, *10*, (17), 2203-2215.
81. Remi Dreyfus, J. B., Marcus L Roper, Marc Fermigier, Howard A. Stone, Jerome Bibette. *Nature* **2005**, *437*, 862-865.
82. Behkam, B.; Sitti, M. *Journal of Dynamic Systems, Measurement, and Control* **2005**, *128*, (1), 36-43.
83. Jiang, H.-R.; Yoshinaga, N.; Sano, M. *Physical Review Letters* **2010**, *105*, (26), 268302.

84. Yang, M.; Ripoll, M. *Soft Matter* **2014**, 10, (7), 1006-1011.
85. Wang, W.; Castro, L. A.; Hoyos, M.; Mallouk, T. E. *ACS Nano* **2012**, 6, (7), 6122-6132.
86. Garcia-Gradilla, V.; Orozco, J.; Sattayasamitsathit, S.; Soto, F.; Kuralay, F.; Pourazary, A.; Katzenberg, A.; Gao, W.; Shen, Y.; Wang, J. *ACS Nano* **2013**, 7, (10), 9232-9240.
87. Kagan, D.; Benchimol, M. J.; Claussen, J. C.; Chuluun-Erdene, E.; Esener, S.; Wang, J. *Angewandte Chemie* **2012**, 124, (30), 7637-7640.
88. Calvo-Marzal, P.; Manesh, K. M.; Kagan, D.; Balasubramanian, S.; Cardona, M.; Flechsig, G.-U.; Posner, J.; Wang, J. *Chemical Communications* **2009**, (30), 4509-4511.
89. Ibele, M.; Mallouk, T. E.; Sen, A. *Angewandte Chemie International Edition* **2009**, 48, (18), 3308-3312.
90. Kagan, D.; Laocharoensuk, R.; Zimmerman, M.; Clawson, C.; Balasubramanian, S.; Kang, D.; Bishop, D.; Sattayasamitsathit, S.; Zhang, L.; Wang, J. *Small* **2010**, 6, (23), 2741-2747.
91. Balasubramanian, S.; Kagan, D.; Jack Hu, C.-M.; Campuzano, S.; Lobo-Castañón, M. J.; Lim, N.; Kang, D. Y.; Zimmerman, M.; Zhang, L.; Wang, J. *Angewandte Chemie International Edition* **2011**, 50, (18), 4161-4164.
92. Wu, J.; Balasubramanian, S.; Kagan, D.; Manesh, K. M.; Campuzano, S.; Wang, J. *Nature Communications* **2010**.
93. Gao, W.; Wang, J. *ACS Nano* **2014**.
94. Soler, L.; Sanchez, S. *Nanoscale* **2014**.
95. Petit, T.; Zhang, L.; Peyer, K. E.; Kratochvil, B. E.; Nelson, B. J. *Nano Letters* **2011**, 12, (1), 156-160.
96. Peyer, K. E.; Zhang, L.; Nelson, B. J. *Nanoscale* **2013**, 5, (4), 1259-1272.
97. Tottori, S.; Zhang, L.; Qiu, F.; Krawczyk, K. K.; Franco-Obregón, A.; Nelson, B. J. *Advanced Materials* **2012**, 24, (6), 811-816.
98. Vicario, J.; Eelkema, R.; Browne, W. R.; Meetsma, A.; La Crois, R. M.; Feringa, B. L. *Chemical Communications* **2005**, (31), 3936-3938.
99. Gibbs, J. G.; Zhao, Y.-P. *Review of Scientific Instruments* **2008**, 79, (8), -.
100. Ebbens, S. J.; Howse, J. R. *Soft Matter* **2010**, 6, 726-738.
101. Stöber, W.; Fink, A. *Journal of Colloid and Interface Science* **1968**, 26, 62-69.
102. Wang, Q.; Liu, Y.; Yan, H. *Chemical Communications* **2007**, (23), 2339-2341.
103. Fang, X.; Chen, C.; Liu, Z.; Liu, P.; Zheng, N. *Nanoscale* **2011**, 3, (4), 1632-1639.
104. Masalov, V. M.; Sukhinina, N. S.; Kudrenko, E. A.; Emelchenko, G. A. *Nanotechnology* **2011**, 22, (27), 275718.
105. Nooney, R. I.; Thirunavukkarasu, D.; Chen, Y.; Josephs, R.; Ostafin, A. E. *Chemistry of Materials* **2002**, 14, (11), 4721-4728.
106. Nozawa, K.; Gailhanou, H.; Raison, L.; Panizza, P.; Ushiki, H.; Sellier, E.; Delville, J. P.; Delville, M. H. *Langmuir* **2004**, 21, (4), 1516-1523.
107. Zhang, Y.; Judkins, E. C.; McMillin, D. R.; Mehta, D.; Ren, T. *ACS Catalysis* **2013**, 3, (11), 2474-2478.
108. Trewyn, B. G.; Nieweg, J. A.; Yannan, Z.; Lin, V. S. Y. *Chemical Engineering Journal* **2008**, 137, 23-29.
109. Ferris, D. P.; Lu, J.; Gothard, C.; Yanes, R.; Courtney, T. R.; Olsen, J. C.; Stoddart, J. F.; Tamanoi, F.; Zink, J. I. *Small* **2011**, 7, (13), 1816-1826.
110. Schlossbauer, A.; Warncke, S.; Gramlich, P. M. E.; Kecht, J.; Manetto, A.; Carell, T.; Bein, T. *Angewandte Chemie International Edition* **2010**, 49, (28), 4734-4737.
111. Baeza, A.; Guisasola, E.; Ruiz-Hernández, E.; Vallet-Regí, M. *Chemistry of Materials* **2012**, 24, (3), 517-524.
112. Bele, M.; Siiman, O.; Matijevi, E. *Journal of Colloid and Interface Science* **2002**, 254, (2), 274-282.
113. Blin, J. L.; Otjacques, C.; Herrier, G.; Su, B.-L. *Langmuir* **2000**, 16, (9), 4229-4236.
114. Esquena, J.; Pons, R.; Azemar, N.; Caelles, J.; Solans, C. *Colloids and Surfaces A: Physicochemical and Engineering Aspects* **1997**, 123-124, (0), 575-586.

115. Hoffmann, F.; Cornelius, M.; Morell, J.; Fröba, M. *Angewandte Chemie International Edition* **2006**, 45, (20), 3216-3251.
116. Walther, A.; Müller, A. H. E. *Chemical Reviews* **2013**, 113, (7), 5194-5261.
117. Lee, K. J.; Yoon, J.; Lahann, J. *Current Opinion in Colloid & Interface Science* **2011**, 16, (3), 195-202.
118. Jiang, S.; Chen, Q.; Tripathy, M.; Luijten, E.; Schweizer, K. S.; Granick, S. *Advanced Materials* **2010**, 22, (10), 1060-1071.
119. Jiang, S.; Schultz, M. J.; Chen, Q.; Moore, J. S.; Granick, S. *Langmuir* **2008**, 24, (18), 10073-10077.
120. Granick, S.; Jiang, S.; Chen, Q. *Physics Today* **2009**.
121. Perro, A.; Meunier, F.; Schmitt, V.; Ravaine, S. *Colloids and Surfaces A: Physicochemical and Engineering Aspects* **2009**, 332, (1), 57-62.
122. Perro, A.; Reculosa, S.; Pereira, F.; Delville, M.-H.; Mingotaud, C.; Duguet, E.; Bourgeat-Lami, E.; Ravaine, S. *Chemical Communications* **2005**, (44), 5542-5543.
123. Maeda, K.; Onoe, H.; Takinoue, M.; Takeuchi, S. *Advanced Materials* **2012**, 24, (10), 1340-1346.
124. Lattuada, M.; Hatton, T. A. *Nano Today* **2011**, 6, (3), 286-308.
125. Simmchen, J.; Baeza, A.; Ruiz, D.; Esplandiu, M. J.; Vallet-Regí, M. *Small* **2012**, 8, (13), 2053-2059.
126. Chen, L. H.; Kenyon, G. L.; Curtin, F.; Harayama, S.; Bembenek, M. E.; Hajipour, G.; Whitman, C. P. *Journal of Biological Chemistry* **1992**, 267, (25), 17716-17721.
127. Anfinsen, C. B. *Science* **1973**, 181, (4096), 223-230.
128. Buchner, E. *Berichte der deutschen chemischen Gesellschaft* **1897**, 30, (1), 1110-1113.
129. Boon, E. M.; Downs, A.; Marcey, D. *Catalase H₂O₂*; 2001.
130. Orozco, J.; García-Gradilla, V.; D'Agostino, M.; Gao, W.; Cortés, A.; Wang, J. *ACS Nano* **2012**, 7, (1), 818-824.
131. Cao, L., Introduction: Immobilized Enzymes: Past, Present and Prospects. In *Carrier-bound Immobilized Enzymes*, Wiley-VCH Verlag GmbH & Co. KGaA: 2006; pp 1-52.
132. Brena, B. M.; Batista-Viera, F., Methods in Biotechnology: Immobilization of Enzymes and Cells., Guisan, J. M., Ed. Humana Press Inc., : Totowa, NJ, 1999.
133. Datta, S.; Christena, L. R.; Rani, Y.; Rajaram, S. *BIOTECH* **2013**, (3), 1-9.
134. Chaplin, M. *Enzyme Technology*.
135. Liu, Y.; Du, J.; Yan, M.; Lau, M. Y.; Hu, J.; Han, H.; Yang, O. O.; Liang, S.; Wei, W.; Wang, H.; Li, J.; Zhu, X.; Shi, L.; Chen, W.; Ji, C.; Lu, Y. *Nature Nanotechnology* **2013**, 8, 187-192.
136. Giandomenico, C. M., Platinum-Group Metals, Compounds. In *Kirk-Othmer Encyclopedia of Chemical Technology*, John Wiley & Sons, Inc.: 2000.
137. Gao, W.; Sattayasamitsathit, S.; Manesh, K. M.; Weihs, D.; Wang, J. *Journal of the American Chemical Society* **2010**, 132, (41), 14403-14405.
138. Solovev, A. A.; Mei, Y.; Bermúdez Ureña, E.; Huang, G.; Schmidt, O. G. *Small* **2009**, 5, (14), 1688-1692.

Objectives and outline

2

This chapter outlines the thesis and briefly introduces the contents that the reader can expect in each chapter.

The generation of movement at the microscale is a fascinating new field of interdisciplinary science. In [chapter 1](#) an extended introduction to micromotors is given, reaching from the history over the physical basics to a review of the state of the art in most motor types. Concerning the chemical part of this thesis, a summary of particle properties are discussed and enzymes which will play an important role in this thesis will be introduced. In summary it can be said that in this joint project with Dr. Baeza from Complutense University in Madrid we focused on the development of particle based micromotors.

[Chapter 3](#) is a collection of all used methods and synthesis strategies throughout the thesis.

[Chapter 4](#) is discussing the results and is divided in 4 subunits. [Chapter 4.1](#) describes the synthesis of silica particles with different characteristics and properties. The obtained particles are an important prerequisite for further steps toward movement at the microscale. In this chapter several tools that will be used at more advanced state of the thesis are developed: of high importance are surface functionalizations and subsequent grafting of catalytically active material on the surface that might be either enzymes or inorganic catalysts. Other biological molecules as DNA were also anchored on the particles and all steps were characterized chemically and their behaviour was documented. In the end all acquired knowledge was combined in the development of a proof of concept motion based DNA sensor. To further develop the utility of the Janus motors, first attempts were taken towards magnetic directionability.

In [chapter 4.2](#) an improvement in the enzyme driven micromotors concerning their lifetime and reusability was achieved by developing of an encapsulation method for enzymes. The capsules themselves were characterized and anchored on different kinds of particles. Some efforts were also dedicated to the evaluation of the stability of those particle micromotors when exposed to elevated temperatures or in presence of proteolytic enzymes.

In [chapter 4.3](#) further efforts were dedicated to the magnetic directionability of the micromotors and several problems were encountered. In order to find an efficient solution, a collaboration with the group of Dr. Sanchez in Dresden was established. Therein an already developed method of multilayer deposition was adopted and particle movement could be guided. Therefore the enzyme had to be replaced by Pt as an inorganic catalyst for peroxide decomposition and movement of Pt driven Janus particles was studied in different fuel containing media. This concept was extended to another type of micromotors, namely microjets and comparative statements about differences between both motor types could be found. The well-known method of Zetapotential measurement was used to further characterize the particle behaviour in presence of different kinds of surfactants. Novel insights into mechanistic details of gradient driven particle movement might be concluded based on those measurements.

In a side project AgCl particles were obtained and due to their potential use as micromotors in [chapter 4.4](#) their synthesis was developed further and their properties were characterized. Their use as micromotors finally led to a first application: waste water cleaning by means of degradation of organic molecules and antibacterial properties.

To summarize, silica materials were functionalized, grafted with different biomolecules or metal based catalysts in order to generate novel micromotors. Their synthesis was carefully characterized and their motion was studied. The newly developed concepts provide a basis for future work and contribute to enlarge the knowledge about movement at the microscale.

3

Experimental details

In this chapter a list of used abbreviations is given, the references for chemicals and materials are listed and all methods are described in detail. Furthermore analytical protocols are listed.

3.1 Abbreviations

A	adenine
AA	acrylamide
AC	alternating current
ADP	adenosine diphosphate
AgNP	silver nanoparticles
AM	2-aminoethyl methacrylate
APS	ammonium persulphate
APTES	3-aminopropyltriethoxysilane
ATP	adenosine triphosphate
AuNP	gold nanoparticles
Au@PS	polystyrene particles half covered with gold
BACl	benzalkonium chloride
bix	1,4-bis(imidazolylmethyl)benzene
C	cytosine
CFU	colony forming unit
CTAB	cetrimonium bromide
DI	deionized water
DNA	desoxyribonucleic acid
DLS	dynamic light scattering
EDC	1-ethyl-3-(3-dimethylaminopropyl) carbodiimide hydrochloride
EtOH	ethanol
F1-ATPase	enzyme that uses a proton gradient to drive ATP synthesis
FAM	fluorescein amidite
FIT	trade name of a dish soap
Fmoc-Cl	fluorenylmethoxycarbonyl chloride
FRET	fluorescence energy transfer experiments
FTIR	fourier transform infrared spectroscopy
G	guanine
GOx	glucose oxidase
HRP	horseradish peroxidase
MBA	<i>N,N'</i> -methylene bisacrylamide
MeOH	methanol
MPA	mercapto propylic acid
MSN	mesoporous nanoparticle
MUA	mercapto undecanoic acid
NADH	nicotinamide adenine dinucleotide
NADP	nicotinamide adenine dinucleotide phosphate
NHS	N- hydroxysuccinimide
NP	nanoparticles
PB	phosphate buffer
PCR	polymerase chain reaction
PDMS	polydimethyl siloxane
pH	decimal logarithm of the reciprocal of the hydrogen ion activity
PS	polystyrene
PTMS	phenyltrimethoxysilane
R	organic residue (in reaction schemes)
SATA	<i>N</i> -Succinimidyl <i>S</i> -Acetylthioacetate
SDS	sodium dodecyl sulfate
SEM	scanning electron microscopy
Sulfo-SMCC	sulfosuccinimidyl 4- <i>N</i> -maleimidomethyl cyclohexane-1-carboxylate
T	thymine
TAMRA	carboxytetramethylrhodamine
TEM	transmission electron microscopy
TEOS	tetraethyl orthosilicate
TGA	thermogravimetric analysis
TMEDA	<i>N,N,N',N'</i> -tetramethylethylenediamine

TPOS	tetrapropyl orthosilicate
UV	ultra violet
wt. %	weight percent
ZP	zeta potential
2D/3D	two /three dimensional

physical constants and symbols

D	diffusion constant
k	Boltzmann constant
T	temperature
r	radius of a sphere
Re	Reynolds number
ρ	fluid density
U	velocity
μ	dynamic viscosity
L	length
f	force (e.g. f_{drag} , $f_{inertia}$, $f_{viscous}$)
ϑ	particle velocity
π	mathematical constant, pi = 3.14159265359
p	pressure
B	magnetic field strength
μ	permanent magnetic moment
R_0	Förster radius
r	distance between the fluorophores
$\tau_{D,0}$	lifetime of the donor
ΔH^\ominus	change of enthalpy
ΔS	change of entropy
Δp	pressure difference

3.2 Chemicals

Name	Sold by
Acrylamide	Sigma-Aldrich Inc.
<i>N</i> -acryloxysuccinimide	Sigma-Aldrich Inc.
Aminoethyl methacrylate	Sigma-Aldrich Inc.
3-Aminopropyltriethoxysilane,	Sigma-Aldrich Inc.
Ammonium persulphate (APS)	Sigma-Aldrich Inc.
Benzalkonium chloride	FlukaChemika
Bicinchinonic acid	Sigma-Aldrich Inc.
Carboxyethylsilanetriol sodium salt	ABCR GmbH & Co. KG.
Catalase from bovine liver lyophilized powder with an activity of >10000units/mg by peroxide assay	Sigma-Aldrich Inc.
Catalase from bovine liver (aqueous suspension, 10,000-40,000 units/mg protein by peroxide assay	Sigma-Aldrich Inc.
Cetyltrimethylammonium bromide	Sigma-Aldrich Inc.
Chloroauric acid	Sigma-Aldrich Inc.
<i>o</i> -Dianisidine(3,3'-Dimethoxybenzidine)	Sigma-Aldrich Inc.
<i>a,a'</i> -Dibromo- <i>p</i> -xylene	Sigma-Aldrich Inc.
Fluorenylmethoxycarbonyl chloride	Sigma-Aldrich Inc.
Fluorescamine (4-Phenylspiro-[furan-2(3H),1-phthalan]-3,3'-dione)	Sigma-Aldrich Inc.
Glucose	Sigma-Aldrich Inc.
Glucose oxidase	Sigma-Aldrich Inc.
Glycerine	Sigma-Aldrich Inc.
Horseradish peroxidase (HRP)	Sigma-Aldrich Inc.
<i>N</i> -Hydroxysuccinimide	Sigma-Aldrich Inc.
<i>N</i> -(3-Dimethylaminopropyl)- <i>N'</i> -ethylcarbodiimide hydrochloride (EDC·HCl)	Sigma-Aldrich Inc.
Dithio-DL-threitol	Sigma-Aldrich Inc.
Imidazol	Sigma-Aldrich Inc.
Iron (II) chloride	Sigma-Aldrich Inc.
Iron (III) chloride	Sigma-Aldrich Inc.
Iron (III) nitrate	Sigma-Aldrich Inc.
Mercapto propanoic acid	Sigma-Aldrich Inc.
Mercapto undecanoid acid	Sigma-Aldrich Inc.
Methylorange	Sigma-Aldrich Inc.
Methylblue	Sigma-Aldrich Inc.
<i>N,N'</i> -methylene bisacrylamide	Sigma-Aldrich Inc.
Paraffin	Sigma-Aldrich Inc.
Peroxide	Mostly Sigma-Aldrich Inc.
Phenyltrimethoxysilane (PTMS)	Sigma-Aldrich Inc.
Polystyrene particles - 1 µm fluorescent	Sigma-Aldrich Inc.
Piperidine	Sigma-Aldrich Inc.
Polystyrene particles -7 µm	Sigma-Aldrich Inc.
Polyvinylpyrrolidone	Sigma-Aldrich Inc.
Potassium hydroxide	Sigma-Aldrich Inc.

Rhodamine 6G	Sigma-Aldrich Inc.
5 µm silica particles	Bang laboratories / Sigma-Aldrich Inc.
10 µm silica particles	Kisker Biotech GmbH & Co. KG
Silver hexafluorophosphate	Sigma-Aldrich Inc.
Sodium acetate	Sigma-Aldrich Inc.
Sodium carbonate	Sigma-Aldrich Inc.
Sodium dodecylsulfate	Sigma-Aldrich Inc.
Sodium hydrocarbonate	Sigma-Aldrich Inc.
Sodium hydride (60% in oil)	Sigma-Aldrich Inc.
Sodium hydroxide	Sigma-Aldrich Inc.
Sodium tartrate	Sigma-Aldrich Inc.
Suberic acid bis(<i>N</i> -hydroxysuccinimide ester)	Sigma-Aldrich Inc.
<i>N</i> -Succinimidyl <i>S</i> -acethioacetate	Thermo scientific
Succinic anhydride	Sigma-Aldrich Inc.
Sulfosuccinimidyl 4- <i>N</i> -maleimidomethyl cyclohexane-1-carboxylate (sulfo-SMCC)	Sigma-Aldrich Inc.
Tetramethylanilium hydroxide	Sigma-Aldrich Inc.
<i>N,N,N',N'</i> -tetramethylethylenediamine (TEMED)	Sigma-Aldrich Inc.
Tetraethyl orthosilicate	Sigma Aldrich Inc.
Tetrapropyl orthosilicate	Sigma Aldrich Inc.
3- (Triethoxysilyl)- propylsuccinic anhydride	ABCR GmbH & Co. KG.
TRIS*HCl (Tris(hydroxymethyl)aminomethane hydrochloride)	Sigma Aldrich Inc.
Trisodium citrate	Sigma Aldrich Inc.
TritonX	Sigma Aldrich Inc.

Deionized water was further purified by passage through a Milli-Q Advantage A-10 Purification System (Millipore Corporation) to a final resistivity of initially 18.2 M/cm. All other chemicals and solvents (hydrochloric acid 37 wt.%, ammonia 30 wt.%, absolute ethanol, acetone, etc.) were of the best quality commercially available and used as received without further purification. Dry tetrahydrofuran was taken from a distillation gadget of the organic department in UAB.

Used DNA was obtained from Sigma-Aldrich Inc. as thiol-conjugated 6FAM -labeled and TAMRA -labeled oligonucleotides (1 mol synthesis scale, desalted).

The (2µ-Cl)dmba-Pt dimer was supplied by Venancio Rodriguez, University of Murcia.

3.3 Material

Membrane filters were made of Nylon with a filter size of 0,22 μm and purchased in Technokroma.




To purify and concentrate enzymes Amicon filters of different molecular weights were purchased from Milipore Merck KGaA.

For diffusion controlled catalysis Corning® Transwell® are used.

G25 Sephadex columns were acquired in GE Healthcare.

Available magnets were characterized by measuring the magnetic field at certain distances from the surfaces, the results are listed in table 3.1.

Table 3.1 Magnetic field strength of used magnets

Cube magnetic - field strength in mT	distance	Upward facing side	Downward facing side	Lateral (central)
	on surface	-540	+534	-190
	0,5cm	-200	/	/
	1cm	-72	/	-35
	2cm	-22	/	-10
	5	-2	/	-1
rod magnetic - field strength in mT	distance	Upward facing side	Downward facing side	Lateral (central pos.)
	on surface	-140	+139	+35
	0,5cm	-69	+75	+28
	1cm	-42	+38	+19
	2cm	-16	+15	+11
	5cm	-2.8	+2.8	+2.2
Small rod - magnetic field strength in mT	distance	Upward facing side	Downward facing side	Lateral (central pos.)
	On surface	-142	+143	+20
	0,5cm	-19.7	+20	+11
	1cm	-6.9	+7	+4.1
	2cm	-1.3	+1.7	+1.1
	5cm	/	/	/

3.4 Detailed description of synthetic methods

3.4.1 Silica particles and enzyme - based micromotors

3.4.1.1 Particle synthesis

*Synthesis of small uniform non porous silica particles*¹

A mixture of TEOS (0.35 mol/L), NH₃ (1.16 mol/L), H₂O (3.1 mol/L), and isopropyl alcohol (123 mL) was stirred at 40 °C for 1h to produce silica beads. Recovered and washed particles were dispersed in concentrated HCl aqueous solution (50 mL, 6 wt.% HCl) and sonicated for 1h before being centrifuged out and washed several times with water.

*Two – step synthesis of uniform non porous silica particles*²

A mixture of 1.9 mL TEOS in 13 mL propanol was prepared. Simultaneously 0.7 mL NH₃ (25%) and 1.4 mL H₂O were mixed and both solutions were united at room temperature under stirring and aged for 60 min at 50 °C to obtain seeds.

A solution of 7 mL TEOS in 300 mL propanol was added to the seed solution under constant stirring and subsequently 20 mL NH₃ (25%) in 40 mL of water were added and heated to 50 °C under stirring. As last step 120 mL of TEOS were added at an addition rate of 0.5 g/min. Several washing steps with water and filtration is required to remove NH₃ and solvent residues.

Synthesis of uniform hollow silica particles^{3, 4}

930 µL of PTMS were added to a 6.6 mmol/L HNO₃ solution kept in an isothermal water bath at 60 °C to form a PTMS/water interface. At acidic conditions at proximity to the interface superficial hydrolysis occurs rapidly. Addition of 10 mL NH₄OH solution (28-30%) initiates the condensation reaction that forms particles. Variation of reaction time leads to different particle shell thicknesses and cavity sizes.

Synthesis of mesoporous silica nanoparticles (MSN)^{5, 6 7}

1 g of CTAB as cationic surfactant was dissolved in a mixture of H₂O/EtOH/NH₃ (vol. ratio 6:4.6:0.7) and stirred for 2h to allow the surfactant to form micelles. 2 mL of TEOS in EtOH were added and precipitates were allowed to form during 2h at 10 °C. After filtration and washing with H₂O and ethanol, the surfactant was removed by extraction with 1% HCl in methanol.

3.4.1.2 Particle functionalization

Asymmetrical amination of mesoporous silica particles (MSN-NH₂)

200 mg of the dried MSN particles were vortexed during 80 seconds with a mixture of 1 g molten paraffin in 22.4 mL H₂O and 4.4 mL EtOH at 80°C. After this time, the suspension was immediately cooled down in order to solidify the paraffin. The obtained particles were filtered, washed and subsequently dispensed in 15 mL water containing 1.5 mL NH₃ (aq. 25%). After addition of 0.7 mL APTES the mixture was shaken overnight on an orbital shaker. The solid was filtered and washed with heptane until there was no paraffin residue measured by FTIR.

Synthesis of carboxylic acid-functionalized particles (MSN-CO₂H)

200 mg of MSN-NH₂ particles were suspended in 4 mL of dry THF under N₂ gas as inert atmosphere. To this solution, 60 mg succinic acid was added and the mixture was stirred overnight at room temperature. The obtained particles were filtered and washed with THF.

Carboxylation of solid 5 μm particles

40 mg of commercial silica particles of approx. 10 μm were dried during 2h at 80 °C. 5mL of dry toluene and a 5-fold excess regarding to the particles surface, considering that 1 nm² silica bears approximately 4.9 OH-groups^{8, 9}. 10 mg of (3-succinimylpropyl)-triethoxysilane were added and reacted overnight. Particles were washed with toluene and EtOH and dried subsequently.

Synthesis of amino-carboxylic acid particles (H₂N-MSN-CO₂H)

In analogy to the previous amination step, 200 mg of MSN-CO₂H particles were dispensed in 15 mL water containing 1.5 mL NH₃ (aq. 25%). After addition of 0.7 mL APTES, the mixture was shaken overnight, followed by filtration and washing steps.

Introduction of thiol groups

100 mg mesoporous silica particles were dispersed in 10 mL dry Toluene under N₂ and heated under reflux to 110 °C. 0.25 mL 3-mercaptopropyltrimethoxysilane (MPTMS) were added and the suspension was stirred during 12 hours, washed with toluene and filtered.

Reaction with cross-linker Sulfo-SMCC

10 mg of H₂N-MSN-CO₂H particles were reacted with 2 mg of sulfo-SMCC for 2 h in 5 mL 0.1 mol/L phosphate buffer (PB), containing 0.2 mol/L NaCl (pH 7.2). After centrifugation the supernatant was removed and excess crosslinker was washed away with H₂O. In case of the cargo-NH₂ particles, the same procedure was followed (see also figure 3.1).

Synthesis of aminated silica particles – cargo (cargo-NH₂)

thiolated products. 10 mg crosslinker containing particles were dispersed in 2 mL 0.1 mol/L PB, 0.2 mol/L NaCl (pH 7.4) and reacted overnight. As mentioned above, the sequence attached to mesoporous silica particle (motor) was 5' 6FAM TTGAATCAGCGATAA ThiC3 , while cargo particles were grafted with 5'- ThiC6 TTCAAGCCGACTAAG TAM. The DNA-immobilized nanoparticles were then washed three times in 10 mmol/L Tris·HCl, 150 mmol/L NaCl, and 0.05% Tween 20 buffer (pH 7.5). The amount of attached DNA was estimated by subtracting DNA accumulated in the supernatant and washing solutions from total DNA, measured by UV/VIS spectrometry.

3.4.1.4 Motor experiments

Motion experiments

10 mg of both particles (motor and cargo) were separately suspended in 0.5 mL of 20 mmol/L Tris·HCl, 37.5 mmol/L MgCl₂ (pH 8). 50 µL of each suspension were mixed and incubated for 20 min in three batches. To one of them, 10 µL of commercial single stranded DNA analyte buffered solution 5'-TTATCGCTGATTCAACTTAGTCGGCTTGAA-3' (1.8 nmol/µL) were added, the other batch received 10 µL of buffer solution, while the last batch receive 10 µL of non-complementary single stranded DNA buffered solution 5'- AACGTTATCATCATTTTCGCCCTATACCTTT-3 (1.8 nmol/µL). Microscope slides were covered with a 5% H₂O₂ in glycerol/water (50:50) and on each a drop of the corresponding particle suspensions was placed. The behaviour of each sample was observed by optical microscopy.

FRET measurements

25 µL of each previously prepared particle suspension (see motion exp.) were mixed in three batches. To one of them, 10 µL of DNA analyte solution (1.8 nmol/µL) were added, the second batch received 10 µL of buffer solution, while the last batch receive 10 µL of non-complementary DNA solution, both solutions contained commercial single stranded DNA, no previous dehybridization was necessary. After 30 min of shaking the samples were diluted with 250 µL 20 mmol/L Tris·HCl, 37.5 mmol/L MgCl₂ (pH 8) buffer and the fluorescence of the probes at an excitation of 480 nm was measured. The efficiency of the fluorescence transfer process is calculated as the ratio of the intensities TAMRA/FAM. Therefore the contributions of FAM and TAMRA to the obtained spectra were determined and the integrals calculated (see chapter 4.1). The ratio of those intensities lead to following FRET efficiencies: 0.919 for the analyte DNA and 0.281 for the non specific DNA. Those values show, that hybridization is 3.2 times stronger than unspecific interactions between oglionucleotides as hydrogen bonds or unspecific absorption.

Synthesis of γ -Fe₂O₃ maghemite nanoparticles¹¹

Superparamagnetic maghemite nanoparticles were obtained by coprecipitation. 10.21 g of FeCl₂·4H₂O (0.052 mol) were dissolved in 1 L of H₂O, pouring a second solution of FeCl₃·6H₂O (28.35 g, 0.104 mol) in 57 mL of HCl 1.5 mol/L under strong stirring, yielding nanometric magnetite (Fe₃O₄). To the previous solution, 100 mL of NH₃ (25%) were added and stirring was stopped 15 minutes later, followed by a two days decantation on a magnet. The black flocculate was dispersed to a 2 mol/L

HNO₃ solution and stirred for 2-3 minutes. After decantation, the particles were oxidized to maghemite in a solution of Fe(NO₃)₃·9H₂O in H₂O (0.3366 mol/L) at 100 °C, keeping this temperature for 30 min. Another decantation (2-3h) was carried out and the product was dispersed in a 0.02 mol/L HNO₃ solution. Those nanocrystals showed an average hydrodynamic diameter of 16 nm measured by dynamic light scattering. To cover iron oxide nanoparticles with silica they were supposed be precoated with APTES and used as nucleation cores in Stoeber synthesis.

Synthesis of rice-shaped Fe₂O₃ hematite nanoparticles^{12,13}

A solution of FeCl₃·6 H₂O (0.02 mol/L) was aged with a NaH₂PO₄ solution (0.0004 mol/L) during 72 hours in a Pyrex bottle at 100 °C. The obtained product was centrifuged and washed with acetone. Oxidation to maghemite particles¹⁴: To oxidize hematite to maghemite, particles were heated to 70 °C during 24 hours and dried under vacuum for 12h. Annealing to magnetite was performed under a continuous stream of Ar (400 mL/min) and H₂ (200 mL/min) during 3h at 360 °C in a furnace. Subsequently the temperature was decreased to 240 °C under air flushing and maintained during 2h to oxidize particles to maghemite. To ensure complete oxidation particles were redispersed in HNO₃ (0.01 mol/L) and after addition of sodium citrate (0.015 mol/L) stirring was continued for 30 min at 90 °C and washed with large excess of acetone.

*Covering with SiO₂*¹⁵⁻¹⁷

20 mg particles were dispersed in a PVP in H₂O solution (400 mg/44 mL) and sonicated during 2h followed by 15h of agitation. Particles were centrifuged and washed with water to remove excess PVP. After redispersion in 2.5 mL H₂O particles were added to 45 mL EtOH, sonicated and stirred at 400 rpm. After 30 min TMAH in EtOH (0.1865 mol/L) is added, followed by 30 min of stirring. 50 µL of APTES are diluted in 200 µL of EtOH and added dropwise. After 30 min of stirring a mixture of APTES, TEOS and EtOH (4:150:1000) is added in 3 portions each 385 µL.

Asymmetrization of rice particles

Pickering solution approach: 1 mL of the silica covered rice particles were vortexed during 80 seconds with a mixture of 1 g molten paraffin in 22.4 mL H₂O and 4.4 mL EtOH at 80 °C. After this time, the suspension was immediately cooled down in order to solidify the paraffin. The obtained particles were filtered, washed and subsequently dispensed in 15 mL water containing 1.5 mL NH₃ (aq. 25%). Resulting precipitation was analyzed by SEM.

Magnetically directed approach: A teflon plate bearing a cavity was placed in between an assembly of 2 cylindrical magnets. In the cavity a drop of solidified paraffin on a glass slide was positioned and a drop silica covered rice particles in solvent was added. The whole assembly was placed in an oven at temperatures varying from 40-80 °C to melt or soften the paraffin and allow the perpendicular entrapment of the rice particles in the paraffin surface. The obtained paraffin drop showed orange enclosures that were analyzed by SEM.

3.4.2 Enzyme encapsulation for micromotors with prolonged lifetime

3.4.2.1 Encapsulation of Enzymes

Pre-purification step of commercial enzymes

Commercially available enzymes mostly contain $(\text{NH}_4)_2\text{SO}_4$ and smaller protein fragments. Therefore a purification step previous to use is recommendable. Commercial enzymes were dissolved in 0.01 mol/L sodium carbonate buffer and filtered through Amicon filters to remove smaller protein fragments and chemical impurities. Using a BCA assay (see 3.6.3) the recovered protein after filtration for catalase was quantified to be around 63% using 100 kDa filter, 93% using a 10 kDa filter. In order to maintain more defined conditions in the polymerization the 10 kDa filter was defined as a standard pre-purification step. In the original enzyme solution, in the obtained filtrate and the washing solution were assessed and only a slight lose in catalytic activity was documented. The washing solution showed some remaining activity, which was insignificant compared to the remaining protein. Therefore it can be assumed that the mayor part of smaller protein fragments are not catalytically active and can be removed without losing significant catalytic activity.

Acroylation of enzymes

Approx. 5 mg of purified enzyme were dissolved in 1 mL 0.01 mol/L sodium carbonate buffer (pH 8.5) and reacted with a 20 fold excess of *N*-acryloxysuccinimide, dissolved in 10 μL DMSO during 30 min at room temperature. Finally, the reaction solution was filtered through Amicon filters of 50 kDa and collected in 100 μL sodium carbonate buffer (0.01 mol/L, pH 8.5). The modification was monitored by DLS and Zetapotential, as well as the protein content and the relative amino-content were compared.

Synthesis of polymer shells on acroylated enzymes

Diluting the acryloylated enzyme in 1000 μL deoxygenated sodium carbonate buffer (0.01 mol/L, pH 8.5) radical polymerization was performed. A ratio of 450-9000 eq. monomer/enzyme, aminoethyl methacrylate (positively charged monomer), 1200-12000 eq. acrylamide (neutral monomer) and 50-2000 eq. *N,N'*-methylene bisacrylamide as crosslinker were added in 2 mL sodium carbonate buffer. The polymerization was initiated by adding 500 eq. of ammonium persulphate and 1000 eq. *N,N,N',N'*-tetramethylethylenediamine dissolved in 1 mL deoxygenated sodium carbonate buffer into the reaction media. The mixture was allowed to react at room temperature during 90 min in nitrogen atmosphere. Unreacted monomers and initiators were removed by filtration and subsequent washing steps applying Amicon filters. The success of capsule formation was monitored by DLS where an increase in size from 7.2 nm (native catalase) to a range from 9.5 up to 60 nm for encapsulated enzyme was observed. These results were confirmed by TEM using phosphotungstic acid as staining agent in order to visualize properly the enzyme-polymer capsules. Zetapotential measurements did not show significative changes. In order to confirm the presence of aminogroups in the capsule the fluorescamine test was employed.

Enzymatic activity assay

Enzyme content was determined through UV-absorption measurement at 280 nm. Native enzyme concentration was adjusted to 3 mg/mL to be identical to the value of encapsulated catalase (2.975 mg/mL). 5 μ L of a tenfold dilution were added to 2 mL of 11 mmol/L peroxide solution in PB and after 1 min of shaking remaining peroxide was determined through absorption at 240 nm.

Enzymatic activity evaluation

The enzymatic activity was determined spectrophotometrically by using H₂O₂ as a substrate following a procedure published elsewhere³³. Briefly, 25 μ L of a solution of enzyme in 50 mM PB pH 7.0 with a concentration of 1mg/mL was added to 11 mmol/L H₂O₂ in 50 mmol/L PB solution with rapid stirring. The decrease in absorbance at 240 nm (with an extinction coefficient of 0.041 mmol⁻¹ cm⁻¹) was recorded after 30 seconds at 20 °C. One unit of catalase will decompose 1 μ mol of H₂O₂ per minute at pH 7.0 and 20 °C. The enzymatic activity was expressed in units per milligram of dry solid.

Enzymatic stability evaluation

Against enzymatic degradation by protease: 1 mg of the catalase capsules or native catalase were dissolved in 1 mL of PB and of 5 mg/mL of protease were added. The mixture was incubated during 2h at 37 °C and 100 rpm. After this time, the enzymatic activity of the enzymes was determined by following the degradation of H₂O₂ by UV-absorption at 240 nm.

Temperature stability: 1 mg of the catalase capsules or native catalase were dissolved in 1 mL of PB and exposed to high temperature (60 °C during 1h) under constant shaking and protected from light. After this time, the enzymatic activity of the enzymes was determined following the degradation of H₂O₂ by UV-absorption at 240 nm.

3.4.2.2 Silica motors

Anchoring of enzyme capsules on silica particles

2 mg particles were dispersed in 0.1 mol/L PB with 1 mg *N*-(3-dimethylaminopropyl)-*N'*-ethylcarbodiimide hydrochloride (EDC) and 2 mg *N*-hydroxysuccinimide (NHS) to activate COOH groups. After 30 min of stirring, 3 mg of catalase capsules or native catalase were added. Further stirring during minimum 2h at room temperature let to covalently anchored enzyme on the particle surface. The whole process was monitored by FTIR spectroscopy (see figure 4.2.7) and other analytical techniques as TGA, amino assay, elemental analysis.

Turn over evaluation of enzyme-silica motors

1 mg of native catalase or capsule catalase functionalized silica particles suspended in 0.2 mL of PB 0.1 mol/L pH 7.2 was placed on the membrane with 0.4 μ m of pore of a Corning® Transwell® well

immersed in 1.5 mL of a solution of 1.5% of H₂O₂. After 30 min, the amount of H₂O₂ was determined by UV-absorption at 240 nm. Then, the liquid was removed and replaced by 1.5 mL of fresh H₂O₂ 1.5% and the procedure was repeated ten times.

Motor movement evaluation

All experiments were performed on microscopy glass slides placed in a 6 well plate. Motor particles were placed in distilled water containing 2.5% of H₂O₂ and 10% glycerine to diminish media movement, to which 1 μL particles dispersed in distilled water were added. The movement was observed in an EVOS xl digital inverted microscope and videos were recorded with a reflex camera. Obtained videos are available in the supporting information.

3.4.2.3 Polystyrene particle motors

Enzyme anchoring on aminated Polystyrene particles

10 μL of a commercial particle solution was diluted in 0.5 mL PB 0.1 mol/L pH 7.2. Then, 0.5 mg of suberic acid bis(*N*-hydroxysuccinimide ester) as crosslinker solved in 10 μL of DMSO was added. After 30 min of stirring, 1 mg of catalase capsules were added. Further stirring at room temperature overnight let to covalently anchored enzyme on the particle surface. The scheme of the reaction is available in figure 4.2.11.

Motor movement evaluation

All experiments were performed on microscopy glass slides placed in a 6 well plate. Motor particles were placed in distilled water containing 2.5% of H₂O₂ and 10% glycerine to diminish media movement, to which 1 μL particles dispersed in distilled water were added. The movement was observed in an EVOS xl digital inverted microscope and videos were recorded with a reflex camera. Obtained videos are available in the supporting information.

3.4.2.4 Janus motors

Gold evaporation on polystyrene

In first instance particles were placed by drop-casting on a previously cleaned inclined glass-surface, leading to a monolayer of particles on the glass. This was carefully dried and placed in the evaporator. In vacuum a thin layer of chromium (approx. 3 nm) was evaporated previously to the gold layer to improve adhesion¹⁸, followed by a gold layer of approx. 10 nm. Finished particles were stored in vacuum in order to minimize passivation.

Sulfyl groups on enzymatic capsules

One batch of enzyme capsules (approx. 5 mg) was diluted in 1 mL PB, 0.05 mol/L and 4 mg of SATA dissolved in 20 μ L of DMSO were added. This mixture was allowed to react during 1h and the unreacted SATA was removed by filtration through Amicon filters. Prior to further experimental use of the thiolated capsules they had to be deprotected by reaction with 1 mL of a 1 mol/L NH_4OH solution, containing 50 mmol/L EDTA during 2h. Deprotected thiolcapsules were purified once more with Amicon filters.

A different approach consisted in the thiolation of AM prior to reaction to capsules. Therefore 500 mg of AM were deprotonized in 0.1 mol/L NaOH and subsequently extracted with dichloromethane. 50 mg of the obtained product were allowed to react with 28 mg of SATA and this molecule was directly used to obtain capsules, as chromatographic purification was not successful.

3.4.2.5 Other enzymes

GOx coupling

Carboxylated silica particles were coupled to glucose oxidase using EDC/NHS coupling as described earlier in chapter 3.4.1.3. Placing such particles in a 5 wt.% glucose solution, pH 5.5, saturated with oxygen did not lead to observable particle movement.

Encapsulation of GOx

was performed analogously to catalase encapsulation, previously described. Briefly in an acrylation step double bonds are introduced to the surface and in the following a mixture of monomers and crosslinker is added, and the reaction is initiated by addition of radicalic ammonium persulphate and *N,N,N',N'*-tetramethylethylenediamine. Molecular ratios between 1:1200 and 1:3000 enzyme:acrylamide were tested.

Coupling of encapsulated GOx

Carboxylated silica particles were coupled to Glucose oxidase capsules using EDC/NHS as presented in chapter 3.4.2.2. Placing such particles in a 5 wt.% glucose solution, pH 5.5, saturated with oxygen did not lead to observable particle movement.

Pure GOx was dissolved in 5 wt.% glucose solution and exposed to a slightly bubbling oxygen flow. To evaluate the generated peroxide concentration 10 μ L of a catalase solution in PB (5 mg/mL) was added. Minimum detectable peroxide concentration was evaluated and found to be 0.1 wt.% by bubbling of catalase. On that account catalase solution was added to the glucose + GOx mixture and no immediate bubble formation was seen. Only after a reaction time approx. 2h a slight bubble

generation was observed. This result indicates that commercial GOx is not suitable to create a micromotor driven by an enzymatic tandem of GOx and catalase.

HRP evaluation

To a solution of 5% peroxide were added 5 mg/mL HRP solution and no bubbles were observed.

3.4.3 Platinum driven micromotors - experiments on motile Janus particles and microtubes

3.4.3.1 Fabrication

Metal covered Janus particles - obtaining a particle monolayer on a glass slide

*monolayer at interface*¹⁹: a Petri dish containing water was covered by a thin layer of heptane and an ethanolic suspension of silica particles (ca. 5 wt.%) was spread onto the interface between water and heptane until the water surface is totally covered with the monolayer. The substrate (precleaned glass slide) was preliminary placed in the bottom of the dish and after monolayer formation carefully lifted up with a tweezer. In this process the monolayer deposits on the glass surface and can be dried.

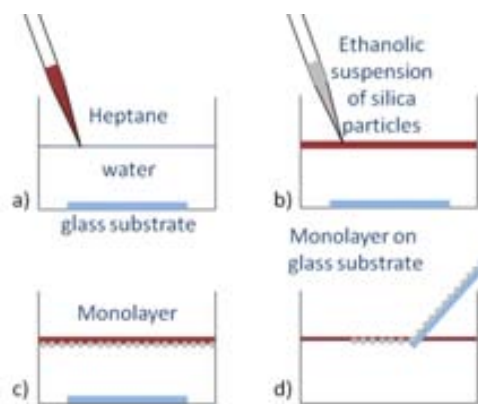


Fig. 3.2 method to obtain a monolayer of particles by a self-assembly process at the interface between two non-miscible solvents that is subsequently transferred to a glass slide.

*drop casting*²⁰: a supporting glass slide is cleaned by ultrasonication in purified water and acetone followed by treatment in oxygen or alternatively UV plasma for 4 min. A droplet of a particle/water dispersion is deposited on a tilted glass slide leading to the self-assembling of the particle monolayers, followed by slow evaporation of the solvent under ambient conditions.

Evaporation of multilayers on microparticles

A suspension of spherical silica colloids is dripped onto a previously cleaned glass substrate as previously described. Afterwards, the particle array samples are introduced to the vacuum chamber

(base pressure of $1 \cdot 10^{-7}$ mbar) of a sputtering machine where deposition of the magnetic multilayer stack consisting of $\text{Co}(0.4 \text{ nm})/\text{Pt}(0.6 \text{ nm})_5$ is carried out at room temperature (Ar sputter pressure, $8 \cdot 10^{-3}$ mbar) as described by Baraban et al.^{21, 22} and a final 5 nm Pt layer was sputtered to guarantee catalytic properties. Afterwards particles have to be placed in a strong magnetic field to magnetize them permanently (here 10 kT).

Fabrication of catalytic platinum microtubes (done by V. Magdanz)

The fabrication method has been described previously^{23, 24}. In brief, Ti/Cr/Fe/Pt microjets were fabricated by e-beam deposition of metallic layers onto lithographically patterned photoresist layers. Square $50 \mu\text{m}$ photoresist patterns were prepared on 28 mm square glass slides. Photoresist AR-P 3510 was spin-coated onto the cleaned glass wafers at 3500 rpm for 35 s, followed by a soft bake using a hotplate at $90 \text{ }^\circ\text{C}$ for 2 min and exposure to UV light with a Karl Suss MA56 Mask Aligner (410-605 nm) for 7 seconds. Patterns were developed in a 1:1 AR300-35:H₂O solution. On-chip rolled-up catalytic microtubes were obtained by a tilted deposition of 5 nm of each metal (Ti, Fe, Cr) at a 75° angle. Subsequently, a 1 nm layer of platinum was sputtered on the glass substrates. By dissolving the photoresist layer in Dimethyl sulfoxide, pre-stressed multilayers automatically roll up into microtubes. The supercritical point dryer was adopted in the fabrication of rolled-up microtubes to avoid the tubes collapsing during drying. The diameter of tubes was tuned to be $5 \mu\text{m}$ (comparable to particle size). As a consequence tubes had approximately 3 windings. In order to self-propel catalytic microjets, aqueous hydrogen peroxide solutions with a volume concentration of 5% were used as chemical fuels, in which certain concentrations of surfactant such as benzalkonium chloride, sodium dodecyl sulfate, Triton X or FIT as common dish soap were added to reduce the surface tension.

3.4.3.2 Speed experiments

Experiments on microtubes were performed in glass recipients containing H₂O₂ solutions of different concentrations in distilled water. A glass substrate bearing tubes was put into the solution and the tubes detached from the surface due to forces generated by bubbles.

All microparticle experiments were performed in a 96 well plate in distilled water containing defined concentrations of H₂O₂ to which $1 \mu\text{L}$ particles dispersed in distilled water were added. Videos were recorded with a Phantom Miro eX2 high speed camera mounted to an inverted Zeiss AxioVision microscope. Evaluation was performed with the Phantom camera software. Considered videos were at least 4 sec long (corresponding to min 82 frames to guarantee high quality videos). Particles could not be followed over a longer distance than one screen width which corresponds to (0.4365 mm ; $512 \cdot 384 \text{ Pixel}$) at a magnification of 100x.

3.4.3.3 Effects of soap on particle- / tube- movement

As synthesized particles or tubes were added to solutions of different soap concentrations (range from 0.00001 wt.% to 10 wt.%), containing 5% of H₂O₂. Videos were recorded using a Phantom

camera with 20 frames per second, with a minimum size of 82 frames, speed evaluation was performed using the integrated mode of the Phantom software.

Zetapotential measurement

Due to methodical limitations original motor particles could not be used to evaluate particle charge (Zetapotential) relative to surfactant concentrations. 10 nm Au and Pt were therefore evaporated on 1 μm silica particles and measured in bidistilled water containing determined surfactant concentrations. Zetapotential was measured in Malvern one-way Zetapotential cells. From the measurements it can be concluded, that surfactants that have strong effects on the behaviour of the motors also strongly change the surface potential. The critical micelle concentration (SDS: 0.23 wt.% , TritonX: $1.375 \cdot 10^{-2}$ wt.% , BACl 0.205 wt.%) does not seem to have an important impact on the surface potential. This is an indication that the coverage of Pt with surfactant molecules only plays a minor part in the mechanism.

3.4.3.4 Effects of thiols on particle- / tube- movement

Surface modification of Pt-particles

A glass slide with Pt-particles of ca 0.25 cm^2 was immersed for different times, ranging from 30 min to 12h, into a 20 mmol/L solution of Mercaptoundecanoic acid (MUA) in isopropanol. Resulting particles did not differ either in the contact angle (data not shown) or in their catalysis properties. Afterwards the particles were rinsed for 5 min in isopropanol, 5 min in water and then removed from the glass slide by sonication.

Surface modification of Pt-tubes

For grafting MUA on the inner Pt surface of microtubes, a piece of 0.25 cm^2 glass slide containing an array of Ti/Fe/Cr/Pt microtubes were immersed for 30 min into a 20 mmol/L solution of MUA in isopropanol. Afterwards the particles were rinsed for 5 min in isopropanol and 5 min in water. The tubes were immersed in a solution containing 5% H_2O_2 , 5% SDS, wherein non functionalized tubes produced a sufficient oxygen to detach from the glass slide and move in solution. MUA modified tubes showed no bubble production at the same conditions.

3.4.5 AgCl - light driven micromotors

3.4.4.1 synthesis of AgCl microstars

In a typical synthesis 10 mg of $2(\mu\text{-Cl})\text{dmbaPt}$ (0,0133 mmol) were dissolved in 4 ml DMSO. A solution of 1 equivalent of an inorganic silver salt (AgPF_6) in 1ml DMSO was added dropwisely and stirred for 1h protected from light. Initially no precipitation of AgCl is observed and in order to shift the equilibrium towards the products 1 eq. of bis(imidazol-1-ylmethyl)benzene or 2 eq. of imidazole were

added and enhanced precipitation of AgCl is observed. The precipitate is filtered and washed with EtOH. In the experiments for figure 4.4.4 the amount of bix was varied from 0,4 eq. to 1,6 eq. of bix.

1,4-Bis(imidazol-1-ylmethyl)benzene (bix) was synthesized following a method published by P.K. Dhal *et al.*: 1.9 g (48 mmol) of a sodium hydride suspension in mineral oil (60%) were washed with 10 mL of dry THF under nitrogen and subsequently dissolved in 30 mL dry THF. Under nitrogen atmosphere 2.85 g (44 mmol) of imidazole dissolved in 15 mL of dry THF were added slowly and the mixture was allowed to stir for 30 min. 5.3 g (20 mmol) *o,o'*-Dibromo-p-xylene in 20 mL of THF were added to the resulting suspension and the resulting suspension was heated to 50 °C for minimum 4h. The reaction mixture was cooled with approximately 25 mL of ice water and stirred for 20 min. Then the product was extracted with chloroform (3 X 50 mL), and the combined organic phases were dried over anhydrous sodium sulfate and after filtration the solvent was removed under reduced pressure the obtained product was found pure in NMR analysis and used without further purification.

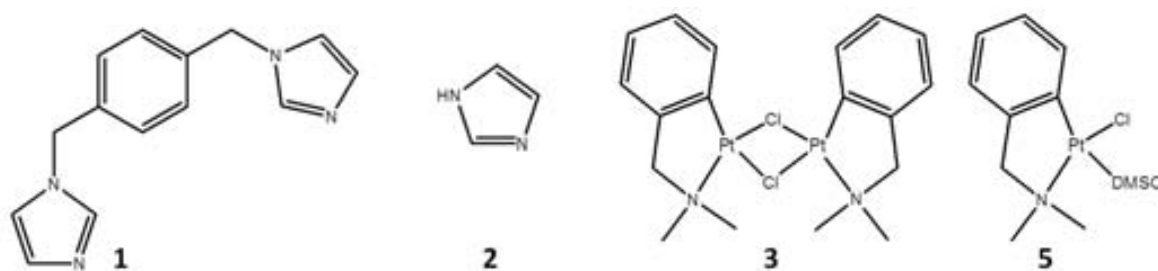


Fig. 3.3 Chemical structures of bix, imidazole, the dimeric Pt complex and an analogous simple Pt complex

3.4.4.2 Degradation of organic molecules²⁵

Microstars were precipitated as described previously, washed in ethanol and water and redispersed in DI water in a concentration of 0.01 mg/μl. Solutions of methyl orange, methyl blue and rhodamine 6G were prepared in a concentration of 10 mg/l. Finally to 5 ml colorant solution 30 μl of microstar suspension were added or for blank experiments 30 μl of pure water. A blank solution and a microstar containing solution of each colorant were kept at a dark place, equally a blank solution and a microstar containing solution of each solution were placed under a UV lamp and another batch of blank and test solutions were placed in the sun. The degradation was found uncompleted after 30 min, therefore the duration of the experiment was extended to 3h when the solutions were either colourless or strongly decolorized. After that time UV absorption was measured in the wavelength range corresponding to the colorant.

catalyst concentration: 0.01 mg/μl

solution of organic compounds: 10 mg/l

add 30 μl of catalyst concentration to each sample

Absorptions were measured in the following ranges (depending on the colorant):

Organic colorant	Initial wavelength in nm	Final wavelength in nm
Methyl orange	250	600
Methyl blue	250	400
Rhodamine 6G	400	600

UV driven micromotors

Experiments were performed in a Zeiss Axiovert microscope coupled to a EXFO lamp (X-Cite) and either an AxioCam MRm or a Thorlab USB 2.0 camera. A sample holder bearing a freshly cleaned glass slide was covered by 100 μl MiliQ water and 2 μl microstars in water were added. When irradiated with white light generally no movement was observed, only after turning on the UV lamp (with DAPI filter) the particles started to move. The particles continued their movement even after turning of the UV light for some time, indicating that the created gradient does not disappear by turning of the light.

3.4.4.3 Bactericide effect

Several concentrations of silver nanoparticles (0, 25, 50, 75 and 100 $\mu\text{g ml}^{-1}$) were tested against E.coli. E. coli cells should always be freshly unfrozen. An agar plate was inoculated with 20 μl of unfrozen glycerol stock and grown overnight. A single colony was used to inoculate 100 ml of THB solution and incubated at 37 °C overnight. Density measurement gave 1.497 after 16 hours. A dilution 1:10 was found to have suitable density for exponential growth (0.322) and used for further experiment. Dilutions of the same solution (10^{-1} to 10^{-6}) were inoculated in Agar plates to count CFU, what resulted in $9,05 \cdot 10^7$ CFU/ml.

The interaction with silver nanoparticles was analysed by adding silver nanoparticles to the solution E.coli solution of $9 \cdot 10^7$ CFU/ml. The homogeneous suspensions of 0-100 $\mu\text{g/ml}$ were allowed to grow overnight under agitation in an orbital shaker to avoid particle sedimentation. Optical density was measured and CFUs were counted in dilutions of 10^{-2} and 10^{-4} . To determine the light sensitivity the same protocol was followed, with the only difference that the growth occurred partially in darkness, partially in irradiation with a USB-LED lamp.

To evaluate the amount of AgCl gone into solution the concentration of Ag^+ -ions in THB and pure inorganic buffer solution was measured. Therefore the synthesized AgCl microstars were added to 5 ml solution (THB or buffer respectively) and shaken for 8 hours before centrifugation to remove all non dissolved particles. Then samples were send to ICP-MS analysis for Ag^+ -ions.

3.5 Analytical techniques

UV-Visible spectra were acquired with a UNICAM UV 500 spectrometer.

FTIR spectra were obtained with a Thermo Nicolet nexus equipped with a Goldengate attenuated total reflectance device.

Zetapotentials as well as dynamic light scattering (DLS) studies of particle sizes and the enzyme nanocomplexes were measured on Zetasizer Nano instrument (Malvern Instruments Ltd., United Kingdom) equipped with a 10 mW helium-neon laser ($\lambda = 632.8$ nm) and thermoelectric temperature controller.

Transmission electron microscope (TEM) images were obtained on different microscopes, each one operating with an acceleration voltage indicated in kV, carried out in the respective Electron Microscopy Center of UCM, UAB or ICN2. Sample preparation was performed by dispersing in distilled water and subsequent deposition onto carbon-coated copper grids.

- JEOL JEM 2000 FX instrument operated at 200 kV, coupled with energy-dispersive X-ray spectroscopy (EDX) and equipped with a CCD camera (KeenView Camera).
- Tecnai G2 F20 microscope (120 kV or 200 kV)

Scanning electron microscope (SEM) images are taken on one of the following microscopes (Electron Microscopy Center UCM and UAB, ICN2). All samples were placed on holders coated by aluminium foil.

- JEOL 6400-LINK AN10000 microscope
- Zeiss Merlin
- SEM Quanta 650 FEG (+ EDS analysis)
- FEI Magellan 400L XHR - either in SEM or STEM mode; on aluminum coated sample holders or carbon-coated copper grids, respectively.

Powder X-ray diffraction (XRD) was carried out on a PananalyticalXpert Pro MPD diffractometer equipped with a Cu K α radiation source ($\lambda = 1.5406 \text{ \AA}$) at 45 kV and 40 mA. The diffraction peaks were collected between 10° and 100° with a scan speed of 0.01696 degree/s.

Fluorescence intensities were measured with a Biotek Synergy 4 plate reader.

Particles and hybrid structures were observed and photographed with a Zeiss Axiovert inverted fluorescent microscope, alternatively with an EVOS microscope.

DSC/TGA measurements were obtained using a Perkin Elmer Pyris Diamond TG/DTA analyzer.

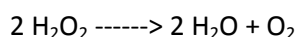
3.6 Detailed description of analytical methods

3.6.1 Enzyme activity catalase^{26, 27}

Unit definition: One unit of catalase will decompose 1.0 μmol of H_2O_2 per minute at pH 7.0 at 25 °C, while the H_2O_2 concentration falls from 11.0 mmol/L to 10.9 mmol/L. The rate of disappearance of H_2O_2 is followed by observing the rate of decrease in the absorbance at 240 nm.

Description

The continuous reduction of spectrophotometric absorbtion (A_{240} , Light path = 1 cm) is based on the following reaction:



Reagents

- (A) 11 mmol/L hydrogen peroxide solution in phosphate buffer (50 mmol/L potassium phosphate buffer, pH 7.4 at 25 °C) – adjust pH with 1 mol/L KOH
- (B) catalase solution – native or elaborated catalase should be dissolved in PB (pH 7.4) at a concentration of approximately 0.01-10 units/ μL .

Procedure

To 1 mL of (A) an aliquote of 10 µL catalase solution (B) is added and after 1 min of mixing the whole solution is transferred to a quartz-cuvette and measured in a spectrophotometer, blank against a cuvette containing phosphate buffer.

A calibration curve in the range of 0 to 11 mmol/L is measured and displayed in figure 3.4.

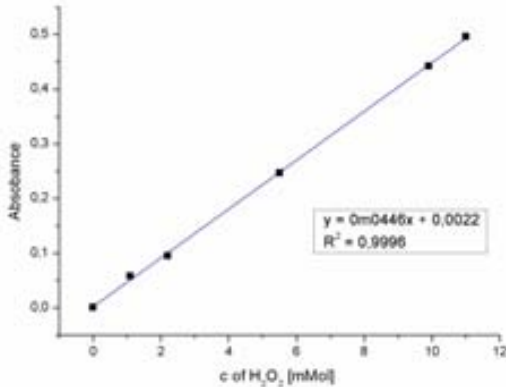
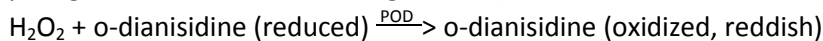
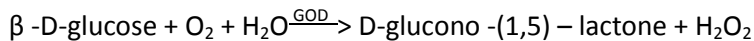


Fig. 3.4 Calibration curve for peroxide concentration

3.6.2 Enzyme activity GOx^{28, 29}

Unit definition: One unit will oxidize 1.0 µmol of β-D-glucose to D-gluconolactone and H₂O₂ per minute at pH 5.1 at 35 °C (equivalent to an O₂ uptake of 22.4 µl per minute). If the reaction mix is saturated with oxygen, the activity may increase by up to 100%.

Description



T=35°C, pH= 5.1, A , light path=1 cm

Reagents

(A) 50 mmol/L sodium acetate buffer, pH 5.1 at 35 °C (buffer)

Prepare 500 mL in MiliQ water saturated with oxygen (saturate the water for five minutes and let it stand overnight before running the assay) using sodium acetate trihydrate. Adjust to pH 5.1 at 35 °C with 1 mol/L HCl.)

(B) 0.21 mmol/L o-dianisidine solution (o-DDH)

Dissolve 20 mg of o-dianisidine dihydrochloride in 8 mL MiliQ water saturated in oxygen using an amber vial or other vial protected from light. Then dilute 5.35 mL to 200 mL with reagent (A)

(C) 10% (w/v) β-D-(+) glucose substrate solution

Prepare 60 mL in purified water using β-D-(+) glucose.

(D) 0.17 mM o-dianisidine and 1.72% (w/v) glucose solution (reaction cocktail)

prepare immediately before use by combining 48 mL of reagent (B) with 10 mL of reagent (C)

Equilibrate to 35°C and adjust to pH 5.1 if necessary with 1 mol/L HCl. Prepare fresh.

(E) Peroxidase enzyme solution

Immediately before use, prepare a solution containing 60 units/mL purpurogallin of POD Type II in cold purified water.

(F) GOx enzyme solution

Prepare immediately prior to use a solution containing 0.4-0.8 units/mL in cold buffer.

Procedure

Pipette the following reagents into suitable cuvettes:

	Test	Blank
Reaction cocktail (A)	2.9	2.9
Peroxidase sol. (E)	0.1	0.1
Glucose oxidase sol. (F)	0.1	-----
Buffer (A)	-----	0.1

Immediately mix and record the increase in $A_{500\text{nm}}$ /min for six minutes. Obtain the maximum linear rate for both the test and the blank solution using a minimum of a 1.0 minute period and a minimum of four $A_{500\text{nm}}$ points.

$$\text{Units/mL enzyme} = \frac{(\Delta A_{500\text{nm}}/\text{minTest} - \Delta A_{500\text{nm}}/\text{min Blank}) * (3.1) * (\text{df})}{(7.5) * (0.1)}$$

3.1=volume (in milliliters) of assay

df=dilution factor

7.5=millimolar extinction coefficient of oxidized o-dianisidine at 500nm

0.1=volume (in mL) of enzyme used

Final assay concentration:

In a 3.10 mL reaction mix, the final concentrations are 48 mmol/L sodium acetate, 0.16 mmol/L o-dianisidine, 1.61% (w/v)glucose, and 6 units peroxidase (concentration of glucose oxidase, might vary depending on used product).

3.6.3 BCA assay^{30, 31}

Description

This method is a simple, sensitive colorimetric assay for proteins based on the fact that proteins reduce alkaline Cu(II) to Cu(I) in a concentration-dependent manner. Bicinchoninic acid forms in alkaline environment a highly specific purple complex with Cu(I) that can be quantified through its absorbance maximum at 562 nm. The absorbance is directly proportional to protein concentration.

Reagents

(A) 1 g BCA, 2 g Na_2CO_3 , 0.15g sodium/potassium tartrate, 0.4 g NaOH, 0.95 g NaHCO_3 are dissolved in 100 mL MiliQ water and the pH is fixed at 11.25 by titration with NaOH.

(B) 0.4 g $\text{CuSO}_4 \cdot 5\text{H}_2\text{O}$ are dissolved in 10 mL MiliQ water.

(C) The stable solutions (A) and (B) are mixed in a v:v ratio 50:1 (A:B)

(D) calibration solutions and samples are prepared in MiliQ water, containing a range of proteins from 0-200 $\mu\text{g/mL}$.

Procedure

500 µl of reagent mixture (C) is prepared and mixed with 500 µl sample or calibration solution. The mixture is incubated during 30 min at 60 °C. After a cooling period of 10 min the spectrophotometric absorbance at 562 nm is measured (A_{562} , Light path = 1 cm). As absorbance depends strongly on temperature and duration of incubation, calibration samples have to be measured in each experiment.

3.6.4 Fmoc assay for amino quantification ³²

Description

The amount of amino groups is determined by protecting the amino groups with highly fluorescent fluorenylmethyloxycarbonyl chloride (FMOC-Cl), followed by intensive washing steps and cleaving the protective group with subsequently measuring the UV/Vis absorption.

Reagents

(A) about 2 mg particles are precisely weighed in an Eppendorf tube, dried under high vacuum overnight and resuspended in 800 µl of dry DMF

(B) solution of Fmoc in DMF

(C) piperidine

Procedure

800 µl of particle suspension (A) is prepared and mixed with 200 µl Fmoc solution (B). The mixture is incubated under sonication during 20 min. After sonication the supernatant is collected by centrifugation at 13000 rpm for 20 min and the spectrophotometric absorbance at 300 nm is measured (A_{300} , Light path = 1 cm). For greater accuracy the UV absorbance should lie between 0.3 and 1.2 absorbance.

3.6.5 Fluorescamine assay for amino determination in proteins ^{33,34}

Description

The heterocyclic dione Fluorescamine reacts with primary amines to form a fluorescent product. The fluorescence of a solution containing protein plus fluorescamine is proportional to the quantity of free amine groups present. Free NH_3 yields a non-fluorescent product. This is the basis of a fluorescent protein assay.

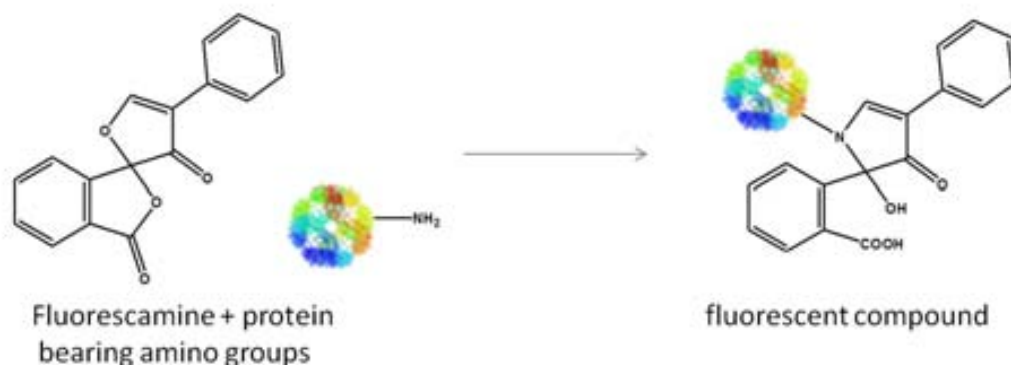


Fig. 3.5 Schematic representation of amine detection in proteins through reaction with fluorescamine

Reagents

(A) prepare a range of protein containing solution of approx 0.05 - 1 mg/mL

(B) Fluorescamine solution in anhydric DMSO 3 mg/mL

Procedure

Pipette 100 μ L of protein solution into a microplate and add 30 μ L of Fluorescamine solution (B). incubate during 60 min at room temperature and measure the emission at wavelength: 465 nm, exciting at wavelength: 360 nm. Calculate calibration.

3.7 Literature

1. Isojima, T.; Lattuada, M.; Vander Sande, J. B.; Hatton, T. A. *ACS Nano* **2008**, 2, (9), 1799-1806.
2. Bele, M.; Siiman, O.; Matijević, E. *J. Colloid Interface Sci.* **2002**, 254, (2), 274-282.
3. Wang, Q.; Liu, Y.; Yan, H. *Chemical Communications* **2007**, (23), 2339-2341.
4. Dong, F.; Guo, W.; Park, S.-S.; Ha, C.-S. *Journal of Materials Chemistry* **2011**, 21, (29), 10744-10749.
5. Nozawa, K.; Gailhanou, H.; Raison, L.; Panizza, P.; Ushiki, H.; Sellier, E.; Delville, J. P.; Delville, M. H. *Langmuir* **2004**, 21, (4), 1516-1523.
6. Stöber, W.; Fink, A. *Journal of Colloid and Interface Science* **1968**, 26, 62-69.
7. Nooney, R. I.; Thirunavukkarasu, D.; Chen, Y.; Josephs, R.; Ostafin, A. E. *Chemistry of Materials* **2002**, 14, (11), 4721-4728.
8. Kiselev, A. V. *Kolloidn. Zhur.* **1936**, 2, 17.
9. Zhuravlev, L. T. *Colloids and Surfaces A: Physicochemical and Engineering Aspects* **2000**, 173, (1-3), 1-38.
10. Jana, N. R.; Gearheart, L.; Murphy, C. J. *Langmuir* **2001**, 17, (22), 6782-6786.
11. Baeza, A.; Guisasola, E.; Ruiz-Hernández, E.; Vallet-Regí, M. *Chemistry of Materials* **2012**, 24, (3), 517-524.
12. Ohmori, M.; Matijević, E. *J. Colloid Interface Sci.* **1992**, 150, (2), 594-598.
13. Ohmori, M.; Matijević, E. *J. Colloid Interface Sci.* **1993**, 160, (2), 288-292.
14. Ngo, A. T.; Pileni, M. P. *Journal of Applied Physics* **2002**, 92, (8), 4649-4652.

15. Rufier, C.; Reufer, M.; Dietsch, H.; Schurtenberger, P. *Langmuir* **2011**, *27*, (11), 6622-6627.
16. Reufer, M.; Dietsch, H.; Gasser, U.; Grobety, B.; Hirt, A. M.; Malik, V. K.; Schurtenberger, P. *Journal of Physics: Condensed Matter* **2011**, *23*, (6), 065102.
17. Reufer, M.; Dietsch, H.; Gasser, U.; Hirt, A.; Menzel, A.; Schurtenberger, P. *The Journal of Physical Chemistry B* **2010**, *114*, (14), 4763-4769.
18. Park, B. J.; Brugarolas, T.; Lee, D. *Soft Matter* **2011**, *7*, (14), 6413-6417.
19. Goldenberg, L. M.; Wagner, J.; Stumpe, J.; Paulke, B.-R.; Görnitz, E. *Langmuir* **2002**, *18*, (14), 5627-5629.
20. Micheletto, R.; Fukuda, H.; Ohtsu, M. *Langmuir* **1995**, *11*, (9), 3333-3336.
21. Baraban, L.; Makarov, D.; Streubel, R.; Mönch, I.; Grimm, D.; Sanchez, S.; Schmidt, O. G. *ACS Nano* **2012**, *6*, (4), 3383-3389.
22. Baraban, L.; Tasinkevych, M.; Popescu, M. N.; Sanchez, S.; Dietrich, S.; Schmidt, O. G. *Soft Matter* **2012**, *8*, (1), 48-52.
23. Mei, Y.; Huang, G.; Solovev, A. A.; Ureña, E. B.; Mönch, I.; Ding, F.; Reindl, T.; Fu, R. K. Y.; Chu, P. K.; Schmidt, O. G. *Advanced Materials* **2008**, *20*, (21), 4085-4090.
24. Solovev, A. A.; Mei, Y.; Bermúdez Ureña, E.; Huang, G.; Schmidt, O. G. *Small* **2009**, *5*, (14), 1688-1692.
25. Tang, Y.; Jiang, Z.; Xing, G.; Li, A.; Kanhere, P. D.; Zhang, Y.; Sum, T. C.; Li, S.; Chen, X.; Dong, Z.; Chen, Z. *Advanced Functional Materials* **2013**, *23*, (23), 2932-2940.
26. Stern, K. G. *Journal of Biological Chemistry* **1937**, *121*, (2), 561-572.
27. Beers, R. F.; Sizer, I. W. *Journal of Biological Chemistry* **1952**, *195*, (1), 133-140.
28. Blaedel, W. J.; Uhl, J. M. *Clinical Chemistry* **1975**, *21*, 119-124.
29. Bergmeyer, H. U.; Gawehn, K.; Grassl, M., *Methods of Enzymatic Analysis* second ed.; Academic Press Inc.: New York, 1974.
30. Smith, P. K.; Krohn, R. I.; Hermanson, G. T.; Mallia, A. K.; Gartner, F. H.; Provenzano, M. D.; Fujimoto, E. K.; Goeke, N. M.; Olson, B. J.; Klenk, D. C. *Analytical Biochemistry* **1985**, *150*, (1), 76-85.
31. Wiechelman, K. J.; Braun, R. D.; Fitzpatrick, J. D. *Analytical Biochemistry* **1988**, *175*, (1), 231-237.
32. Yoon, T.-J.; Yu, K. N.; Kim, E.; Kim, J. S.; Kim, B. G.; Yun, S.-H.; Sohn, B.-H.; Cho, M.-H.; Lee, J.-K.; Park, S. B. *Small* **2006**, *2*, (2), 209-215.
33. Underfriend, S.; S, S.; Bohlen P; W., D. *Science* **1972**, *178*, 871-872.
34. Håkanson, R.; Larsson, L. I.; Sundler, F. *Histochemistry* **1974**, *39*, (1), 15-23.

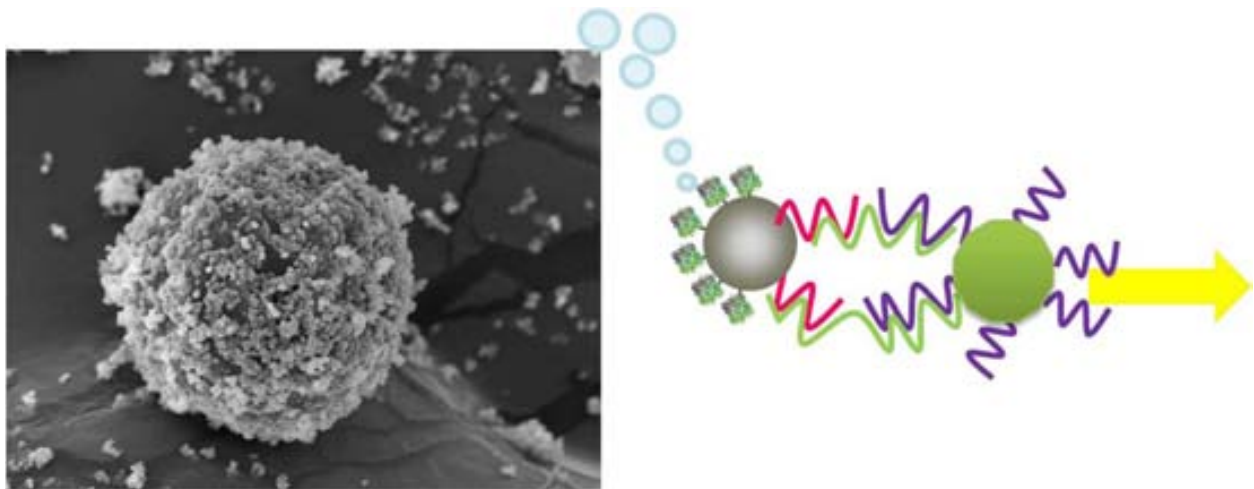
4

Results and Discussion

In this chapter the results are presented and discussed. The work is divided in four main parts, each indicated as a subchapter. In chapter 4.1 the synthesis of silica particles is introduced, as well as its functionalization and grafting of biomolecules to create self-propelled motion. In chapter 4.2 the lifetime of catalase driven micromotors is improved by previously encapsulating the enzyme. In chapter 4.3 the directionality of micromotors is approached and the enzymes are replaced by a more robust catalytic platinum surface. And finally in 4.4 we attempt to replace the peroxide by energy harvested from UV light.

4.1 Silica particles and enzyme - based micromotors

In this chapter the main working material is introduced, namely silica particles, as well as their surface functionalization and more in detail their asymmetric functionalization. Then the principle of the microassembly of a motor particle connected to a signaling particle is presented, which consists of a smaller motor particle with grafted DNA on its surface which binds to a ten micrometer large particle through a DNA sandwich structure. Benefitting from the catalytic reaction on the surface of the motors the signaling particles move, which enables us to use this device for easy motion based DNA detection.



4.1.1 Motion-based DNA sensors

4.1.1.1 Introduction to DNA

Deoxyribose nucleic acid is the macromolecule that is used by almost all forms of life to encode their genetic information. Chemically seen DNA is a kind of organic polymer built up of four different monomers where each monomer is composed of a phosphate group, a single-ring sugar and one of four bases: adenine, thymine, cytosine and guanine. The revelation of its chemical composition started already in 1869 with a Swiss biochemist called Friedrich Miescher, who isolated what today is known as DNA and found that its chemical composition contains carbon, oxygen, hydrogen and nitrogen, but also an important quantity of phosphorus. By 1900 the components were identified as phosphates, a sugar and the four bases, but the actual structure gave reason to many speculations. The final solution was then given by theoretical physicist Francis Crick and biochemist James Watson by suggesting a double helix structure formed by two coupled single-stranded DNAs ¹. Their findings were based on X-ray diffraction data collected by R. Franklin in Kings College London. Those long polymer strands were called polynucleotide and they are built up by bonding the sugars and the phosphate groups. Those single strands bear their bases in the centre of the helix and as all four bases are planar single- or double-ring aromatic compounds they can pair through hydrogen bonds with each other. In figure 4.1.1 can be seen that adenine (A) pairs with thymine (T) through 2 hydrogen bonds, while guanine (G) pairs with cytosine (C) in 3 hydrogen bonds. Therefore high G/C content leads to higher stability in DNA. The whole structure is characterized by the chirality of sugars and the optimization of hydrogen bond angles, leading to the formation of a regular helical structure with 10.4 base pairs per turn and a radius of 3.4

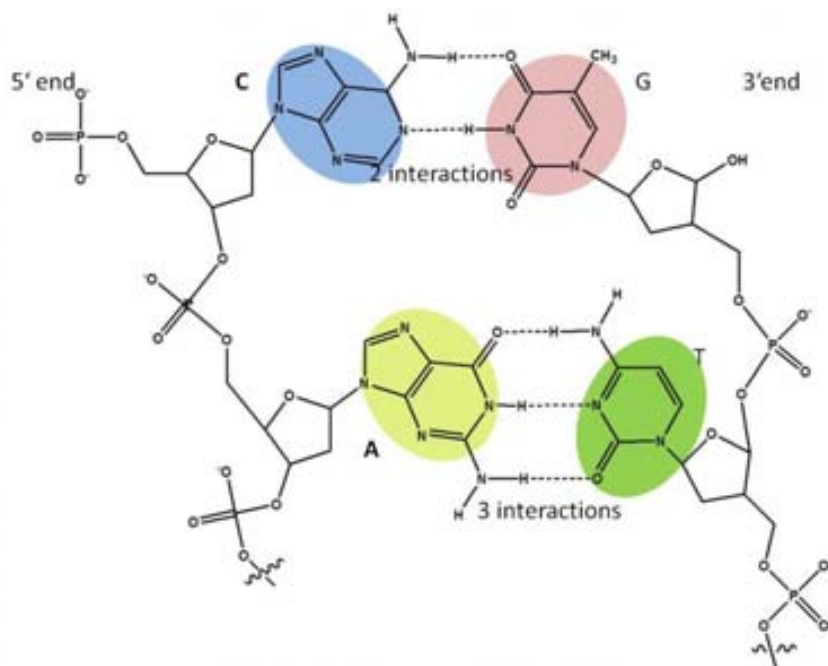


Fig. 4.1.1 Chemical structure of DNA, consisting of a two sugar-phosphate backbone strands, each carrying one of four nucleobases (C=cytosine, G=guanine, A=adenine, T=Thymine), that pair up by formation of base pairs, hydrogen bonds are depicted as dotted lines.

nm¹. This assembly is ideally suited for encoding biological information as one irregular single strand of n monomers can bear $4n$ different combinations of bases, i.e. $22n$ bits of information. Even though double-stranded DNA does not carry more information than single strands almost all organisms rely on double-stranded DNA to encode their genetic information. Nowadays not only biochemists, but material scientists, nanotechnologists and engineers work with DNA due to their unique properties e.g. as molecular valves^{2,3} or material to do tiny origamis⁴.

4.1.1.2 DNA nano detection devices

The detection of this important molecule was for a long time based on a multiplying method for DNA invented by Cetus Corporation in Berkeley, the polymerase chain reaction (PCR). Together with gel electrophoresis PCR formed the base for DNA fingerprinting. In this method after amplification the DNA is separated through gel electrophoresis and subsequently visualized through different methods as silver staining, radiolabelling or fluorescent dyes⁵. Further methods are based on mass spectroscopy, electrochemical approaches or DNA digestion, among others. Nowadays nanotechnology aims to develop methods able to detect and identify DNA without previous isolation and amplification. One of the pioneers in the field is Chad Mirkin from Northwestern University. An early approach of his group is based on the coupling of DNA strands to gold nanoparticles (AuNPs), that selectively aggregate in presence of complementary DNA and induce a color change in the solution⁶. Later the same group presented a follow-up where the target DNA binds in a sandwich assay to another complementary strand bearing a gold nanoparticle. Through catalytic reduction of silver in the sample hybridized assays can be detected scanometrically⁷, a concept that is later developed into a nanostructure-based bio-barcode amplification assay⁸. Further strategies are detailed in a recent review⁹.

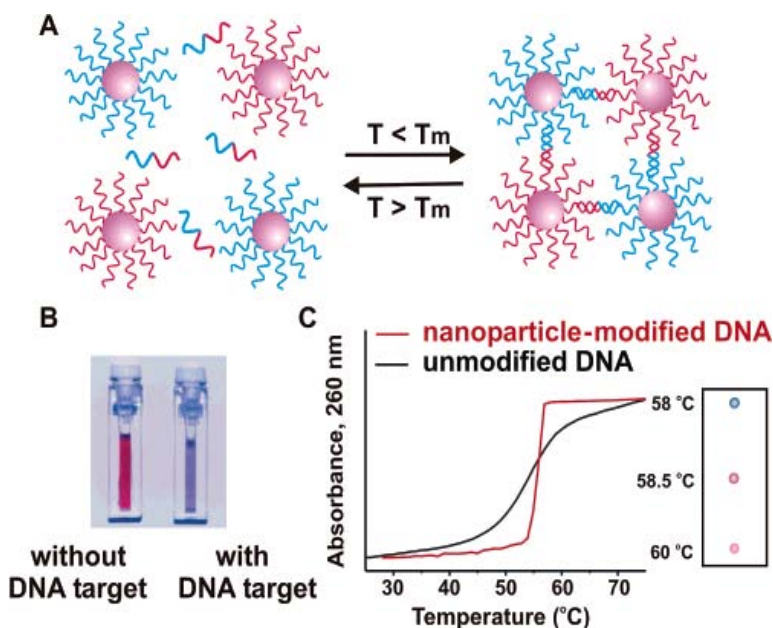


Fig. 4.1.2 DNA assay developed by Mirkin's group: A) in the presence of complementary target DNA, oligonucleotide-functionalized gold nanoparticles aggregate resulting in a color change that is depicted in B) and can be monitored by UV/Vis spectroscopy, image from reference 9.

4.1.1.3 Motion based sensors

Critically evaluating the applications for micromotors in the close future, sensing tasks are among the more feasible near term uses of micromotors, especially because the use of peroxide as fuel does not limit their realization. Several sensor designs including synthetic nano- or micromotors have been proposed, for example the single-molecule detection of DNA via sequence-specific links between F1-ATPase motors and gold nanorod sensors presented by York *et al.*¹⁰. Another early example based on a natural motor is the dust sensor developed by Hess' group. This device is powered by kinesin that transports dust particles to the detection region¹¹. Joseph Wang's group is leading in motion based detection sensors using artificial micromotors. In 2009 this group discovered that the speed of catalytic nanowire motors increases in the presence of silver ions and used this phenomenon for silver detection¹². This principle was further developed to a sandwich DNA hybridization assay. The assay is based on DNA grafted micromotors that couple through the target DNA to a third DNA strand tagged by a silver particle. Dissolution of the Ag nanoparticles increases the concentration of Ag^+ ions, enhancing the performance of the motors. The more the concentration of the target DNA, the more Ag tags can be bound to the motor and therefore the Ag-concentration increases, enabling a quantification of the target down to the attomole level¹³. The same group further improved the method until isolation of single-strand DNA from raw biological samples and implemented it into a lab-on-chip device for both nucleic acid isolation and detection¹⁴. An anti-protein A modified microengine is finally used to demonstrate the selective capture, transport and convenient label-free optical detection of protein A containing bacteria in the presence of a large excess of non-target cells¹⁵. The group around A. Merkoci recently studied the enhancing effects of micromotors for surface based biodetection. They detected a 3.5-fold increase of signal intensity for proteins and envisioned the extension of this novel feature to DNA detection and cell analysing¹⁶.

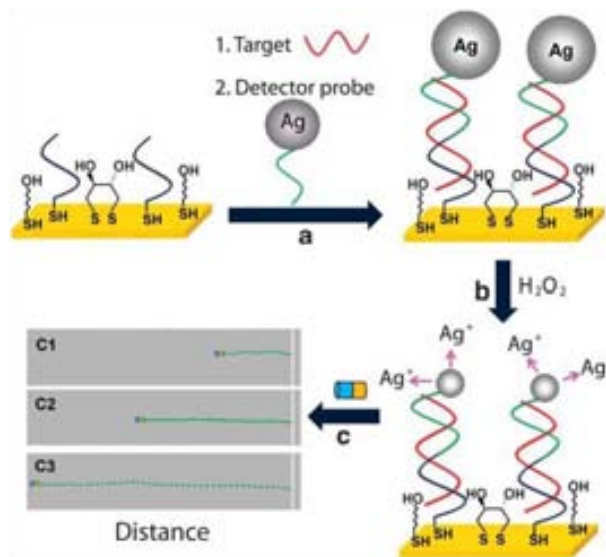


Fig. 4.1.3 a) Target hybridization and capture of the AgNP-tagged detector probe in a typical sandwich assay b) Dissolution of AgNP-tags in the peroxide($\Rightarrow \text{Ag}^+$ -enriched fuel) c) detection of motor speed, C1, C2 and C3 represent hypothetical and increasing target nucleic acid concentrations, image from reference 13.

4.1.1.4 Particle tandem based micromotors for DNA analysis

Our proposal to detect single stranded DNA is likewise a sandwich assay, both the motor silica particles (asymmetrically functionalized with catalase) and the cargo particles are grafted with single stranded DNA (see figure 4.1.4). Both DNA strands are not complementary to each other, but each is complementary to one of the terminal fragments of a larger strand (analyte) that acts as bridge between the particles, in virtue of the high selectivity of the DNA hybridization process. After selective sandwich coupling the big and visible cargo particle is moved by the motor particle, offering an easy detection method by direct visual tracking of the cargo. Without hybridization on both sides of the analyte DNA the motor is not connected to the detection system (cargo) and no easy detectable movement is observable (by optical microscopy) because the bigger cargo particles do not move. This practical approach differs from earlier presented assays (which use either fluorescent tags or other more indirect methods for hybridization detection) as it requires only one single step. This straightforward strategy is very promising for the design of lab on chip devices for pathogen DNA detection or other interesting applications. However first we will introduce silica particles as they form the base of our micromotors. Subsequently the asymmetrization and surface functionalization will be described and then we move on to the proof-of-concept DNA detection device.

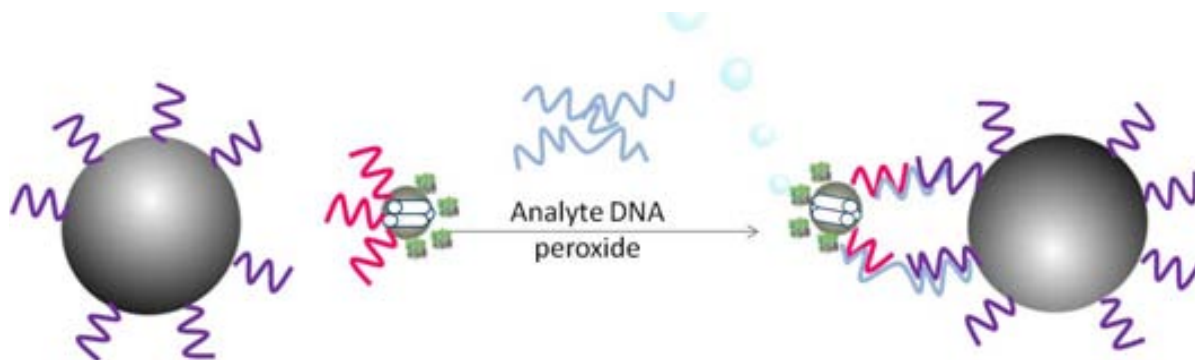


Fig. 4.1.4 Concept of our motion based DNA assay: the assay consists of a cargo and a motor particle, both grafted with non complementary DNA and the motor particle additionally bears catalase to achieve motion in hydrogen peroxide. In presence of an analyte DNA a both DNA types hybridize to the analyte DNA forming a sandwich assay and enable the movement of the cargo particle.

4.1.2 Synthesis of silica particles

As mentioned in chapter 1 there are innumerable synthetic methods for silica particles described in literature. To dispose of a stock of possibly useful particles several synthesis conditions were tried. Different families of silica particles were achieved depending on the experimental conditions. Following the method given by Lattuada *et al.*¹⁷ uniform particles with a size average around 400 nm were obtained through condensation of TEOS in an ammoniacal - isopropanoic - aqueous solution (see figure 4.1.5 a-b). Larger particles with an average size around 1 μm were produced in a seed-based approach in ammoniacal isopropanol solution without water addition (shown in figure 4.1.5 g-h)¹⁸. Hollow particles were synthesized using a pH mediated emulsion-polymerization strategy (see figure 4.1.5 c-d). Instead of hydrophilic TEOS the more organophilic phenyltrimethoxysilane (PTMS) was used as a precursor in

this case, leading to an emulsion in acidic water¹⁹. The diameter of the shell could be manipulated by changing reaction times. In accordance with theory and literature it was found that the use of surfactant leads to porous particles and further addition of a swelling agent increased the pore size^{20, 21}, until making particles more fragile. As can be seen in figure 4.1.5 e-f those particles suffer from rupture and irregularities. As large pores are not crucial to build micromotors the final synthesis was carried out without swelling agent (see experimental section 3.3). Size tuning was possible by modifying the reaction temperature, the ratio solvent/silane/surfactant and the molecular size of the initial product (TPOS instead of TEOS)²². The control of the addition rate proved to be a very useful tool to obtain particles with a narrow size range²³. The base type was found responsible for the particle shape, wherein ammonia favors a near spherical shape. To obtain surfactant free pores several methods as calcinations, extraction with a NaNO₃ solution and an acid extraction in MeOH were tested and last one turned out to be the best combination of efficacy and sensibility.

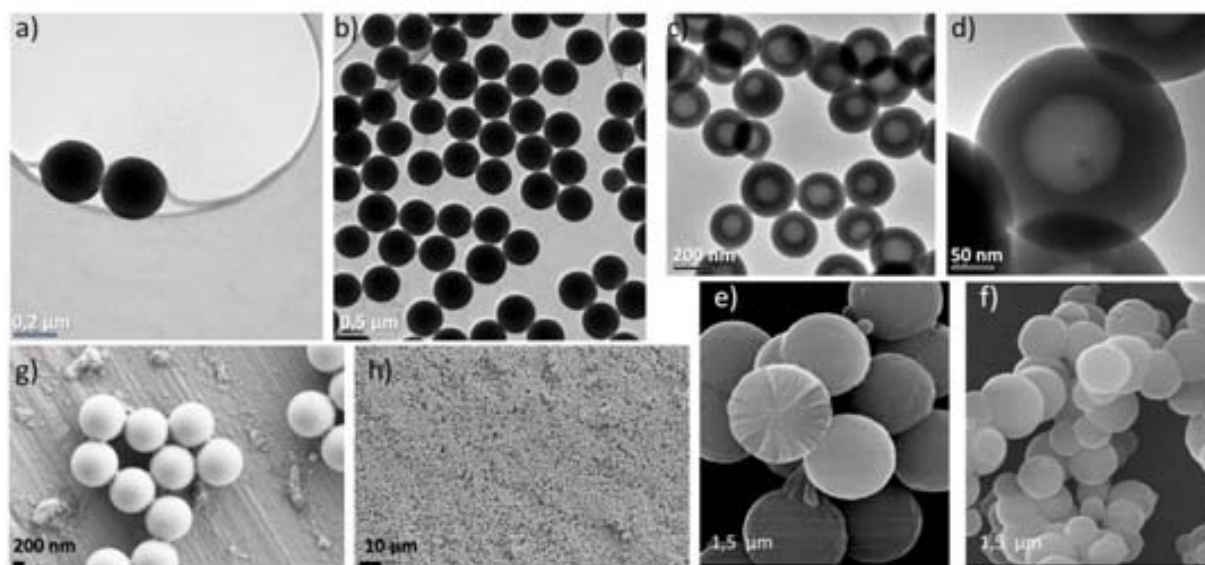


Fig. 4.1.5 a-b) TEM image of silica particles obtained following the approach of Lattuada *et al.* c-d) TEM image showing hollow particles obtained after Wang *et al.* e-f) SEM image of mesoporous particles from a modified Stoeber process; g-h) SEM image showing the result of a two step procedure published by Bele *et al.*

4.1.3 Asymmetrization and surface functionalization

The next step was the asymmetric functionalization of the silica particles. Several methods to achieve this have been presented in the literature, as electrochemical functionalization²⁴, use of elastomeric stamps²⁵ or metal sputtering²⁶. Here an optimized version based on the formation of Pickering solutions was chosen. This method had been previously described and was chosen for its simplicity, scalability and its excellent results^{27, 28}. Briefly, the particles were added to a wax-in-water solution forming a stable Pickering emulsion. When the temperature is decreased below the melting temperature of the wax (53-57 °C), the paraffin solidifies leading to the immobilization of the porous silica particles at the surface of the wax droplets (figure 4.1.6 b). Homogeneous solid 1 μm particles were not adequate for asymmetric functionalization (see figure 4.1.6 c and e) because their higher

density did not favor the accumulation at the interface of Pickering solutions. As asymmetrization was considered important for catalytic micromotors the mesoporous particles were chosen as starting material for the motors. This was a compromise between bigger particles to improve visibility in optical microscopy, uniformity of particle shape and maximum surface for following asymmetric functionalization. The average particle size was tuned to approximately 700 nm and confirmed by SEM microscopy. The removal of the surfactant was performed by acidic extraction in methanol.

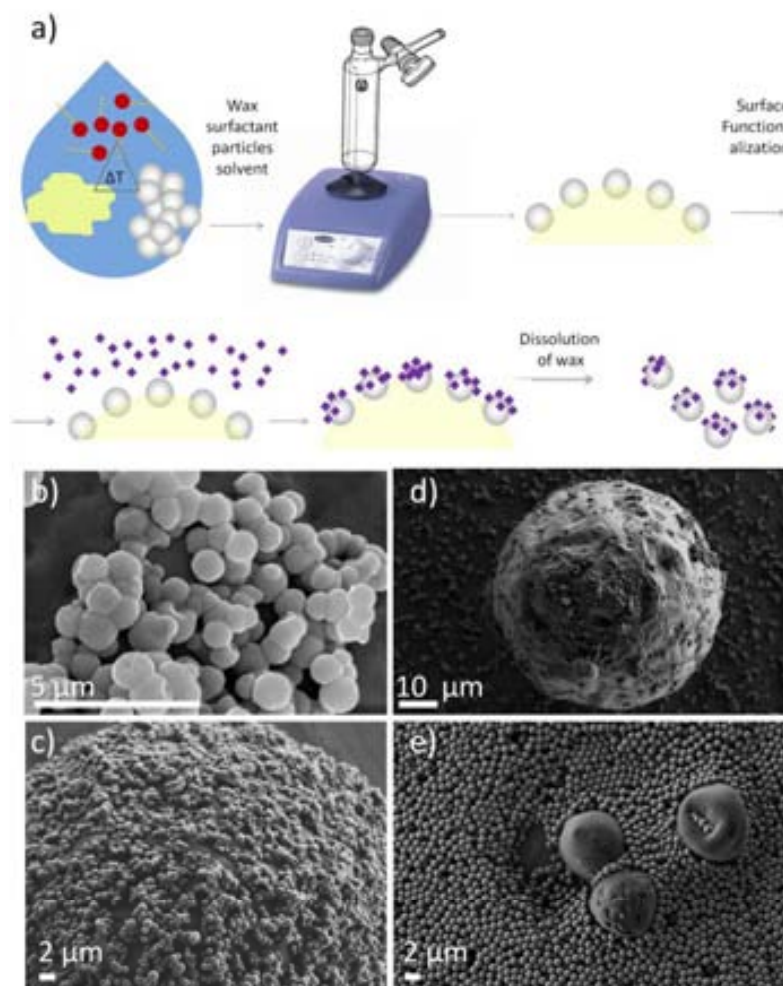


Fig. 4.1.6 a) Schematic representation of the methodology followed for asymmetric functionalization b) SEM picture of porous silica particles embedded in paraffin c) magnification of a paraffin ball with attached porous silica particles d) solid silica particles presenting a low coverage of paraffin ball e) solid particles that do not assemble on the wax.

In case of the mesoporous particles the surface that emerges towards the aqueous phase was functionalized in an aqueous solution, here 3-aminopropyltriethoxysilane (APTES) was used (as described in detail in chapter 3). Thus, after paraffin dissolution in heptane, asymmetrically functionalized particles have been obtained. The quality of the asymmetrization can be controlled by exposing these particles to a solution of gold nanoparticles (AuNP). Due to affinity differences, the

AuNPs cover specifically the modified parts, e.g. amino or thiol groups feature a tendency to form bonding with gold. Treated particles analyzed by TEM microscopy clearly show that AuNPs hardly deposit on non-modified silica particles (see figure 4.1.7 a), but a selective covering occurs on the functionalized nanoparticles as shown in figure 4.1.7 b-e.

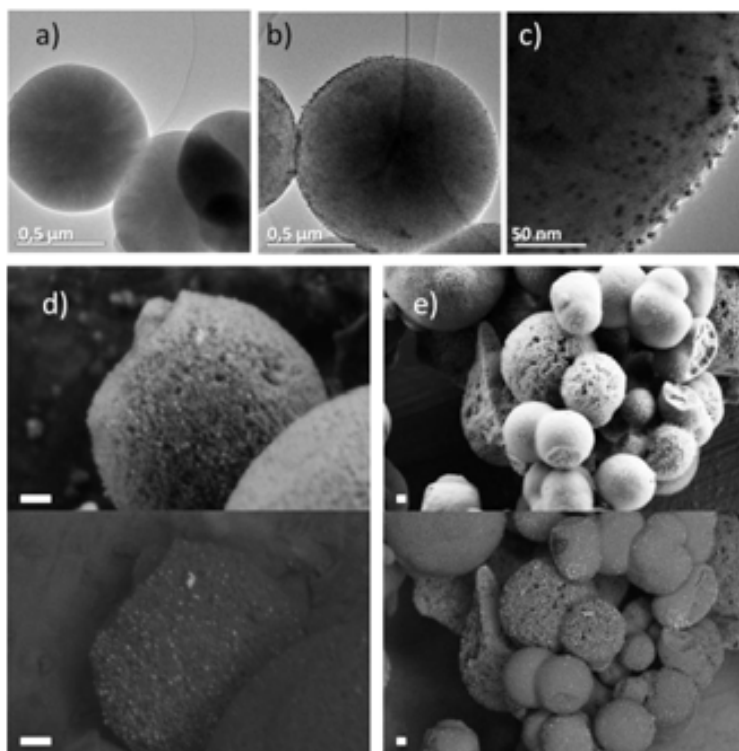


Fig. 4.1.7 a) TEM image non-functionalized mesoporous particles b) TEM image of an asymmetrically functionalized particle with AuNPs on one hemisphere c) TEM image showing a magnification of surface with AuNP d-e) SEM images of AuNP - decorated silica, image mode up: secondary electrons, down: energy selective backscattered electrons, the scale bar corresponds to 100 nm.

In average silica surfaces present 4.9 silanol groups per nm^2 which enables chemists to modify their surface chemistry^{29, 30}. Widely employed for that use are for example silanes that can condense on the particle surfaces and a variety of functional groups can be grafted using commercially available molecules. If the desired moiety is not accessible, easily obtained functionalities as amino groups can be introduced and chemically transformed in the chosen functionality. Using Janus particles selective functionalization can be performed, so that the asymmetric properties of particles can be maintained.

Amino group functionalization - The silane reagent APTES reacts readily with the silica surface in ethanolic solution. After reaction the amino content of the particles was determined by UV/Vis absorption resulting in a value of $0.134 \mu\text{mol/g}$ for half-sphere aminated particles (figure 4.1.8 a). This procedure was carried out employing fluorenylmethyloxycarbonyl chloride (FMOC-Cl) assay for amino quantification described in detail in the experimental section 3.6.4³¹.

Carboxyl group functionalization - Even though a silane reagent bearing COOH-moieties (carboxyethylsilanetriol sodium salt) is commercially available all attempts to attach carboxylic groups on the particles through direct reaction in one step only led to a very small percentage of carboxylated particles. This low yield was probably due to the low affinity of the charged sodium salt to the negative surface of silica particles. Therefore carboxyl groups were obtained following a two-step strategy: the primarily introduced aminogroups were reacted with succinic anhydride in dry tetrahydrofuran. An alternative method was based on the use of a silane bearing an ethyl chain and a succinic anhydride moiety that can be grafted on the surface that through further hydration provides a terminal acid group.

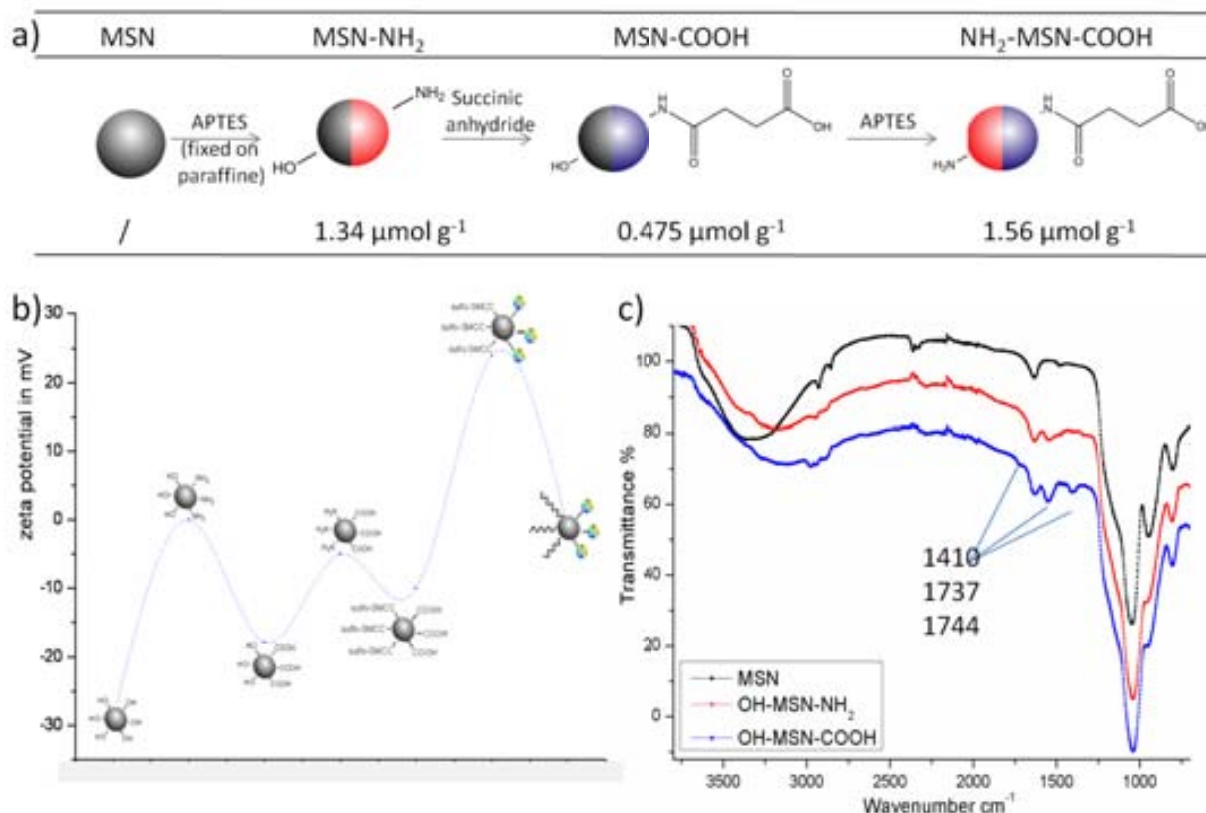


Fig. 4.1.8 a) Scheme of asymmetric functionalization and amino content of asymmetrically functionalized mesoporous nanoparticles (MSN) b) Zetapotential changes experienced by the silica particles along the asymmetric surface functionalization process c) changes on the surface during the process monitored by FTIR.

Synthesis of amino-carboxylic acid functionalized silica - Finally the particles were treated with APTES in order to introduce amino groups on the free hemisphere (see scheme within figure 4.1.8 a). The success of the modification is reflected in stepwise changes of the amino content (see table in figure 4.1.8 a). The overall process was monitored by FTIR and Zetapotential measurements. FTIR spectra show the typical NH₂-scissoring band at 1537 cm⁻¹ after the first reaction with APTES, whereas after the reaction with succinic anhydride, the peaks corresponding to C=O and C-O (acid) stretching vibrations at 1744 cm⁻¹ and 1410 cm⁻¹ respectively, are clearly visible (Figure 4.1.8 b). Zetapotential measurements of the suspended particles in phosphate buffer solution (pH 7.2) confirm the success of the functionalization process (Figure 4.1.8 a). The introduction of amino groups on the particle surface led to a clearly

observable increase in the positive charge. The second modification led to the opposite effect because the amino groups were transformed into negatively charged carboxylic entities. Finally, the attachment of more amino groups on the other face introduces positively charged moieties, neutralizing the surface potential.

4.1.4 Enzyme attachment

The anchoring of enzymes on the particle surface was performed through a covalent immobilization strategy linking the carboxylic acids of the particles to free amine groups in catalase. Considering that the particles bear both, amino as well as carboxylic groups on their surface cross reactions between particles might lead to aggregation. Therefore amino moieties have to be blocked before activating the carboxylic groups. Instead of introducing additional steps by using protective groups, particles were treated with the crosslinker sulfo-succinimidyl 4-*N*-maleimidomethyl cyclohexane-1-carboxylate (Sulfo-SMCC) in PB (pH 7.2), which selectively reacts with their aminated half-spheres. This linker bears a maleimide group on the unreacted end which will be used to bind DNA single strands in further steps. Once the amino groups have been blocked with Sulfo-SMCC, the carboxylic groups were activated through the water-soluble cross-linker *N*-(3-Dimethylaminopropyl)-*N*'-ethylcarbodiimide hydrochloride (EDC-HCl) and *N*-hydroxysuccinimid (NHS) and subsequent addition of catalase led to amide bond formation with free amine groups (see figure 4.1.9). After the activation a solution of catalase in phosphate buffer was added to the suspension and the mixture was stirred overnight. Subsequently, several vigorous washing steps guarantee that no significant amount of enzyme remains physically retained on the surface. The success of the enzyme grafting reaction was determined by suspending the particles in a diluted hydrogen peroxide solution and measuring the decrease of the UV absorption at 240 nm³². The amount of enzyme covalently bound was estimated at 0.98 mg protein/g particles, which corresponds to an anchorage yield of 2%.

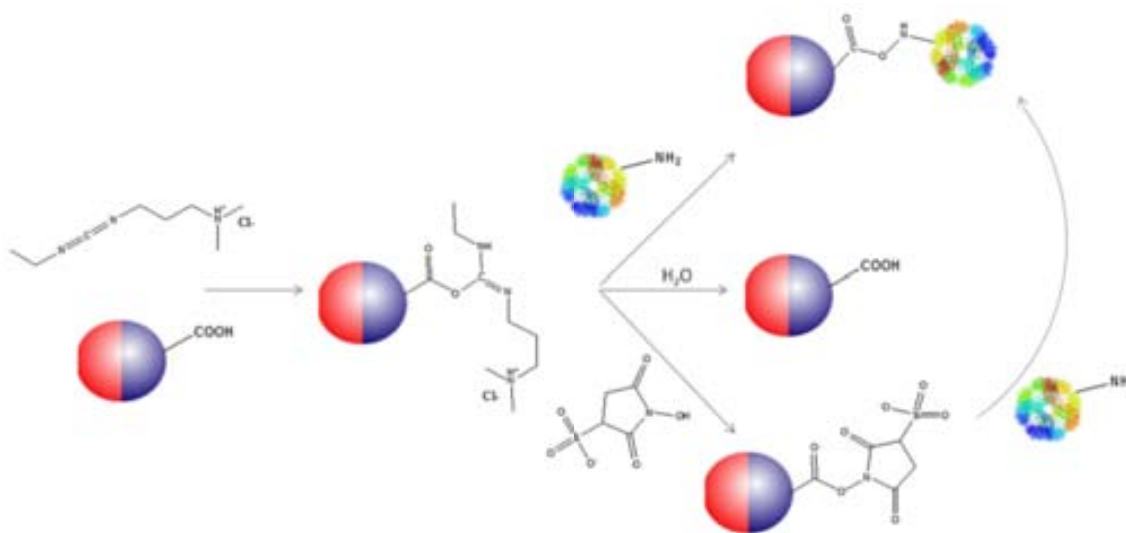


Fig. 4.1.9 Scheme of covalent enzyme attachment on carboxyl bearing silica particles and using carbodiimide chemistry and amino groups present on the enzyme surface.

4.1.5 DNA micromotor

4.1.5.1 DNA grafting

As mentioned above, Sulfo-SMCC has been used as protecting agent of the amino groups present on one side of the mesoporous particle (to avoid cross reaction due to the presence of free amino groups) during the coupling with EDC/NHS. In this step the presence of this group allows the direct immobilization of the 3'-thiol-modified oligonucleotide sequence 5'TTGAATCAGCGATAATHiC3 using a previously reported method (for the chemical details see experimental section 3.4.1)³. The total amount of grafted DNA was 50-57%, which was indirectly calculated by UV-Vis spectroscopy measurements of free DNA remaining in the reaction media.

4.1.5.2 DNA recognition and motion

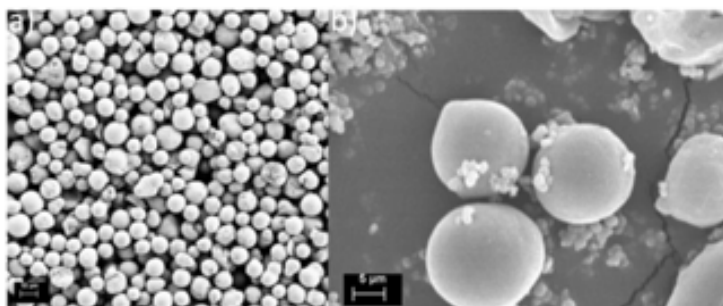


Fig. 4.1.10 a) commercial 10 µm silica particles used as cargo and b) motor - cargo assembly

The ability of enzyme grafted microparticles to perform ballistic motion and its capability to transport cargo was evaluated through the following experiment. In order to demonstrate the capacity of the motor particles to move themselves and also transport a charge larger load, commercially available silica particles of approx. 10 µm (figure 4.1.10) were chosen as cargo system. They confer the additional advantage of clear visibility in optical microscopy to the whole assembly. The functionalization procedure was similar to the one used with the mesoporous particles, in order to introduce the amino functionality we treated a suspension of these particles with APTES. After the reaction with the cross-linker sulfo-SMCC, a specially designed oligonucleotide sequence 5'-ThiC6TTCAAGCCGACTAAG, with a 5'-thiol-end and in 3'-end, was grafted onto the surface. The grafting of DNA in this case was similar to the one mentioned above (40-50 %).



Fig. 4.1.11 Hybridization of the DNA sandwich assay, the blue analytical DNA binds selectively in a sandwich assay, connecting the DNA strands attached to both types of particles. Without complete hybridization no movement of the signal particles can be observed.

In order to assess the capacity of the motor particles to recognize, capture and transport the cargo, only in the presence of a specific oligonucleotide sequence, a mixture of motor and cargo particles was incubated in a Tris-HCl buffered solution, with and without a commercial specific single strand DNA sequence 5'-TTATCGCTGATTCAACTTAGTCGGCTTGAA-3' (analyte).

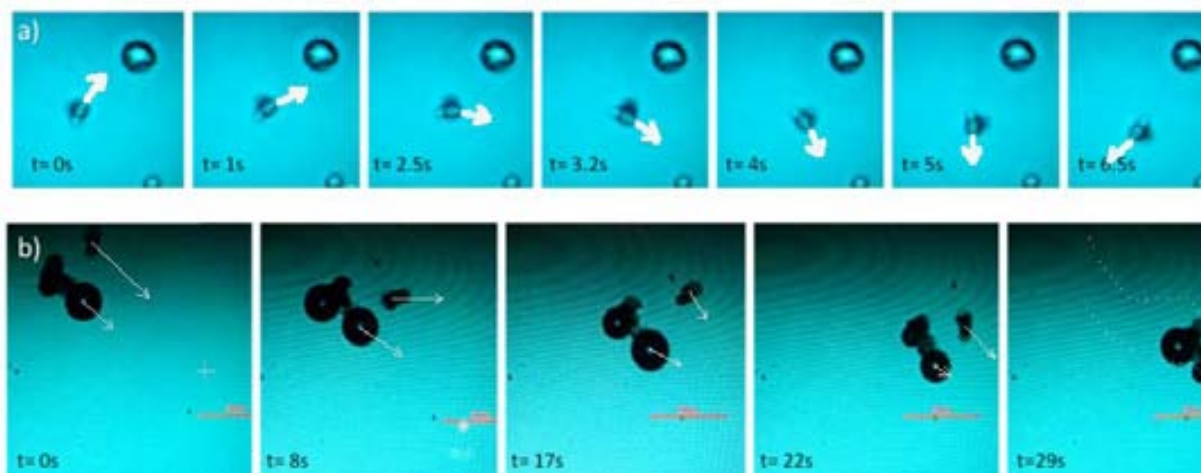


Fig. 4.1.12 Chemically powered self-assembly device: time-lapse images for the movement in 5% hydrogen peroxide solution. a) Movement of one cargo-particle covered by motor nanoparticles and b) assembly of several cargo particles.

This sequence has been designed in order to be complementary to both of the DNA strands attached to the motor and cargo particles, acting as a bridge between them. This special sandwich assay enables us to use the motor assembly for analytical purposes. As can be seen in figure 4.1.11 only when the analyte is present the motor particle can capture and transport the signal particle. Therefore the motion of the signaling particles can be used as a means to qualitatively determine the presence of analyte DNA (blue in figure 4.1.11). Experimentally the two kinds of particles and the DNA were mixed and after an appropriate incubation time for the recognition and hybridization process (ca. 30 min) a drop of this suspension was placed on a microscope glass slide containing a thin film of 5% H_2O_2 in a glycerol/water (1:1) mixture. Glycerol was employed to increase the viscosity of the media reducing the speed of the assembly in order to record the motion properly. A blank experiment was performed in absence of DNA and no movement of the signal particles was observed. The presence of a miss-matched DNA did not lead to motion either. Only after addition of the analyte sequence we could identify motion of the cargo particles. Formation of oxygen bubbles is clearly visible providing the driving force that moves the motor particles. After addition of analyte DNA the direction of the movement was defined by oxygen generation at the trailing end of the particles which is in accordance with the previously reported systems of Whitesides³³ and Feringa³⁴. In our system, the non-symmetric nature of the assembly can determine the directionality of the motion. Figure 4.1.12 a) shows one kidney shaped assembly that is executing a circular translation motion, probably due to bubble formation taking place only in one point and in figure 4.1.12 b) random movements of two particles relative to each other can be seen. This kind of motion is dominating in the here presented system, and is caused by particles or their aggregates which expulse oxygen bubbles from more than one zone on their surface. As mentioned above, motor

and cargo particles were also mixed and treated in the same conditions and at equal times without presence of the DNA analyte. As expected, smaller motor particles catalyze the decomposition of H_2O_2 and oxygen bubble formation is clearly visible, but no motion of the big particles was observed. Figure 4.1.10 b) shows a SEM picture of small motors attached on the surface of the bigger cargo particles. This procedure can be employed to detect, capture and isolate DNA fragments present in biological samples.

4.1.5.3 FRET -experiments

In order to provide a free-of-doubt proof that the motion of the cargo particles is due to a selectively-induced analyte self-assembly process, instead of simple physisorption of motor particles on the cargo surface, combined fluorescence energy transfer experiments (FRET) were performed. This term describes a phenomenon in a sample that contains a pair of fluorescent dyes, in presence of light of the exciting wavelength of the donor molecule. The acceptor molecule is not excited by the light itself, but can be excited by internal conversion of energy from an excited fluorescent donor molecule if both are spatially close. In the 1940s Foerster observed this process for the first time and modelled it correctly^{35, 36}. Without the energy transfer the acceptor would not be excited by the given wavelength and only through long range dipole Coulomb interactions between excited donor and acceptor the transfer can occur. Even though the process is based on transition densities a model considering both as dipoles describes the experiment very well

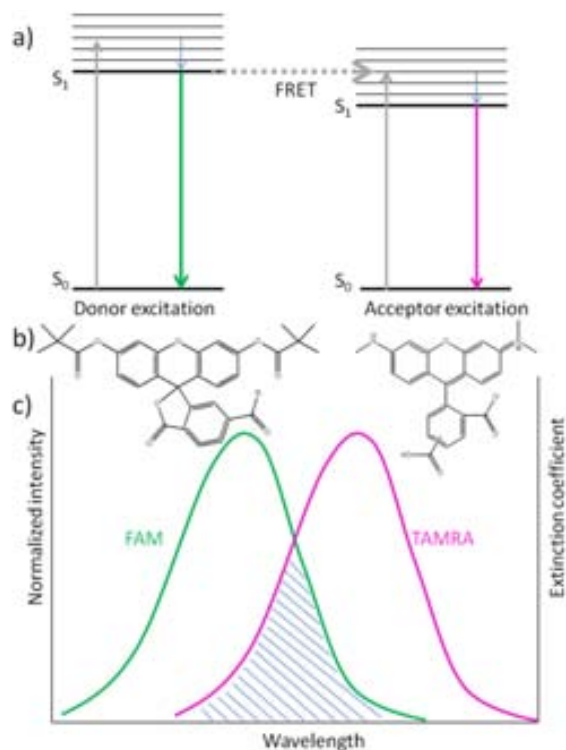


Fig. 4.1.13 a) Fluorescence Resonance Energy Transfer principle (FRET) results from the transfer of energy from an excited state of the donor molecule to the acceptor molecule, b) molecules of FAM and TAMRA, c) schematic of donor and acceptor spectra.

$$k_{FRET} = \left(\frac{R_0}{r}\right)^6 * \frac{1}{\tau_{D,0}} \quad (4.1)$$

with R_0 the Förster radius, r the distance between the fluorophores, $\tau_{D,0}$ the lifetime of the donor. This equation shows the strong dependence of energy transfer rate on the distance between the donors, hence FRET experiments can be performed in order to access a "molecular ruler". R_0 is a characteristic distance for each donor-acceptor pair. One characteristic pair typically used to signal oligonucleotides are FAM (Fluorescein amidite) and TAMRA (5(6)-carboxytetramethylrhodamine succinimidyl ester) as displayed in figure 4.1.13. Therefore instead of normal DNA strands fluorescently tagged strands are used, both fluorophores form a FRET pair and in close spatial proximity the energy transfer occurs and detection of the FRET acceptor signal proves the low distance between them. The motor particle carries a DNA strand tagged with group 6-FAM, incorporated at the 5'-end, while the cargo particles bear DNA strands tagged with a TAMRA dye on the 3' of the DNA strand. As mentioned this allows further characterization of the hybridization state by fluorescence resonance energy transfer.

Similar weights of particles containing FAM-tagged strand (motor) and particles containing TAMRA-tagged strand (cargo) were added to two batches of 250 μL of the same Tris-HCl buffer solution employed for the motion experiments. 50 μL of DNA analyte solution (ca. 30 equivalents) were added to one of the batches whereas the second one was treated with the same amount of buffer, this time without specific analyte. After shaking for 30 min, the emission fluorescence was measured in the 500-700 nm range upon excitation of FAM at 480 nm. The obtained spectrum in the absence of analyte reveals the lack of any energy transfer to the TAMRA, with most of the emitted energy coming from the same FAM at 516-520 nm (figure 4.1.13). Only a slight increase of emission at 580 nm compared to the pure FAM signal can be observed, most likely caused by a residual excitation of the TAMRA at the working wavelengths and/or to a small extent of FRET by to Brownian motion or non-specific Van-der-Vaals absorption of motor particles on the bigger cargo particles. The signal increase obtained upon

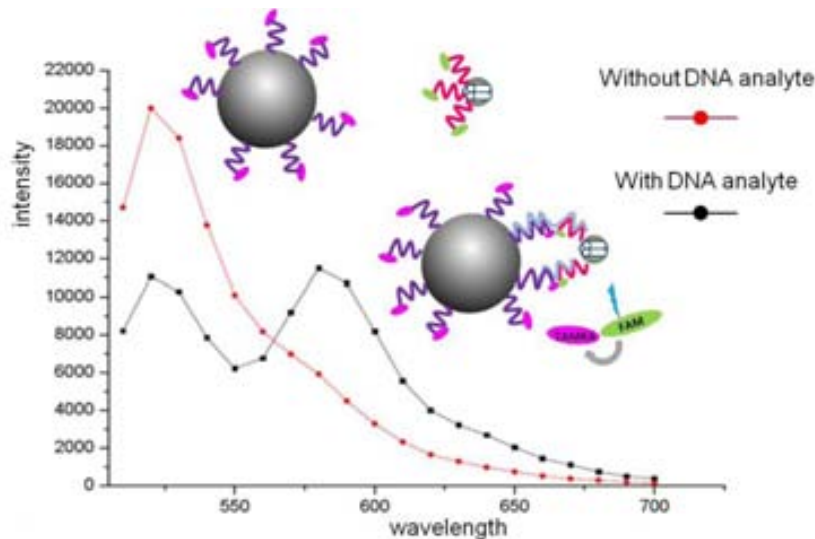


Fig. 4.1.14 FRET measurement: Visible spectra of the cargo - motor mixture with (black line) and without (red line) analyte show that in absence of analyte DNA only the motor particles are excited, after hybridization an energy transfer can occur, exciting the dyes bound to the cargo particles as well.

analyte addition is about one order of magnitude larger, caused by the hybridization process with the complementary DNA strand due to which both fluorophores get spatially closer and energy transfer gets enabled. Thus, an emission at 580 nm characteristic of TAMRA has been observed (figure 4.1.13), owing the energy transfer occurring between the two dyes in close contact ($R_0 = 5$ nm).

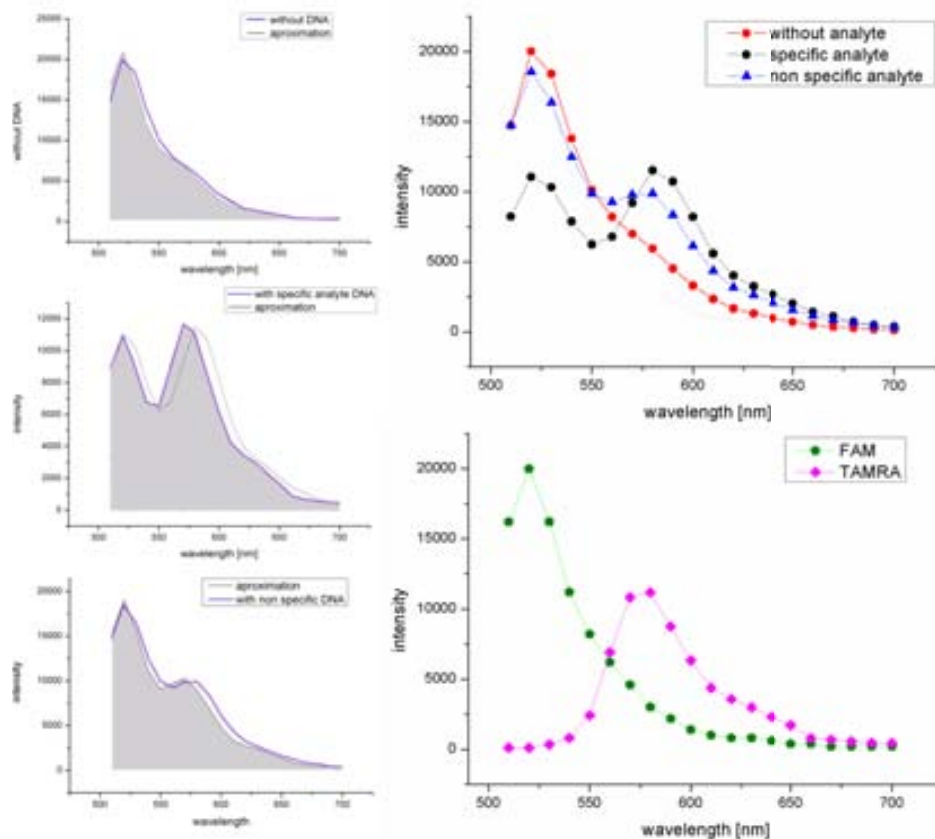


Fig. 4.1.15 Fluorescence spectra of motor and cargo particle tagged with the fluorophores FAM and TAMRA, in absence and presence of analyte DNA, as well as a non-specific DNA strand are depicted, down the individual spectra of FAM and TAMRA and on the left the areas are determined to calculate E_{FRET} and the percentages of energy transfer.

Finally, as mentioned above, a mismatched DNA single strand 5'-AACGTTATCATCATTTCGCCCTATACCTT-3' has been used in order to assess the selectivity of this process. In addition to the absence of motion of the cargo particles, the lack of a significant FRET effect as that previously described for the specific analyte (figure 4.1.15) confirms the selectivity of this strategy for specific DNA detection. Though an increase of the emission at 580 nm is observed, most likely due to the higher intensities of non specific interactions such as hydrogen bonds between the DNA strands of the cargo and motor particles (the FRET-radius of 5 nm allows energy transfer even at close proximity of the dyes without complete hybridization), it is still considerably smaller than when a specific analyte is used. While the non specific interactions lead to a value of 0.281, hybridization resulted in the 3.2-fold of this value 0.919 (table 4.1.1). This result proves that FRET-experiments can easily differentiate between specific hybridization and non specific interactions.

Table 4.1.1 intensity of fluorescence signals of FAM and TAMRA relatively for the cases without analyte, with analyte DNA and with non-specific DNA

	Without analyte	Analyte DNA	Non-specific DNA
Intensity of TAMRA I_{TAMRA} unity	134090	400130	303559
Intensity without Brownian part I_{TAMRA} unity	/	266040	169469
Intensity of FAM I_{FAM} unity	665438	357628	620420
$E(FRET) = I_{TAMRA}/I_{FAM}$	/	0.7439	0.2731
Percentage %	/	74.4	27.3

It is important to note that these particles could be stored in the fridge for several days or even weeks, without significant loss of activity, showing that the used enzyme (catalase) and the attached oligonucleotide strands are robust systems and substitution by other alternatives is not necessary.

4.1.6 Directionality of the movement

It was shown that micromotors are able to capture DNA strands and detect them through motion of signaling particles. To improve this system and bring it into stages that range further than proof of concept the motion needs to be controllable. Motion with defined directionality is required for efficient sensing, therefore the next aim should be a deterministic guidance of the micromotors. Among the different external stimuli used in literature to achieve directed movement, light represents an elegant and functional approach. Weibel *et al.* guided the movement of photosynthetic algae through visible light³⁷. Phototactic directionality turns out very difficult to be reproduced on synthetic micromotors and only very recently Huang *et al.* published the control by UV light of molecular imprinted Janus particles bearing silver nanoparticles on one hemisphere. The presence of UV light enhanced the speed and shifted the movement from random to ballistic³⁸. An alternative is temperature; Wang's team has shown a temperature dependent modulation of motor speed though at this stage they did not achieve directional control³⁹.

More successful is the chemotaxis approach where micromotors are directed by chemical concentration gradients. So far, most motors are not able to sense any gradients apart from fuel, so only movement towards high fuel areas has been shown yet by "powered diffusion"^{40,41}. One single example was found in literature where polymer beads containing palladium nanoparticles moved towards a higher NaOH concentration⁴².

However precise gradient generation is complicated and the propelling mechanism should rather be independent from the method of directing motion. An approach that has been used widely in nanorods, and nanotubes is the application of homogeneous magnetic fields. One advantage lies in the fact that no gradient has to be created, but a homogeneous field can already orient particles and therefore direct their movement. The viability of this approach has been proven for nanorods, tubes and helical structures⁴³⁻⁴⁶. Therefore magnetism was chosen as means to achieve directional motion, bringing up

the requirement to use materials with magnetic properties that allow interactions with applied magnetic fields.

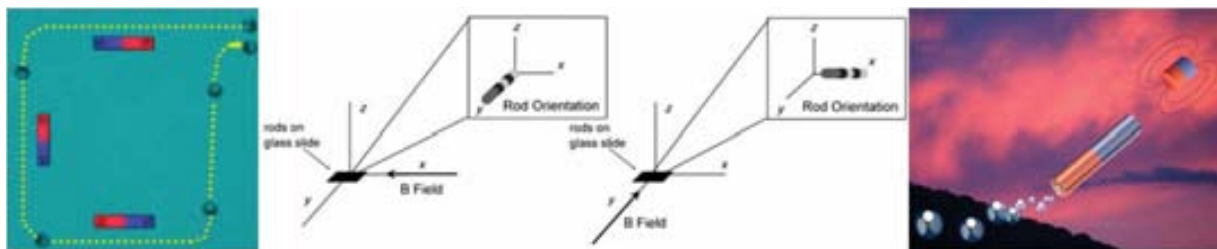


Fig. 4.1.16 Examples from several groups that published previously the use of magnetic motor properties fields for guidance of particles, rods and microtubes. respectively from Baraban 2012 (ref #29), Kline 2005 and Zhao 2012

4.1.6.1 Attempts to introduce directionality using magnetic fields

Simple encapsulation of iron oxide nanoparticles would probably lead to isotropic distribution of the iron oxide nanoparticles inside the silica. This approach would confer magnetic properties to the particles and a strong heterogeneous magnetic field would be able to attract them but a simple directing of peroxide degrading particles uncoupled from propulsion cannot be achieved with this approach. Therefore this strategy was abandoned as no defined orientation of particles can be expected. To avoid this limitation, the obvious and direct choice was to use intrinsically anisotropic rice-shaped iron oxide particles⁴⁷⁻⁵⁶. Many nanostructures magnetize along one of their most extended directions, i.e. in rice particles the c-axis. When an external field is applied opposing the direction of particle magnetization there are two possibilities to minimize energy: change either the magnetization or the orientation of the rice particle. As anisotropy forces which hold the magnetization in an "easy" direction are stronger than in isotropic nanoparticles to change magnetization it must rotate through the disadvantageous direction to reach the new "easy" direction⁵⁷. Thus the coercivity is large and particle turning to adapt to the magnetic field seemed to be favored (see figure 4.1.17 e,f). Hematite needles with a size of about 400 nm length and 120 nm diameter were obtained using a forced hydrolysis of iron(III) chloride in the presence of $\text{HNa}_2\text{PO}_4 \cdot \text{H}_2\text{O}$ as described previously by Ohmori *et al.*^{49, 58}. Afterwards, carefully dried particles were annealed under argon and hydrogen and subsequently oxidized at low temperature and air flux (see experimental section for more details) to obtain the maghemite phase. To ensure complete oxidation particles were redispersed in hot nitric acid solution⁵⁹. Maghemite is a thermodynamically stable phase of magnetic iron oxide and even though magnetite presents magnetic properties as well this more stable phase was chosen as base for the directionality approach.

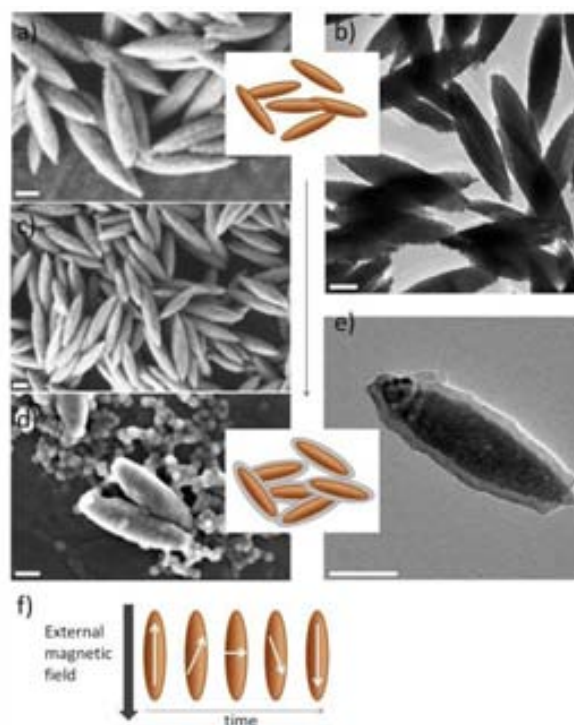


Fig. 4.1.17 a-c) SEM and TEM images of rice particles as synthesized and d, e) silica covered rice particle (SEM/TEM image). The central inset schematically shows the uncovered vs. covered Fe_2O_3 rice particles. f) Scheme of magnetization rotation in single domain rice particles, the scale bar corresponds to 100 nm.

To obtain silica coated rice particles the colloidal solution was stabilized by polyvinylpyrrolidone and subsequently covered by a layer of approximately 20-25 nm silica (see figure 4.1.17 e). This coverage is of particular interest for enhanced colloidal stability at neutral pH and it further enhances biocompatibility and enables us to use well known silica based functionalization strategies.

4.1.5.2 Asymmetrization

The objective of this part of the work was to obtain Janus particles and couple the rice particles as guiding part to the earlier described motor particles. Considering that rice particles are quite small for observation in optical microscopy the asymmetrization is required to couple them with some bigger signaling particles conferring visibility to the assembly. Asymmetrization in longitudinal sense would allow different functionalization of both ellipsoid ends of the rice particle taking advantage of their hydrodynamic shape (compare 4.1.18 a).

First attempts to obtain surface silica covered asymmetric functionalization of the rice-shaped magnetic particles was through a Pickering emulsion of wax stabilized by our magnetic particles, as previously described. However, experiential results showed that a flat accommodation of rice particles on the interface of paraffin and solvent is preferred (see figure 4.1.18). Those findings are in accordance with recent publications by Madivala *et al.*^{60, 61}. Additionally the average covering with rice particles is low which makes longitudinal asymmetrization impossible.

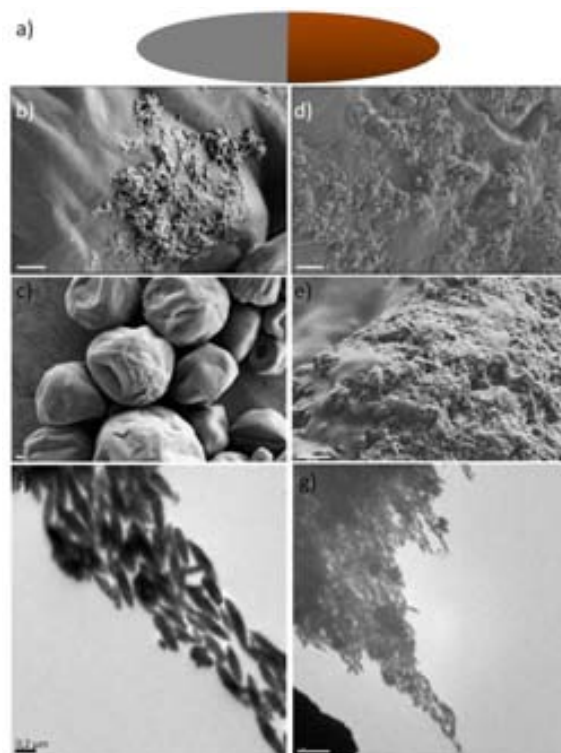


Fig. 4.1.18 a) Schematic picture of target asymmetry; b-e) trials to obtain asymmetric rice particles: b,c) immobilization through Pickering solution, d,e) immobilization on wax surface, f,g) formation of magnetic chains in magnetic field.

The second approach was also based on immersion in wax, several attempts were made to direct the immersion vertically into the wax by applying a homogeneous magnetic field as shown in the scheme below (see figure 4.1.19). Therefore a teflon plate bearing a cavity was placed in between an assembly of two cylindrical magnets. In the cavity a drop of solidified paraffin on a glass slide was positioned and a drop silica covered rice particles in solvent was added. The whole assembly was placed in an oven at temperatures varying from 40-80 °C to melt or soften the paraffin and allow the perpendicular entrapment of the rice particles on the paraffin surface. The obtained paraffin drop showed orange enclosures that were analyzed by SEM but no half immersed particles were found. Temperature control was expected to give margin to influence the depth of immersion, but no satisfying results could be obtained, in spite of several attempts with varied experimental conditions. Therefore this strategy had to be abandoned due to non feasibility. Later Tierno *et al.* used different rice shaped polymer particles with encapsulated iron oxide NPs covered with catalytic Pt against their hydrodynamically preferential orientation and obtained motile ellipsoid particles. Those particles were directable by magnetic fields

but due to their higher hydrodynamic resistance they were found to have slower speeds compared to spherical Janus particles⁶². The same approach could not have been realized with the here used rice particles because their size range was too small for optical microscopy and the hydrodynamic orientation that results from this flat asymmetrization is not considered beneficial for micromotor movement.

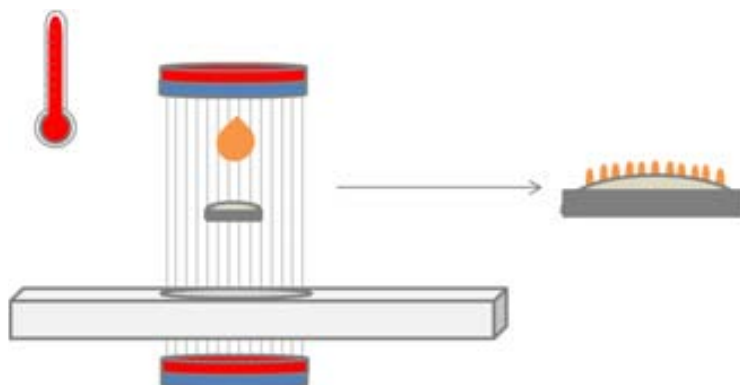


Fig. 4.1.19 Principle of intended asymmetrical functionalization of silica covered rice particles by partial immersion in wax directed by an applied homogeneous magnetic field.

4.1.7 Summary

Several kinds of silica particles were synthesized with different characteristics from porous structures to hollow particles and their properties were evaluated, being mesoporous particles the most suitable for surface functionalization and asymmetrization. Those particles were successfully functionalized and after grafting of different biomolecules (ADN and catalase) they could be coupled to signaling particles. The junction of this assembly is achieved by DNA hybridization enabling us to directly visually track of the cargo particles. The movement was found to be heterogeneous, including translational, rotational and circular movements, as well as combination of those. As the hybridization of the different DNA strands is crucial for the function of the micromotor the selectivity of the DNA hybridization has been proved by employing a molecular ruler: DNA strands tagged with two fluorophores forming a FRET pair were grafted on the particles and by observing Foerster energy transfer the distance between both fluorophores could be evaluated as less than 5 nm. This proves that hybridization is occurring and the movement of cargo particles is not due to any non-specific absorption. Non matching DNA gave a far lower signal compared to the original analyte DNA, showing the excellent selectivity of DNA. The motion of this assembly is enzymatically powered by the oxygen bubble formation upon catalase-based degradation of hydrogen peroxide solution. To the best of our knowledge this was the first catalase-driven particle based micromotor.

Finally attempts to make this movement directional were done by synthesizing rice-shaped core shell particles of iron oxide encapsulated by silica. However all approaches to obtain proper Janus particles out of them were unsuccessful.

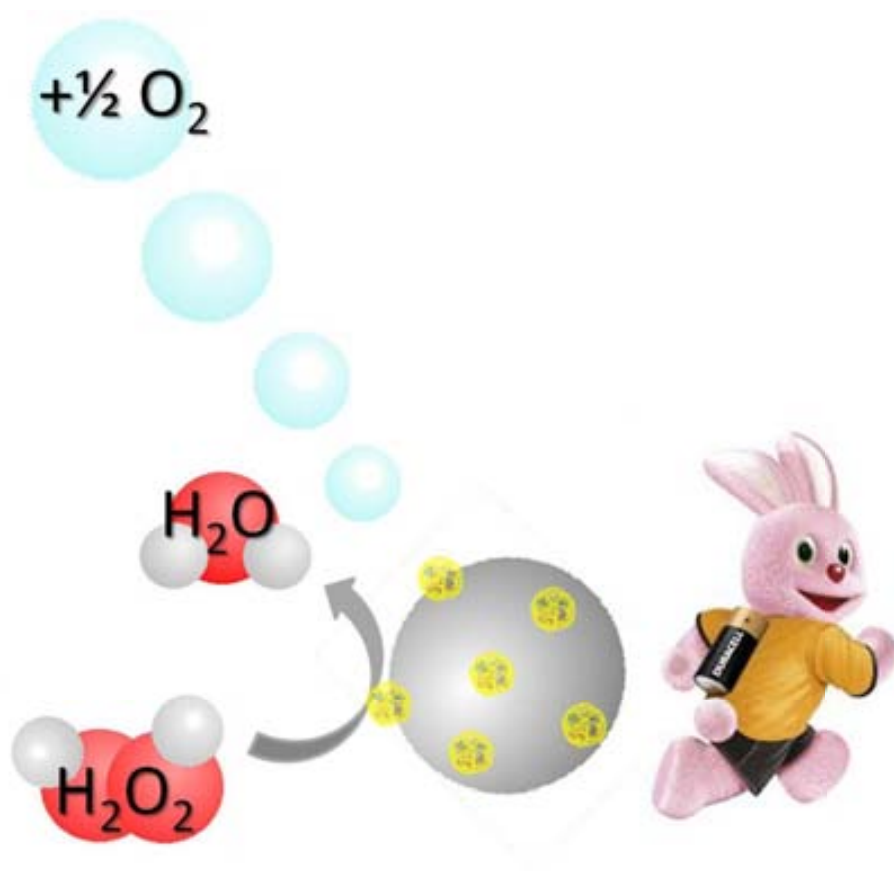
4.1.8 Literature

1. Watson, J. D.; Crick, F. H. *Nature* **1953**, 171, 737-738.
2. Schlossbauer, A.; Warncke, S.; Gramlich, P. M. E.; Kecht, J.; Manetto, A.; Carell, T.; Bein, T. *Angewandte Chemie International Edition* **2010**, 49, (28), 4734-4737.
3. Ruiz-Hernández, E.; Baeza, A.; Vallet-Regí, M. *ACS Nano* **2011**, 5, (2), 1259-1266.
4. Andersen, E. S.; Dong, M.; Nielsen, M. M.; Jahn, K.; Lind-Thomsen, A.; Mamdouh, W.; Gothelf, K. V.; Besenbacher, F.; Kjems, J. *ACS Nano* **2008**, 2, (6), 1213-1218.
5. Ebert, A.; Delay, G. DNA Detection, Chapter 13.
http://www.uvm.edu/~biology/Classes/296D/13_Detection.pdf
6. Mirkin, C. A.; Letsinger, R. L.; Mucic, R. C.; Storhoff, J. J. *Nature* **1996**, 382, (6592), 607-609.
7. Taton, T. A.; Mirkin, C. A.; Letsinger, R. L. *Science* **2000**, 289, (8), 1757-1760.
8. Cao, Y. W. C.; Jin, R. C.; Mirkin, C. A. *Science* **2002**, 297, (30), 1536-1540.
9. Rosi, N. L.; Mirkin, C. A. *Chemical Reviews* **2005**, 105, (4), 1547-1562.
10. York, J.; Spetzler, D.; Xiong, F.; Frasch, W. D. *Lab on a Chip* **2008**, 8, (3), 415-419.
11. Fischer, T.; Agarwal, A.; Hess, H. *Nat Nano* **2009**, 4, (3), 162-166.
12. Kagan, D.; Calvo-Marzal, P.; Balasubramanian, S.; Sattayasamitsathit, S.; Manesh, K. M.; Flechsig, G.-U.; Wang, J. *Journal of the American Chemical Society* **2009**, 131, (34), 12082-12083.
13. Wu, J.; Balasubramanian, S.; Kagan, D.; Manesh, K. M.; Campuzano, S.; Wang, J. *Nature Communications* **2010**.
14. Kagan, D.; Campuzano, S.; Balasubramanian, S.; Kuralay, F.; Flechsig, G.-U.; Wang, J. *Nano Letters* **2011**, 11, (5), 2083-2087.
15. Garcia, M.; Orozco, J.; Guix, M.; Gao, W.; Sattayasamitsathit, S.; Escarpa, A.; Merkoci, A.; Wang, J. *Nanoscale* **2013**, 5, (4), 1325-1331.
16. Morales-Narváez, E.; Guix, M.; Medina-Sánchez, M.; Mayorga-Martinez, C. C.; Merkoçi, A. *Small* **2014**, n/a-n/a.
17. Isojima, T.; Lattuada, M.; Vander Sande, J. B.; Hatton, T. A. *ACS nano* **2008**, 2, (9), 1799-1806.
18. Bele, M.; Siiman, O.; Matijevi; E. *Journal of Colloid and Interface Science* **2002**, 254, (2), 274-282.
19. Wang, Q.; Liu, Y.; Yan, H. *Chemical Communications* **2007**, (23), 2339-2341.
20. Blin, J. L.; Otjacques, C.; Herrier, G.; Su, B.-L. *Langmuir* **2000**, 16, (9), 4229-4236.
21. Guo, W.; Luo, G.; Wang, Y. *China Particuology* **2003**, 1, (4), 151-155.
22. Nooney, R. I.; Thirunavukkarasu, D.; Chen, Y.; Josephs, R.; Ostafin, A. E. *Chemistry of Materials* **2002**, 14, (11), 4721-4728.
23. Nozawa, K.; Gailhanou, H.; Raison, L.; Panizza, P.; Ushiki, H.; Sellier, E.; Delville, J. P.; Delville, M. H. *Langmuir* **2004**, 21, (4), 1516-1523.
24. Lodget, G.; Kuhn, A. *Nature Communications* **2011**, 2, 535.
25. Jiang, S.; Granick, S. *Langmuir* **2009**, 25, (16), 8915-8918.
26. Love, J. C.; Gates, B. D.; Wolfe, D. B.; Paul, K. E.; Whitesides, G. M. *Nano Letters* **2002**, 2, (8), 891-894.
27. Giermanska-Kahn, J.; Laine, V.; Arditty, S.; Schmitt, V.; Leal-Calderon, F. *Langmuir* **2005**, 21, (10), 4316-4323.
28. Perro, A.; Meunier, F.; Schmitt, V.; Ravaine, S. *Colloids and Surfaces A: Physicochemical and Engineering Aspects* **2009**, 332, (1), 57-62.
29. Kiselev, A. V. *Kolloidn. Zhur.* **1936**, 2, 17.
30. Zhuravlev, L. T. *Colloids and Surfaces A: Physicochemical and Engineering Aspects* **2000**, 173, (1-3), 1-38.
31. Yoon, T.-J.; Yu, K. N.; Kim, E.; Kim, J. S.; Kim, B. G.; Yun, S.-H.; Sohn, B.-H.; Cho, M.-H.; Lee, J.-K.; Park, S. B. *Small* **2006**, 2, (2), 209-215.

32. Wang, Y.; Caruso, F. *Chemistry of Materials* **2005**, 17, (5), 953-961.
33. Ismagilov, R. F.; Schwartz, A.; Bowden, N.; Whitesides, G. M. *Angewandte Chemie International Edition* **2002**, 41, (4), 652-654.
34. Vicario, J.; Eelkema, R.; Browne, W. R.; Meetsma, A.; La Crois, R. M.; Feringa, B. L. *Chemical Communications* **2005**, (31), 3936-3938.
35. Forster, T. *Naturwissenschaften* **1946**, 33, (6), 166-175.
36. Förster, T. *Annalen der Physik* **1948**, 437, (1-2), 55-75.
37. Weibel, D. B.; Garstecki, P.; Ryan, D.; DiLuzio, W. R.; Mayer, M.; Seto, J. E.; Whitesides, G. M. *PNAS* **2005**, 102, (34), 11963-11967.
38. Huang, C.; Shen, X. *Chemical Communications* **2014**, 50, (20), 2646-2649.
39. Balasubramanian, S.; Kagan, D.; Manesh, K. M.; Calvo-Marzal, P.; Flechsig, G.-U.; Wang, J. *Small* **2009**, 5, (13), 1569-1574.
40. Hong, Y.; Blackman, N. M. K.; Kopp, N. D.; Sen, A.; Velegol, D. *Physical Review Letters* **2007**, 99, (17), 178103.
41. Baraban, L.; Harazim, S. M.; Sanchez, S.; Schmidt, O. G. *Angewandte Chemie International Edition* **2013**, 52, (21), 5552-5556.
42. Dey, K. K.; Bhandari, S.; Bandyopadhyay, D.; Basu, S.; Chattopadhyay, A. *Small* **2013**, 9, (11), 1916-1920.
43. Baraban, L.; Makarov, D.; Streubel, R.; Mönch, I.; Grimm, D.; Sanchez, S.; Schmidt, O. G. *ACS Nano* **2012**, 6, (4), 3383-3389.
44. Fischer, P.; Ghosh, A. *Nanoscale* **2011**, 3, (2), 557-563.
45. Gao, W.; Feng, X.; Pei, A.; Gu, Y.; Li, J.; Wang, J. *Nanoscale* **2013**, 5, (11), 4696-4700.
46. Kline, T. R.; Paxton, W. F.; Mallouk, T. E.; Sen, A. *Angewandte Chemie International Edition* **2005**, 44, (5), 744-746.
47. Mendoza-Reséndez, R.; Bomati-Miguel, O.; Morales, M. P.; Bonville, P.; Serna, C. J. *Nanotechnology* **2004**, 15, (4), S254.
48. Ocaña, M.; Morales, M. P.; Serna, C. J. *Journal of Colloid and Interface Science* **1999**, 212, (2), 317-323.
49. Ohmori, M.; Matijević, E. *Journal of Colloid and Interface Science* **1993**, 160, (2), 288-292.
50. Wiogo, H.; Lim, M.; Munroe, P.; Amal, R. *Crystal Growth & Design* **2011**, 11, (5), 1689-1696.
51. Dagallier, C.; Dietsch, H.; Schurtenberger, P.; Scheffold, F. *Soft Matter* **2010**, 6, (10), 2174-2177.
52. Liu, L.-H.; Dietsch, H.; Schurtenberger, P.; Yan, M. *Bioconjugate Chemistry* **2009**, 20, (7), 1349-1355.
53. Reufer, M.; Dietsch, H.; Gasser, U.; Grobety, B.; Hirt, A. M.; Malik, V. K.; Schurtenberger, P. *Journal of Physics: Condensed Matter* **2011**, 23, (6), 065102.
54. Reufer, M.; Dietsch, H.; Gasser, U.; Hirt, A.; Menzel, A.; Schurtenberger, P. *The Journal of Physical Chemistry B* **2010**, 114, (14), 4763-4769.
55. Rufier, C.; Reufer, M.; Dietsch, H.; Schurtenberger, P. *Langmuir* **2011**, 27, (11), 6622-6627.
56. Sánchez-Ferrer, A.; Reufer, M.; Mezzenga, R.; Schurtenberger, P.; Dietsch, H. *Nanotechnology* **2010**, 21, (18), 185603.
57. Almeida, T. Hydrothermal Synthesis and Characterisation of α -Fe₂O₃ Nanorods. University of Nottingham, 2010.
58. Ohmori, M.; Matijević, E. *Journal of Colloid and Interface Science* **1992**, 150, (2), 594-598.
59. Ngo, A. T.; Pileni, M. P. *Journal of Applied Physics* **2002**, 92, (8), 4649-4652.
60. Madivala, B.; Fransaer, J.; Vermant, J. *Langmuir* **2009**, 25, (5), 2718-2728.
61. Madivala, B.; Vandebril, S.; Fransaer, J.; Vermant, J. *Soft Matter* **2009**, 5, (8), 1717-1727.
62. Tierno, P.; Albalat, R.; Sagués, F. *Small* **2010**, 6, (16), 1749-1752.

4.2 Enzyme encapsulation for micromotors with prolonged lifetime

In this chapter a method to encapsulate enzymes in thin permeable polymer shells with reactive groups on the surface is described. After optimization and careful characterization for catalase as our model enzyme the capsules are anchored onto silica particles. The motion endurance is found to be enhanced and even in harsh conditions as high peroxide concentrations, elevated temperatures or the presence of proteolytic enzymes higher enzyme resistance was proven.



4.2.1 Enzyme encapsulation

In the previous chapter covalent attachment of catalase on silica particles enabled us to build micromotor assemblies. Though we observed that the durability of the catalase itself in peroxide was not very promising. To immobilize enzymes on surfaces several more elaborated methods than covalent attachment have been developed, e.g. entrapment or encapsulation. In order to minimally hinder diffusion of peroxide and facilitate anchorage on the particle surface, the use of a thin polymer shell wrapping the enzyme shall be studied. Additionally the need to protect the activity of catalase and improve its performance as catalytic motor, considering the life-time and the resistance to external influences is addressed. Subsequent covalent attachment of the enzyme-capsules on the silica surface requires the presence of functional groups on the surface of both, silica and enzyme capsules. A promising approach was recently published and shall be introduced quickly¹⁻³.

4.2.1.1 Enzyme encapsulation using acrylate-type monomers

As previously described the encapsulation of enzymes in different materials results in enhanced stability but the coating may hinder the transport of substrate and the release of product, resulting therefore in decreased biocatalytic activity. Yan *et al.* proposed in 2006 a promising solution by coating enzymes with a thin polymeric capsule. The first step consists in the introduction of reactive acryl groups on the surface, followed by capsule forming *in situ* polymerization. They used horseradish peroxidase (HRP), a widely used but relatively sensitive enzyme that catalyzes the decomposition of peroxide. As fundamental monomer acrylamide (AA) was employed while N,N'-methylenebisacrylamide (MBA) served as cross-linker, and N,N,N',N'-tetramethylethylenediamine (TMEDA)/ammonium persulfate (APS) as the initiator¹.

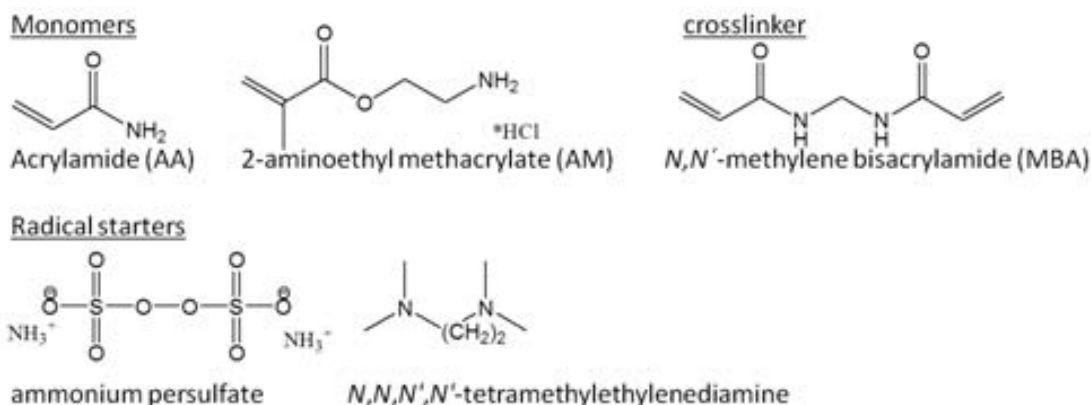


Fig. 4.2.1 Chemical formula and names of all compounds used to form acrylamide capsules.

Moreover, a degradable and a non-degradable version of the capsules were developed by exchanging the crosslinker. The non-degradable capsules show long-term stability, whereas the degradable ones break either in dependence of pH or up on irradiation³. Another publication of the same group described the delivery of apoptosis inducing caspase-3 to cancer cells and the protease mediated degradation process². The encapsulation of complementary functional enzyme complexes was published by Liu *et al.*⁴. One example of those co-localized

nanocomplexes contained alcohol oxidase and catalase. This complex was able to reduce blood alcohol levels in intoxicated mice. The authors suggested this as a possible antidote and prophylactic for alcohol intoxication ⁴.

A very similar method to that presented by Liu *et al.* was chosen to produce enzymatic capsules to propel micromotors. In our approach we also used AA as neutral monomer, MBA as crosslinker and a hydrochlorid salt of 2-aminoethyl methacrylate (AM) as positive monomer in order to introduce amino groups on the capsule surface. As radical starters APS/TMEDA were used. The main change consisted in the use of AM as positive monomer; all formulas can be seen in figure 4.2.1 and for a detailed description and illustration of the polymerization mechanism see 4.2.2.

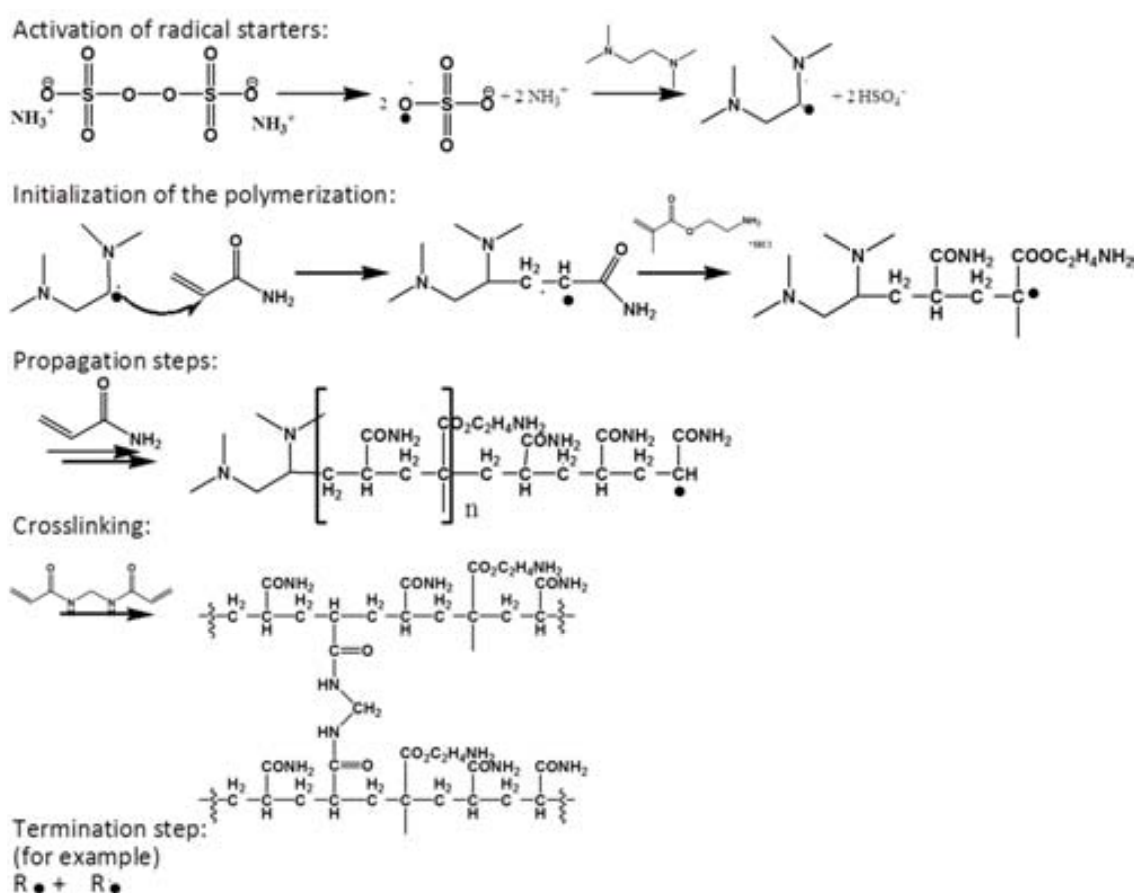


Fig 4.2.2 Schematic illustration of the mechanism of a radical polymerization with the above mentioned monomers, crosslinker and starters. Traditionally a polymerization consists of an activation step, the initialization of the reaction itself, several propagation steps, the crosslinking and one or more termination steps.

The polymerization mechanism follows the typical course of a radical polymerization, starting with the activation of the radical starters, the initiation of the reaction, several propagation steps and finally the termination, caused either by disturbing factors or by the consumption of monomers, as depicted in figure 4.2.2.

4.2.1.2 Encapsulation of catalase



Fig. 4.2.3 Scheme of encapsulation process with acryloylation of the enzyme as a first step and subsequent capsule formation on the introduced acryloyl groups.

To optimize the capsule formation in the first step the monomer ratio (AA:AM:MBA) was fixed to 6:4.5:1 and different conditions varying the acrylamide:enzyme ratio between 1200:1 and 12000:1 were tested. Low monomer content was found favorable (Table 4.2.1, entry a), as higher monomer content led to formation of bulk polymer. In the following experiments the optimal enzyme:AA relation was maintained and different proportions of the monomers and the crosslinker were checked. A trend can be observed that increasing the crosslinker content leads to more gelification, followed by entrapment of the enzyme capsules in the gel and low recovery ratio (see table 4.2.1). Lower content of AM led to a lower amino content on the capsule surface. The grade of crosslinking seems to affect this parameter as well, as it is capable of reacting with free amine-side chains in the polymer (table 4.2.2). As optimal conditions the capsules with high recovery, defined size and high grade of accessible amino groups on the surface were chosen. They correspond to entry d, table 4.2.2: the optimal ratio was found to be enzyme/AA/AM/MBA 1/1200/900/100. The size of these was confirmed by TEM. Considering that organic molecules do not absorb many electrons they do not produce a strong contrast in transmission electron microscopy. Therefore it was necessary to enhance the contrast using phosphotungstic acid as staining agent.

Table 4.2.1 Variations of the ratio monomer/enzyme to optimize capsule synthesis, chosen conditions were marked grey in both tables.

Table 1 Entry	Monomer ratio			Capsules	
	AA	AM	MBA	Recovered Mass mg	DLS Nm
a	1200	900	200	3.71	9.57
b	3000	2250	900	< 1 mg	19.3
c	6000	4500	1000	< 1 mg	60.6
d	12000	9000	2000	Gel formation	

Table 4.2.2 Having fixed monomer/enzyme ratio according to the results from table 4.2.1 the relations between the monomers were varied

Table 2 Entry	Monomer ratio			Capsules		
	AA	AM	MBA	Recovered Mass mg	DLS nm	NH ₂ %*
a	1200	900	200	3.71	9.57	87.5
b	1200	450	200	2.55	9.93	65.6
c	1200	900	300	< 1 mg	64.6	x
d	1200	900	100	3.77	14.2	175
e	1200	900	50	1.56	41.84	220

In figure 4.2.4 the native enzyme and the capsules are compared, with the capsules showing an average size of 30 nm. The presence of amino-groups has been proven by a fluorescamine assay and the capsule presents approximately 75% more accessible amino-groups than native catalase, for more experimental details on the assay see chapter 3.

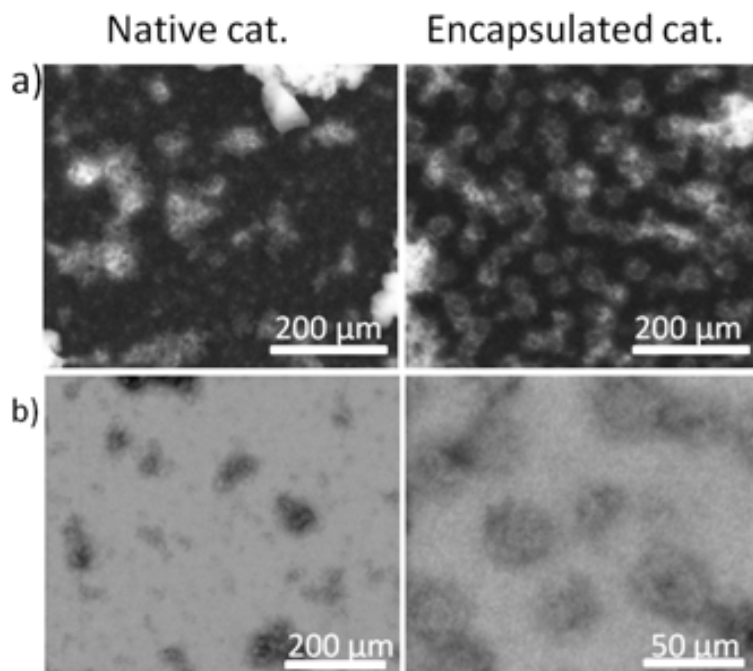


Fig. 4.2.4 STEM image of native (left) vs. encapsulated (right) enzyme stained with 1% phosphotungstic acid solution a) STEM image in dark field, b) STEM acquired in bright field.

4.2.1.3 Activity evaluation for encapsulated catalase

The enzymatic activity of the enzyme capsules was determined following the decomposition of a H_2O_2 solution by UV-absorption at 240 nm. The acryloylation step scarcely modified the activity retaining more than 95% of the activity. The encapsulated enzymes obtained after the polymerization process lost almost 50% of the initial activity (see figure 4.2.5). The enzymatic activity was expressed in units per mg of dry solid residue. The presence of the polymer coat increases the weight of the enzyme in a proportion difficult to determine with precision and this fact is considered the main reason for this activity lost. Other reasons that can diminish the activity of the encapsulated enzyme are active site blockage and lower peroxide diffusion into the polymer shell. The encapsulated catalase shows significant increase in its thermal stability and resistance to protease degradation. Despite the decrease in the activity, the encapsulation of the enzyme achieves a great improvement in its thermal stability and resistance to harsh external condition as oxidizing agents such as peroxide or proteolytic enzymes like protease that might degrade the catalase. After 1 hour at 60 °C, the enzyme capsules retain more than half of their initial activity, which is a loss of only about 45% whereas the native enzyme lost almost 80% of its activity.

In order to evaluate the potential application of these motors in biological fluids, where proteolytic enzymes can be present, the stability of the capsules against enzymatic degradation was tested. Therefore enzyme capsules were incubated in a solution of 5 mg/mL of protease at 37 °C for 2h. After this time, the remaining activity was evaluated following the decomposition of H₂O₂ as in the previous cases. The native enzyme practically loses all the activity whereas the encapsulated enzyme retains more than 90% of its initial activity. This shows that the capsule covers the sites where the protease can attack the enzyme in order to degrade it.

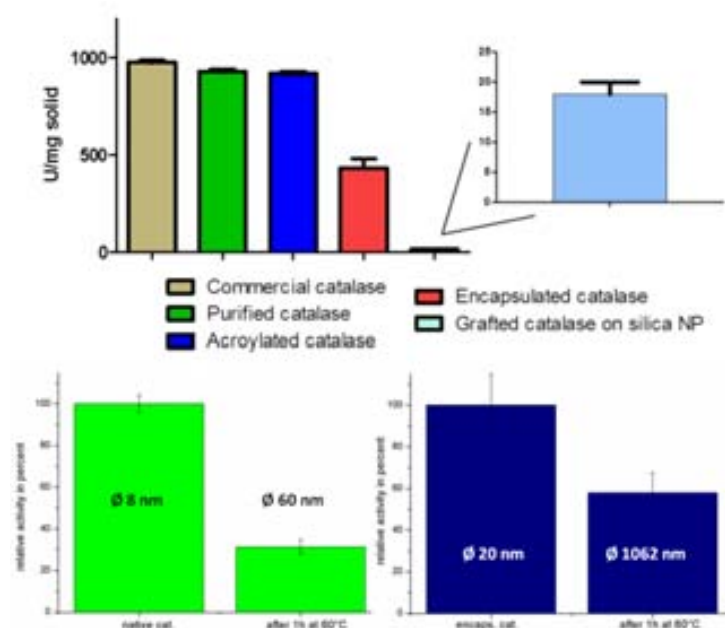


Fig 4.2.5 Catalase activity loss after encapsulation compared to native catalase, evaluated by peroxide solution degradation. Evaluation of the relative thermal stability of native catalase vs. encapsulated catalase, and hydrodynamic diameter of the units.

4.2.2 Micromotors powered by encapsulated catalase

4.2.2.1 Silica motors

To synthesize the micromotors the surface of the silica particles was functionalized with carboxylic groups in order to allow the attachment of the catalase capsules. This reaction was performed using (3-succinimylpropyl)-triethoxysilane in toluene at 80 °C under nitrogen atmosphere. The introduction of carboxyl groups was monitored with FTIR comparing the initial spectrum which is typical for silica (shown in figure 4.2.6) with the modified particles. In the inset the appearance of the COOH-band at 1708 cm⁻¹ after COOH-grafting is enlarged. The functionalization is reflected in thermogravimetric analysis (TGA) as well, indicating around 22 wt.% of carboxyl groups. A monolayer of carboxyl groups on the particle surface would correspond to approx. 6.5 wt.% and as an excess of 3-succinimylpropyl-triethoxysilane was used, we conclude that polycondensation occurred. This can additionally facilitate the enzyme capsule attachment. Once functionalized with acid groups, the capsules were covalently

attached on the surface using EDC and NHS for activating the carboxylic groups. In the FTIR the disappearance of the carboxylbands after reaction with EDC/NHS and the enzyme can be observed. Last point also indicates that the enzymes are covalently bound and not only physically absorbed (Figure 4.2.6).

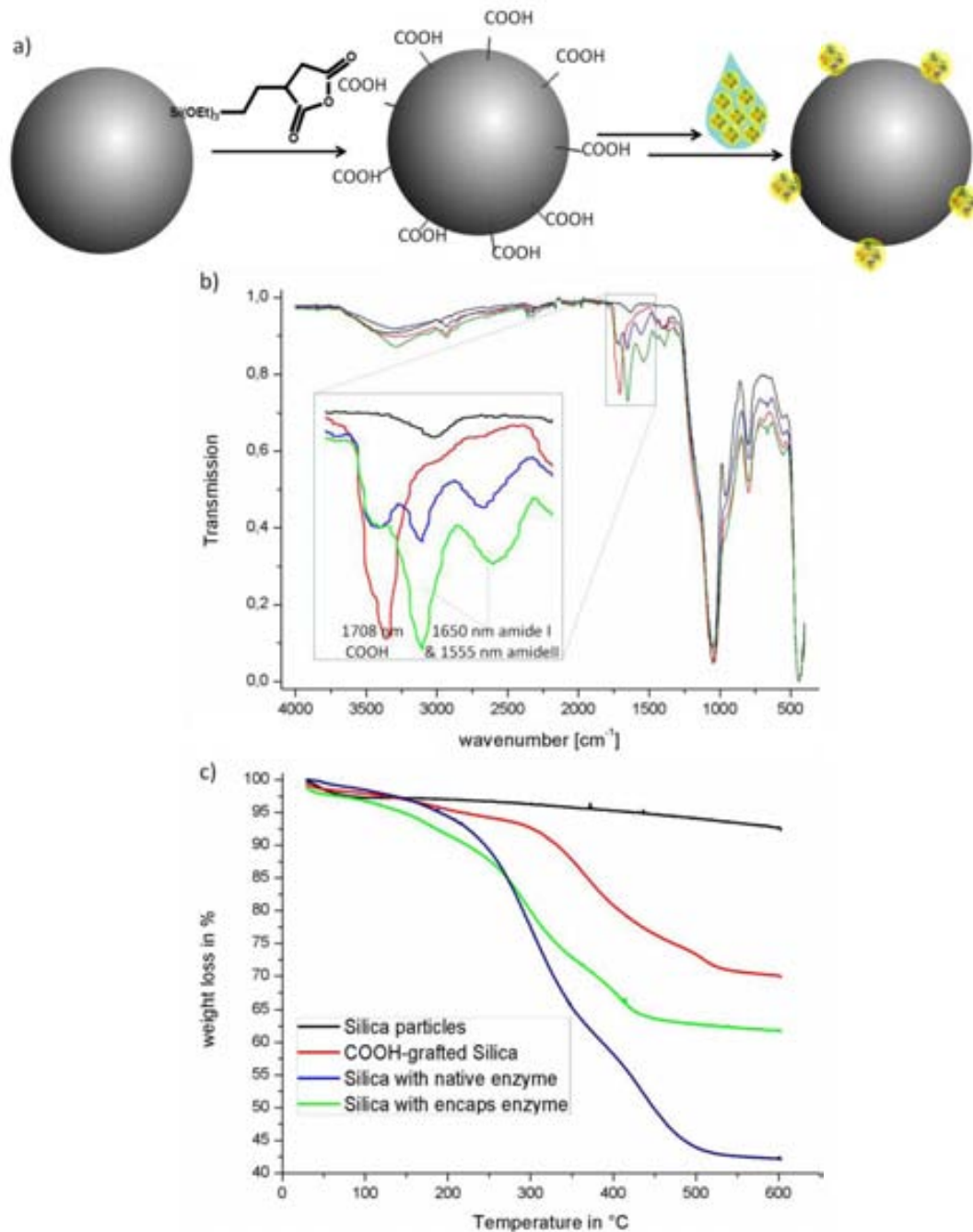


Fig. 4.2.6 a) Schematic representation of the surface functionalization, chemical modifications were monitored by b) FTIR and c) TGA.

In order to compare the covalent anchoring, native catalase was grafted using the same procedure. According to the thermogravimetric analysis, the amount of native enzyme bounded to the silica surface was 8%, whereas the encapsulated catalase reached 25% (figure

4.2.7). This discrepancy can be associated to two factors: in first instance the polymer capsules increase the average weight of each enzyme unit. Additionally the capsules present a higher number of amino groups on their surface compared to the native catalase and therefore grafting is favored. Amino assay through fluorescence measurement after reaction with fluorescamine (see detailed scheme in chapter 3) resulted in an approximately 75% higher amine content in the polymer shell than in native catalase. The grafting reaction activated by EDC/NHS benefits from those amino groups and the protein grafting is more efficient. The higher amount of protein bound to the silica surface was confirmed by S-selective elemental analysis, which is completely selective to the enzyme, as neither the silica particles nor the methacrylate capsules contain any sulfur. The S-content in a sample of particles bearing encapsulated enzyme was approximately 5 times higher than in particles with native enzyme on their surface.

4.2.2.2 Comparative evaluation of enzymatic activity

The peroxide as substrate for catalase is a factor that might oxidize the catalase enzyme. Even though some forms of this enzyme contain a NADH factor in each subunit to protect themselves from oxidation exposure to peroxide is critical for the enzyme stability. Relatively high concentrations deactivate the enzyme rapidly, while the polymeric capsule protects the enzyme quite efficiently from oxidation. In figure 4.2.7 we can see that 150 μg of silica particles bearing encapsulated catalase completely convert 1% H_2O_2 into water and oxygen, while the same amount of particles with native enzyme is oxidized and the reaction stops at approximately 5% decomposed peroxide. This result is not really surprising when one considers that the enzyme was designed to operate at extremely low concentrations of peroxide inside cells.

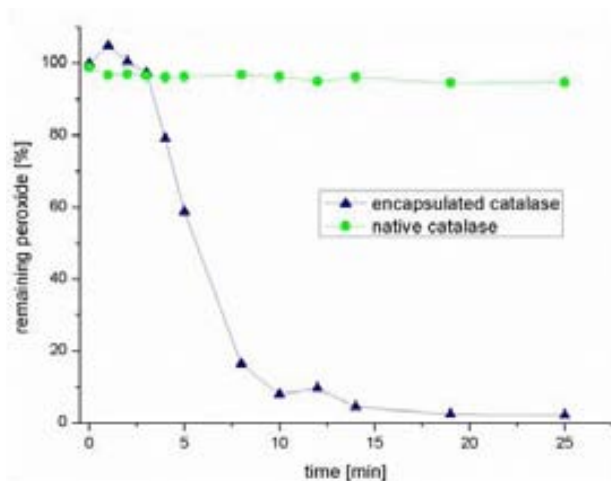


Fig. 4.2.7 Degradation of 1% peroxide in presence of silica particles bearing native catalase vs. encapsulated catalase. It can be observed that the degradation of peroxide is stopped after few minutes with native catalase while the encapsulated enzyme degrades almost all the peroxide.

This is especially important when one considers the reusability of enzymes. If the enzyme is oxidized by the substrate itself the recycling of enzyme grafted particles is not possible. Therefore an experiment was designed in order to show the enhanced recycling properties of encapsulated catalase. Silica particles decorated with enzyme capsules are able to decompose

an almost constant amount of hydrogen peroxide during more than 10 cycles, whereas the silica particles covered by native enzymes show a significant activity decrease after 2 or 3 cycles. This result demonstrates that enzyme encapsulation not only achieves higher covalent grafting but also allows an impressive stability increase of the attached enzyme (figure 4.2.8).

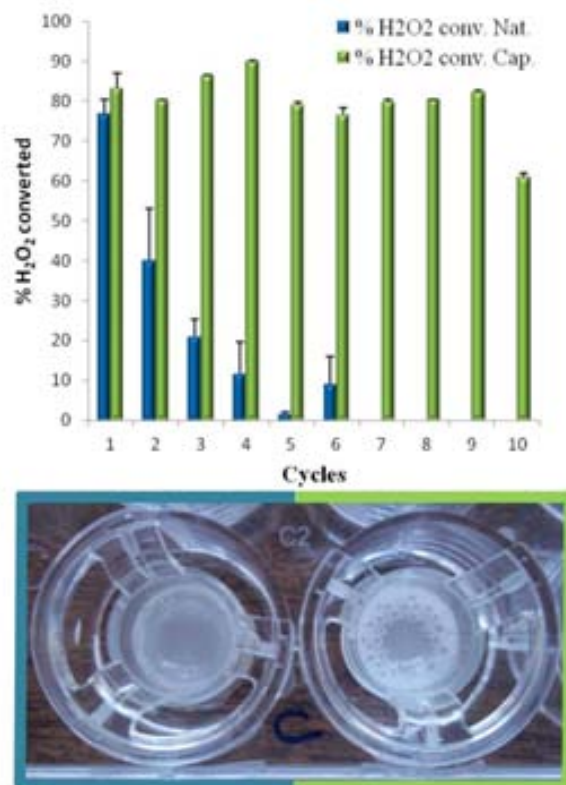


Figure 4.2.8 H₂O₂ conversion by native enzyme vs. encapsulated enzyme grafted on silica particles, down picture taken after 10 cycles, left well: native catalase, right well: capsules.

4.2.2.3 Motion experiments

Silica particles decorated with encapsulated enzymes are placed in a 2.5% peroxide solution and show immediate bubble production, which is visibly located on the surface of the

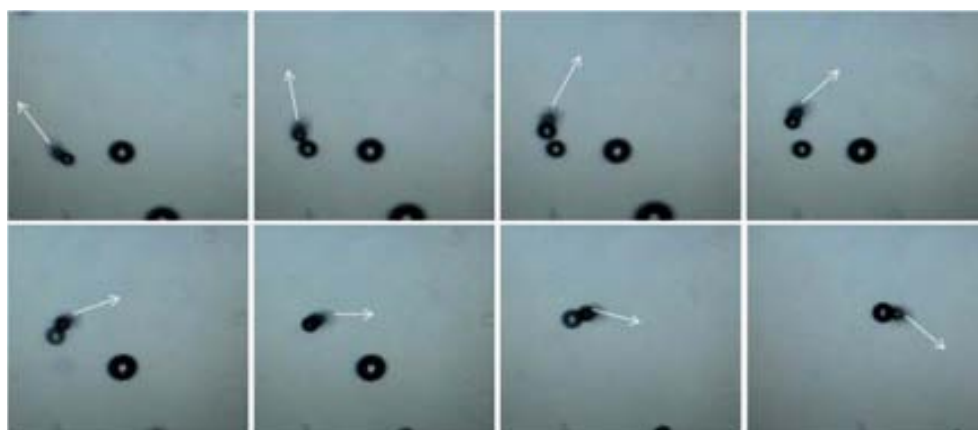


Fig. 4.2.9 Circular translation of silica motors with encapsulated catalase grafted on the surface, the motion is propelled bubble ejection

microparticles. The direction of the movement is determined by bubble creation. Videos prove that fast bubble production leads to a jet propulsion, i.e. the fast exit of bubbles propels a forward movement. A slow reaction rate that creates bigger bubbles is not able to produce this effect, but has an equal influence on particle position. The bursting of slowly growing large bubbles produced creates an "empty space" that is subsequently filled by media, creating a flux that seems to push the particle backward. Manjare *et al.* have observed similar behavior for large Pt driven Janus motors ⁵. Contrary to the tube-shaped motors, particle based motors seemed to favor non bubble driven mechanisms, as the degradation products are not confined and their free diffusion more commonly leads to gradient driven mechanism. Anyway here we could not observe any particles moving by mechanisms other than bubble propulsion, which is probably due to high reaction rates of the used enzyme. The high activity leads to strong accumulation of O₂ due to which surface tension is rapidly overcome and bubbles are formed. These results are similar to what was found in previous work ^{6,7}. Important improvement is achieved by encapsulation concerning the "durability" of micromotors. Using native catalase in peroxide for propulsion, it is observed that after short time the movements stop, as the enzyme itself gets oxidized by the fuel. Using encapsulated enzymes the stalling of particle movement takes far longer (depending on experimental conditions in the range of 30 min) and is reversible by adding more peroxide fuel. This indicates that the stalling is not due to degradation of the enzyme, but due to the consumption of fuel. This observation was confirmed in a separate experiment to determine the turn over number (particles with anchored native catalase vs. catalase capsules @ silica particles, see figure 4.2.8).

4.2.2.4 Polystyrene motors

Amino groups as quite reactive moiety present a high level of versatility and allow manifold coupling. To demonstrate that amino coupling is not limited to carboxyl groups we coupled the encapsulated enzyme to fluorescent polystyrene (PS) particles with amino groups on their surface. Where silica particles still benefit from the presence of silanol groups on the surface that facilitate enzyme immobilization by hydrogen bonding and electrostatic interaction, PS hardly interacts with the enzymes ⁸. Here we used a suberic acid bis(*N*-hydroxysuccinimide ester), able to crosslink between two amino groups.

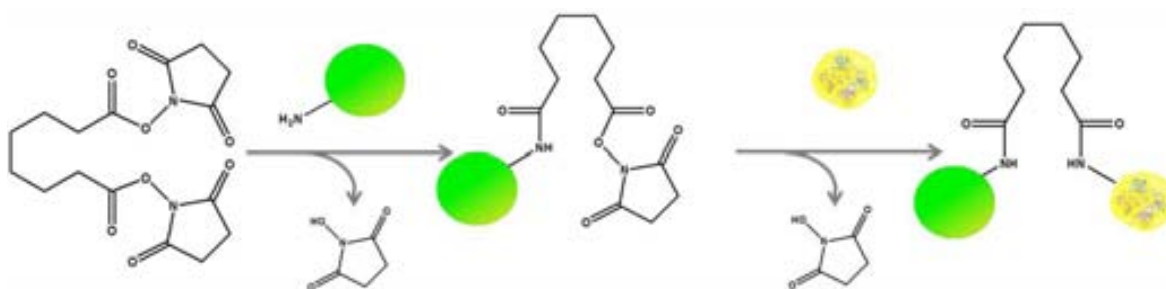


Fig. 4.2.10 scheme of di-amine crosslinking of fluorescent amino grafted PS particles to amino groups on the surface of enzyme capsules by suberic acid bis(*N*-hydroxysuccinimide) ester.

Movement could be mainly observed in particle agglomerations, which might be due to several factors. In the first instance due to the particle size of 1 μm the observation of single particles is more difficult, so bigger agglomerates are more likely to be observed by the experimentalist. On the other hand the anchoring of enzymes might be more favored in agglomerations due to increased van der Waals forces. Analogous observations as in silica motors could be made, the movement is long-lasting and after stalling the movement could be reactivated by addition of new fuel.

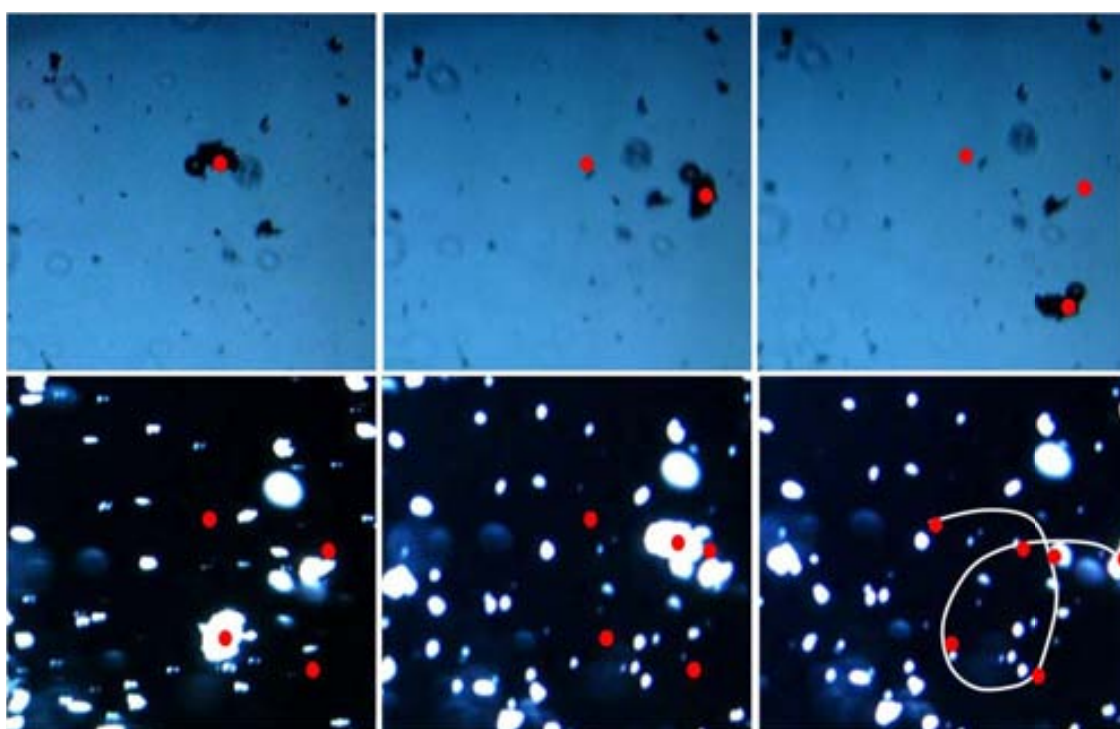


Fig. 4.2.11 Movement of agglomeration of fluorescent PS particles through catalase grafted on the surface, up: seen by optical microscopy with visible light, down: seen by an optical microscope in fluorescence mode. The positions of the agglomerate are marked with red dots in all images and tracked in the last image.

4.2.3 Janus motors

Micromotors produced in previous experiments show rather by chance one pattern of bubbling or another. The amount and positioning of grafted enzymes strongly depend on statistical probability of the reaction. To enhance the probability of co-grafting several enzymes that are spatially close and therefore obtain an increased likelihood of a "forward movement", enzyme capsules should be anchored on asymmetric particles. Here, commercial polystyrene beads of an average diameter of 7 μm were chosen, due to their excellent homogeneity and visibility in optical microscopy. Particles were covered by a 2 nm thin layer of chromium to increase their "stickyness" for the gold-layer, which were then coated by 10 nm of gold. As polystyrene itself is not very reactive and functionalized particles of this size are hardly available, the gold half-sphere was chosen for functionalization. Gold is easily covered by self-assembly of thiols on its surface. Therefore thiolation of enzyme capsules was chosen to introduce thiol functionalities that might bind to the gold surface and attach the enzyme semi-covalently to the particles^{9,10}.

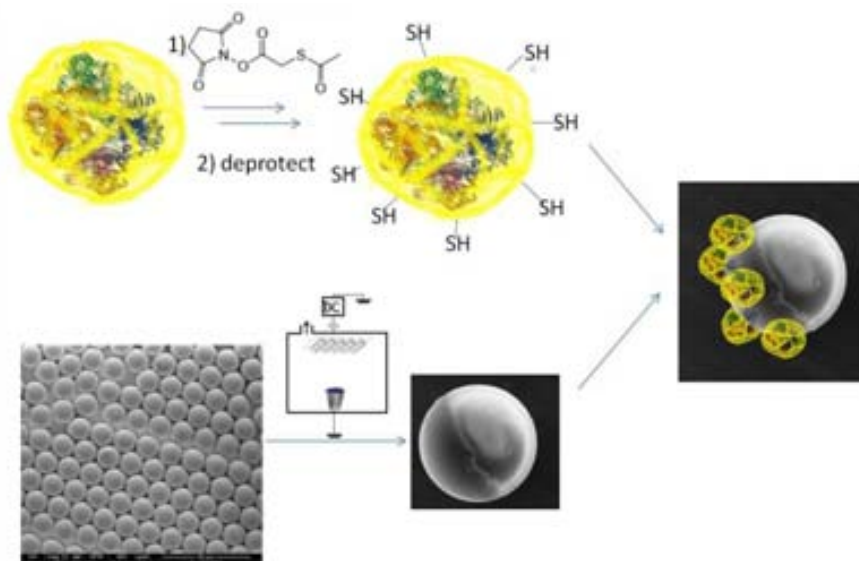


Fig. 4.2.12 Thiolation of catalase capsules by reaction of amino surface groups with SATA and subsequent deprotection and down: production of Au-covered PS particles and anchorage of thiolated catalase capsules on the Au-hemisphere.

Two different strategies were followed to introduce thiol groups into enzyme capsules. The first is similar to an approach used by Kuhn *et al.*¹¹ displayed in figure 4.2.12: on previously synthesized aminated capsules protected thiols were grafted using *N*-Succinimidyl *S*-Acetylthioacetate (SATA) and deprotected subsequently. Systematic studies showed that amine content after thiolating amino groups on polymeric capsules lowered by approximately 60%, so that it can be concluded that thiol groups entered the capsule surface. Due to the low sensitivity of available tests for thiols the exact quantity of thiol groups could only be determined indirectly. In the purification step after deprotecting the enzyme capsules form S-S bonds and agglomerate strongly.

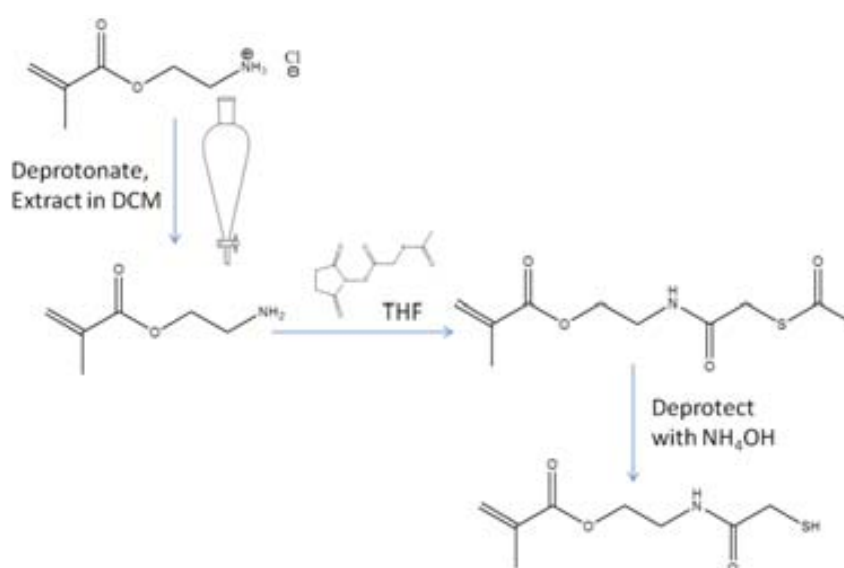


Fig. 4.2.13 Synthesis of thiolated monomers: extraction of deprotonated AM and reaction with a thiolated succinimidyl molecule and subsequent deprotection.

Therefore as alternative strategy the use of thiolated monomers in capsule synthesis was suggested. As no such monomers are commercially available, the aminated monomer had to be transferred to thiols, following a synthetic route depicted in figure 4.2.13. Briefly the hydrochloric salt of the aminated monomer was deprotonized in an NaOH solution and extracted into a dichlormethane organic phase. The thiolation reaction is carried out in dry THF with 1 eq. SATA. In a first trial the product is dried and analyzed by NMR. In a first attempt the desired product was detected and the whole batch was used without further purification in the capsule synthesis, leading to capsules with a reasonable size of 13.4 nm and the Zetapotential shifted to very negative values. This seems logical for thiolated products. However, as no direct chemical analysis for thiol groups was feasible a purification of the monomer was necessary to quantify the amount of thiol groups in the capsule. Several extraction conditions and washing procedures have been tried but still several impurities were found. A chromatographic purification failed because the silica gel decomposes the product. As SATA is very expensive this approach was not followed any further.

Table 4.2.3 Analysis of polymeric capsules containing different functional groups

	Pure polymeric capsules	Amine containing capsules	Capsules with protected, grafted thiols	Capsules with thiol containing monomer
DLS nm	14.6	19.3	20.8	13.4
ZP mV	-37	-32.4	-27.4	-56.3

In the following different reversed strategies similar to those used for tubes by Sanchez *et al.*⁷ have been tried. On the gold covered half sphere of the PS particles a monolayer of mercapto undecanoic acid (MUA) / mercapto propionic acid (MPA) should be assembled to subsequently activate the acidic groups and graft catalase. The functionalization with MUA/MPA is commonly carried out in propanol or similar alcoholic solvents, in which PS undergoes swelling processes. Prior to activation of the COOH groups a solvent change to aqueous medium is required. Janus Au@PS particles are not stable under those conditions and suffer from exfoliation of the metal caps. Another hypothesis is that the affinity of MUA/MPA to the metal surfaces is so much higher than PS to the metal, so that the assembly is favored, which benefits the restacking of the metal caps. Due to those encountered difficulties this strategy was abandoned.

4.2.4 Other enzymes

Nano- and micromotors are said to have very promising applications *in vivo*, the most cited future application was already presented about 60 years ago - micromachines for human medicine in the film "fantastic voyage" in 1966. Most of today's micromotors are based on peroxide as fuel, which is incompatible with cells as high concentrations of hydrogen peroxide cause immediate death by cell lysis (necrosis)¹² and even concentrations down to 0.05 mmol/L induce cell death¹³. Therefore much attention was paid to glucose oxidase (GOx) as motor enzyme, which on itself it could possibly propel motors through ion gradients. In a enzymatic tandem with catalase the motor would even be able to propel by bubble production in a

glucose solution. However the anchoring of GOx on silica particles did not lead to any movement. The encapsulation of catalase showed that enzyme driven micromotors benefitted strongly from encapsulation of the enzyme. In a recent work on enzyme immobilization strategies the author claims that encapsulation stabilizes those biomolecules in many cases and may even improve enzyme performance ⁸. Therefore GOx was encapsulated using the same method as described for catalase

However when the amount of peroxide produced by GOx was evaluated by adding a small amount of catalase to the glucose solution containing GOx only after approx. 15 min first bubbles appeared. This does not seem practicable to propel motors. This result leads to the conclusion that the conversion rate of commercial GOx is too low to produce a sufficient gradient for propulsion and not enough peroxide to allow efficient catalase operation. To test the validity of this conclusion, horseradish peroxidase was tested, as an enzyme catalysing the same reaction as catalase does, but with an activity comparable to GOx activity. A drop of 5 mg/mL solution was added to a 2.5% peroxide solution and no bubble formation could be observed. For comparison: the same concentration of catalase causes wild bubbling. Therefore we tentatively conclude that the activity of enzymes is crucial for their use in micromotors, even though further studies have to be designed to quantitatively evaluate this thesis.

4.2.5 Summary

Based on the work of Liu *et al.* ^{1,3,4} a method to encapsulate catalase in a novel capsule type bearing amine groups by co-encapsulation of aminated monomers was developed. The capsules were characterized in morphology and surface properties and their catalytic performance was evaluated. A method for covalent grafting of the enzymatic capsules on motor particles was presented and the improved performance of those motors was evaluated. We found that the durability of our micromotors bearing enzyme capsules was manifold increased compared to motors with native enzyme. The reusability of both types was compared and the capsules were more stable in thermal and enzymatic treatment, as well as in peroxide rich environment.

In conclusion it can be said that encapsulation of catalase strongly improved the endurance of catalase based micromotors, as it protects the enzyme against oxidation and enzymatic degradation. This might be the way to go to use other enzymes as propelling force for motors and therefore access novel, probably less oxidation and aggressive fuels.

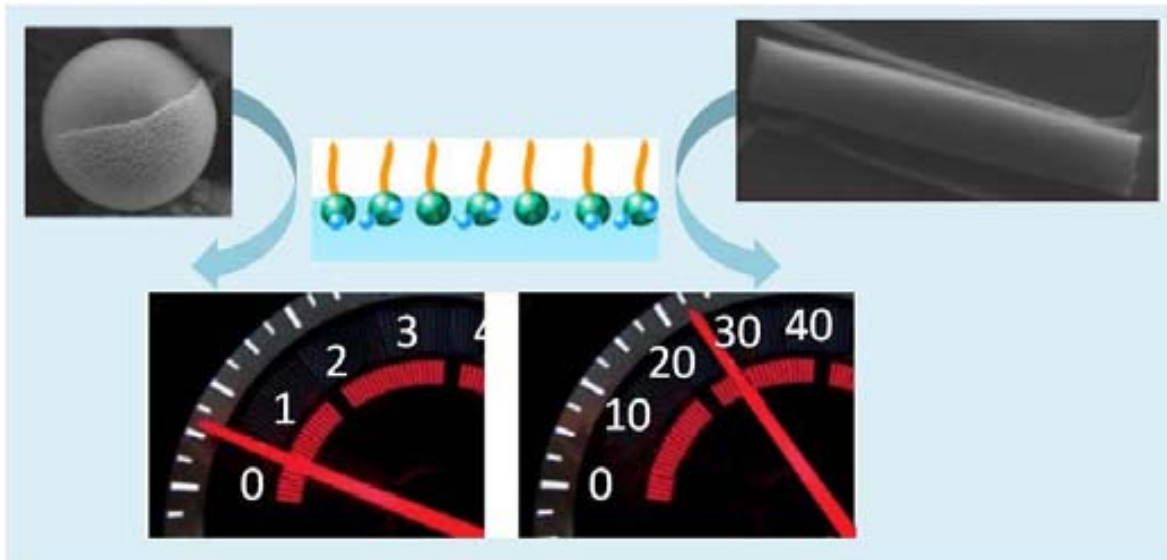
A brief evaluation of other enzymes as glucose oxidase and horseradish peroxidase indicated that at least commercial enzymes without further purification steps are not suitable to propel nano-or micromotors - however it should not be excluded to add additional purification and concentration steps and search for an ideal encapsulation method to improve enzyme performance.

4.2.6 Literature

1. Yan, M.; Ge, J.; Liu, Z.; Ouyang, P. *Journal of the American Chemical Society* **2006**, 128, (34), 11008-11009.
2. Gu, Z.; Yan, M.; Hu, B.; Joo, K.-I.; Biswas, A.; Huang, Y.; Lu, Y.; Wang, P.; Tang, Y. *Nano Letters* **2009**, 9, (12), 4533-4538.
3. Yan, M.; Du, J.; Gu, Z.; Liang, M.; Hu, Y.; Zhang, W.; Priceman, S.; Wu, L.; Zhou, Z. H.; Liu, Z.; Segura, T.; Tang, Y.; Lu, Y. *nature Nanotechnology* **2010**, 5, 48-53.
4. Liu, Y.; Du, J.; Yan, M.; Lau, M. Y.; Hu, J.; Han, H.; Yang, O. O.; Liang, S.; Wei, W.; Wang, H.; Li, J.; Zhu, X.; Shi, L.; Chen, W.; Ji, C.; Lu, Y. *Nature Nanotechnology* **2013**, 8, 187-192.
5. Manjare, M.; Yang, B.; Zhao, Y. P. *Physical Review Letters* **2012**, 109, (12), 128305.
6. Simmchen, J.; Baeza, A.; Ruiz, D.; Esplandiu, M. J.; Vallet-Regí, M. *Small* **2012**, 8, (13), 2053-2059.
7. Sanchez, S.; Solovev, A. A.; Mei, Y.; Schmidt, O. G. *Journal of the American Chemical Society* **2010**, 132, (38), 13144-13145.
8. Cao, L., Introduction: Immobilized Enzymes: Past, Present and Prospects. In *Carrier-bound Immobilized Enzymes*, Wiley-VCH Verlag GmbH & Co. KGaA: 2006; pp 1-52.
9. Nuzzo, R. G.; Allara, D. L. *Journal of the American Chemical Society* **1983**, 105, (13), 4481-4483.
10. Boeckl, M.; Graham, D. *Material Matters* **2006**, 2, (1), 3.
11. Kuhn, S. J.; Finch, S. K.; Hallahan, D. E.; Giorgio, T. D. *Nanoletters* **2006**, 6, (2), 306-312.
12. Ager, A.; Gordon, J. L. *Journal of Experimental Medicine* **1984**, 159, 592-603.
13. de Bono, D. P.; Yang, W. D. *Atherosclerosis* **1995**, 114, (2), 235-245.

4.3 Platinum driven micromotors

In this chapter the magnetic guidance of micromotors is approached and in order to obtain a more homogeneous motion the enzyme based fuel degradation is exchanged. As alternative catalyst an inorganic catalytic Pt layer is employed, which leads to more uniform motion, enabling us to characterize the movement and draw conclusions considering the mechanism of motion. To systematically acquire knowledge in the field, particle based micromotors are compared with tube-shaped motors to see if conclusions obtained for one shape can be adopted for other motor geometries and shapes.



4.3.1 Conferring directionality to micromotors using Janus motors

4.3.1.1 Introducing magnetism

As described earlier a big advance for our micromotors would be the ability to guide and direct them by external means. As explained in part 4.1 magnetism has been found to be the most promising way to control the orientation of motion. In a first attempt we tried to adapt the results of some recent publications ^{1, 2} that described the fabrication of magnetic Janus particles by evaporation of magnetic layer under the protective gold layer. At that time the team around Dr. S. Sanchez published a similar approach to confer "out-of-plane" magnetism to Janus particles, which leads to deterministic behaviour in a magnetic field. This system is based on alternating deposition of Pt and Co in form of a multilayer $[\text{Co}/\text{Pt}]_n$, a method that has been developed for information storage applications ^{3, 4}. The multilayer structure allows coupling of the magnetic moments of the single cobalt layers and therefore the resulting magnetic moment is oriented along the main symmetry axis of the cap structure (see figure 4.3.4). It has been shown that this multilayer coating is applicable to an arrays of spherical particles with sizes ranging from 50 nm to 5 μm without losing its perpendicular magnetic anisotropy ^{3, 4}. As Baraban et al. did we used this approach to create directable micromotors. To ensure that the Janus motors are well directable a more homogeneous motion than can currently be achieved by catalase is desirable and for this reason Pt was chosen as catalyst.

4.3.1.2 Replacing the catalase by Pt catalysts

The overall reaction of the degradation of hydrogen peroxide by Pt is the same as when catalyzed by the corresponding enzyme. As can be seen in figure 4.3.1 the hydrogen peroxide decomposes to oxygen and water, which means more molecules of reaction product are generated than reactants are consumed. The whole process has a ΔH^\ominus of -98.2 kJ/mol and a ΔS of $70.5 \text{ J}/(\text{mol}\cdot\text{K})$ and is therefore thermodynamically favourable. Many transition metals and their composites are good catalysts for this composition, as for example silver, palladium, manganese dioxide or platinum. The multistage decomposition on an iron catalyst was described by Fenton in 1894 and it can be assumed that in presence of a catalyst many of those reactions happen simultaneously ^{5, 6}. This chemical reaction can be used to generate mechanical work from chemically stored energy and it creates an asymmetric distribution of product around the particle.

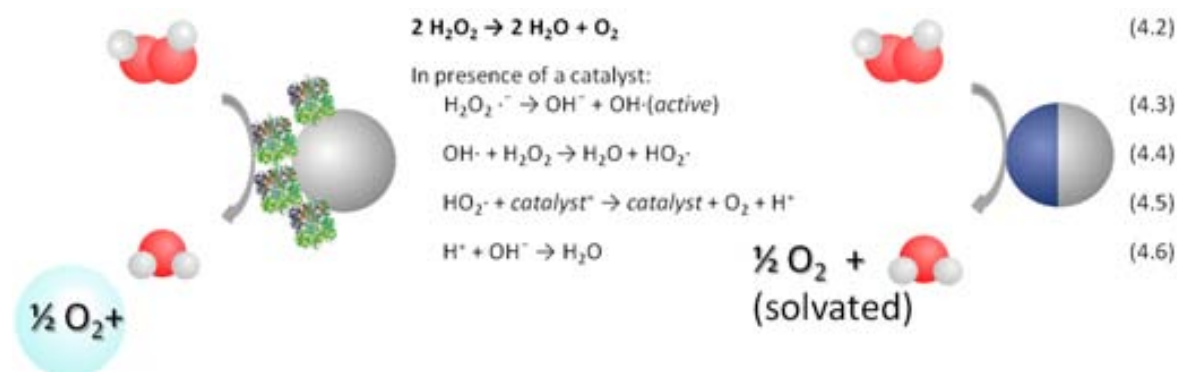


Fig. 4.3.1 Decomposition of peroxide, respectively on catalase and Pt bearing particles and equations summarizing chemical reactions occurring in the process.

4.3.1.3 Mechanism of motion

For the previously described enzyme driven micromotors we found that the movement originated from a constant bubble ejection due to the high catalytic activity of catalase that causes a sufficiently high oxygen volume to saturate the surrounding water and overcome the surface tension. The resulting jet-like mechanism leads to effective movement.

As can be seen from several sources in literature in case of Pt driven micromotors the asymmetric distribution of reaction products leads to a propulsion by a self-diffusiophoretic process⁷. Diffusiophoresis is the propulsion of a particle in a solute gradient, due to interactions between the solute and the particle surface. In self-diffusiophoresis this gradient is created by asymmetric reactions on the surface of the particle itself. For the case of Pt particles Howse *et al.* proposed that an O₂ gradient is responsible for the motion⁷, but other mechanisms as ionic diffusiophoresis or electrophoresis have also been proposed^{6,8,9}. In ionic diffusiophoresis the creation of ions within a chemical reaction leads to an increased concentration of ionic species on the particle surface, causing an ion gradient. Howse *et al.* characterized the diffusiophoretic movement of Janus particles as predominantly directed motion with a velocity depending on the concentration of the fuel concentration for short times, while at long time the motion turns into random walk by rotational diffusion⁷. The same group observed that Janus particles move away from their catalytic Pt patch¹⁰ and found a dependence of particle speed on the particle radius¹¹, a result that can be explained considering the Stokes equation (see chapter 1). All early publications did not achieve long range motion, only enhanced random movements. The first real directed motion was achieved using this approach by Baraban *et al.* combining a macroscopic field with the peroxide based propulsion to obtain fully directed motion⁶. Baraban explained the movement employing a local gradient of the chemical potential around the particle, that resulted in a difference in a pressure difference Δp . On the other hand she also considers a peroxide degradation mechanism as described by Fenton, where charged ions OH⁻ and protons H⁺ were formed around the particle during the reaction. They could induce short time polarization of the particle and possibly could play an important role in an ionic diffusiophoresis based particle propulsion mechanism⁶. Golestanian *et al.* give a detailed explanation of phoretic mechanisms in their paper "designing phoretic micro- and nanoswimmers"¹² and state that for phoretic swimmers the spherical geometry is better than a rod geometry, because the velocity for rods is reduced by an aspect ratio dependent factor¹².

In literature only few examples of jet-mechanism for Pt-driven Janus particles are described. Gibbs and Zhao published in 2009 a work on bubble driven silica particles and discussed the mechanism as a coalescence of concentrated oxygen to bubbles that grow due to a continuous oxygen flow towards the bubble. This growth continues until the buoyancy force wins over surface adhesion and the bubble detaches, conferring a driving force to the particles¹³. Later another particle based micromotor that moved through bubble propulsion was presented by Manjare *et al.* but only particles with diameters larger than 10 μm were found to be bubble driven¹⁴. A system that seems to strongly benefit from the bubble propelled motion are catalytic microtubes. The degradation of peroxide occurs on sputtered catalysts in the inside of the tubes, which spatially confines the reaction products and helps to overcome the surface tension. The first paper on rolled up microtubes by Mei *et al.* found that silver catalyzes peroxide decomposition and bubbles thrust out of the tube causing a fast and directional movement¹⁵. Solovev *et al.* from the same group described the motion of microjets as caused by gas bubbles that eject from one end of the tube.

They found the microjet velocity to be dependent on the product of the bubble radius and the bubble ejection frequency¹⁶. Later also enzyme propelled microtubes were created that still moved by bubble propulsion¹⁷ and other fabrication methods as electrochemical deposition were introduced¹⁸. Zhao's group produced rolled up multilayered heterostructures built up from graphene oxide with a vapour deposited Pt layer at the inside. They have examined the spiral motions of several scrolls and found speed and direction depending on frequency and size of the bubbles, as well as the location of the bubbles with respect to the central axis and other factors¹⁹.



Fig. 4.3.2 Schematic view on the bubble creation inside a microtube, image from Sanchez 2010 #250

4.3.1.4 Role of surfactants in bubble driven motion

It has been claimed that the use of surfactant is necessary in bubble driven catalytic motors in order to reduce the surface tension and stabilize the generated bubbles^{20, 21} and for that a large number of different surfactants have been “randomly” used by different groups. In nearly all papers on microtubes the use of surfactant has been reported and surfactant addition was associated to lower surface tension and a more frequent formation of smaller bubbles¹⁸. As far as known to the authors the only exception was published by Manjare *et al.* who demonstrated the performance of catalytic microparticles¹⁴ and tubular graphene oxide-Ti-Pt engines²² in 5% H₂O₂ without surfactants depending on their geometry. Generally in literature a variety of surfactants have been applied as for example benzalkonium chloride (BACl)²¹, sodium dodecyl sulfate (SDS)²³, the commercial dish soap Fit²⁴, sodium cholate²⁵, isopropanol²⁶, Triton X²⁷. Sanchez *et al.* described the effects of the surfactants as mediator for capillary fluid filling, stabilizer for bubbles and reductor of surface tension without deeper investigation of the detailed effect of the surfactants on the micromotors²⁴. Manesh *et al.* report partially controversial results, as they found reduced speed using surfactant (Triton X). They explained this observation by lower propulsion forces generated by bubbles of smaller radius¹⁸. In spite of this observation of Wang's group the general understanding is that surfactant addition enhances tube performance, as the surfactant Triton X-100 was found "essential for the microengine movement"²⁰. Only very recently Pumera's group analysed the influence of some surfactants on the motion of bubble-propelled tubular microjets²⁸. They observed an enhanced motion of microjets in the presence of SDS, an anionic surfactant. The authors claimed that Tween 20, a non-ionic surfactant with a large molecular mass (four times the mass of the other surfactants employed) slows down the microjets drastically. Their catalytic microjets were not active in cetrimonium bromide (CTAB), a cationic surfactant containing an ammonium moiety with high affinity to platinum, which may be the reason of their surprising results since other cationic surfactants have been previously used in the literature²⁹. As can be seen from chapter 4.1 and 4.2 we obtained bubble driven motion from enzyme based micromotors without adding any surfactant. However in all experiments glycerine was added to reduce excessive motion of the medium and it cannot be excluded that glycerine also lowers the surface tension. In order to evaluate the effects of surfactants in this chapter we compare the behaviour of Pt driven Janus particles and microjets in presence of several kinds of surfactants.

4.3.2 "out-of-plane magnetized" Janus particles as micromotors

4.3.2.1 Fabrication

In figure 4.3.3 Janus particles obtained by evaporation of metallic layers on silica particles are shown, as well as a scheme explaining the evaporation process. It can be concluded that this method is suitable for a wide size range. In the following experiments particles with a diameter of 5 μm are used to ensure good visibility of the motors in optical microscope. Particle monolayers were deposited by drop casting on previously cleaned glass slides. The covering by multilayer stacks as described in 4.3.1 was done in collaboration with Dr. D. Marakov and consists of evaporation of ordered alloys at room temperature in order to obtain the desired high magnetic anisotropy³. The special texture required to stabilize the uniaxial magnetic easy axis perpendicular to the surface on amorphous SiO_2 substrates can be checked by measuring magneto-optical properties of the obtained particles. The results of are displayed in figure 4.3.3. The saturation of all magnetic moments of the particle in a strong magnetic field guarantees that its magnetization will not be affected by weak magnetic fields that it might encounter in a laboratory setup.

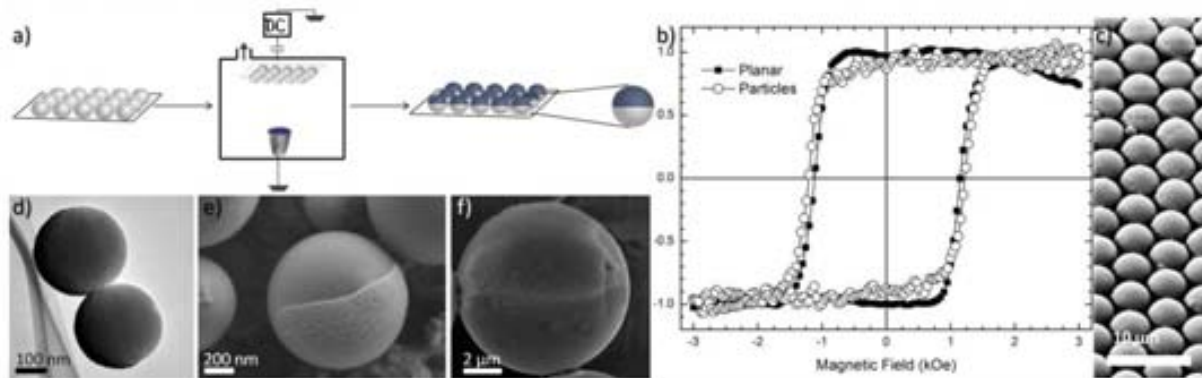


Fig. 4.3.3 a) Scheme of evaporation of metallic layers on monolayers of Janus particles b) magneto-optical measurement of $[\text{Co}/\text{Pt}]_n$ multi-layer evaporation on a flat substrate compared to silica particles c) SEM image of a particle array after evaporation d) TEM image of an initial trial where a metal layer was evaporated on 300 nm silica particles e) SEM image of an initial trial of 1 μm Janus particle with evaporated metal layer f) SEM image image of 5 μm Janus particle with a Co/Pt multilayer.

4.3.2.2 Directing motion

Baraban et al. illustrated the remanent "out of plane" magnetization of the Janus particles using the model in figure 4.3.4. This magnetic state of the particles adopts a preferred orientation in a magnetic field and rotates with the field, which allows deterministic guidance by applying a magnetic field, as is tentatively shown in figure 4.3.4. To avoid magnetic attraction on the particles by a heterogeneous field we had to make sure that the directing conditions were homogeneous. Due to previous experience of the Sanchez group it was known that no complicated setup of magnetic coils is required, but normal Neodyn magnets are sufficient. To check the field conditions and make sure they are nearly homogenous from the particle perspective the properties of the magnets were measured. All experiments were conducted in the lateral zone, 2-5 cm distance of the magnet surface where nearly parallel magnetic field lines can be expected. Measurements on the strongest of the three used magnets gave a difference of the magnetic field of approx. 20 mT per 3 cm (see detailed measurements in chapter 3).

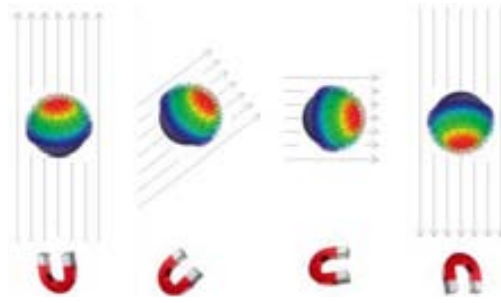


Fig. 4.3.4 The model from extracted from Baraban *et al.* shows schematically the distribution of magnetic moments in the cap at remanence after magnetic saturation and we show the behaviour of the corresponding capped Janus particles in a rotating magnetic field.

This is an average change of 0.0033 mT/particle length, that might be neglected. Blank experiments placing motor particles in this magnetic field without fuel showed, that particles string up, but no movement can be observed (showed in figure 4.3.5 a). So it can be assumed that the local magnetic field experienced by the particle is nearly homogeneous, due to the macroscopic dimensions of the magnet. As control experiment the micromotors were placed in peroxide fuel in absence of a magnetic field and as expected only random movement was observed. The combination of peroxide fuel to propel particles and magnetic field for directionality led to controlled movement of Janus particles. In figure 4.3.5 c) several states of particles moving in a magnetic field that changes direction are shown. Changes of the orientation of the magnetic field cause an increased energy content that is minimized by particle rotation as the magnetization of the particles was fixed by exposing them to a very strong magnetic field. Thus a deterministic motion can be caused by applying a weak homogeneous field.

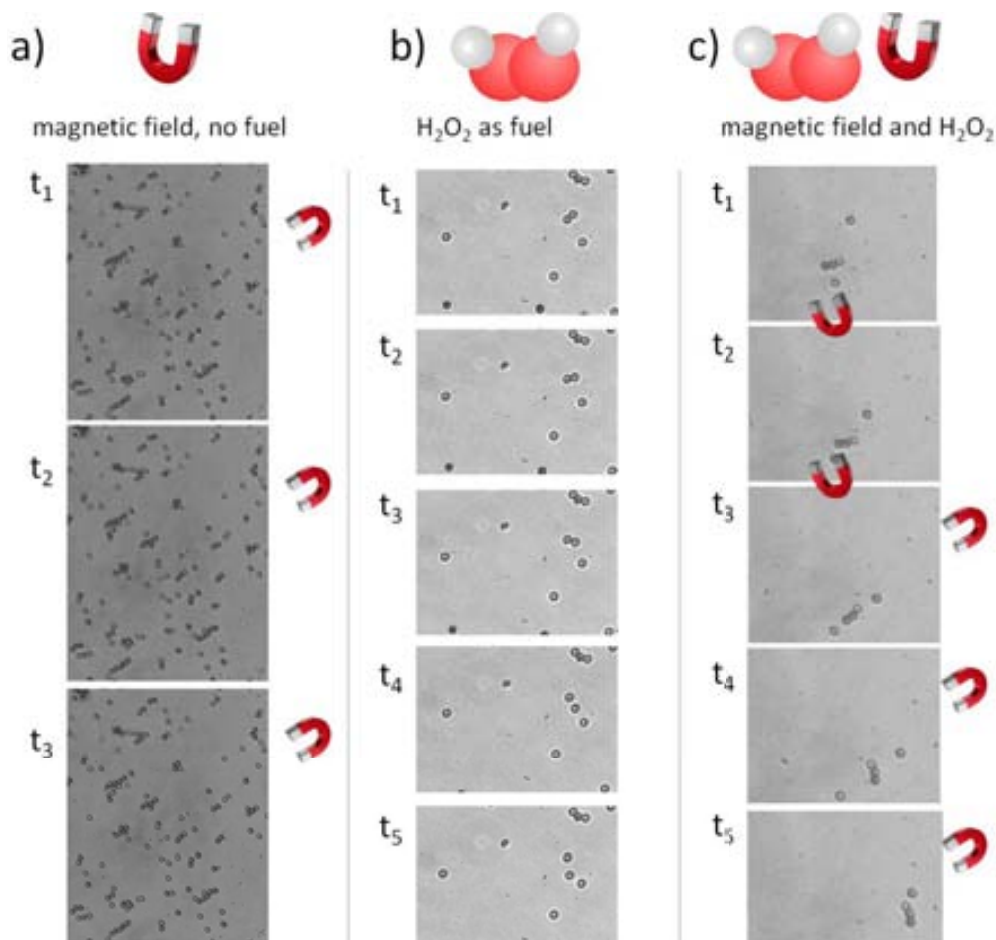


Fig. 4.3.5 a) particles string in the homogeneous magnetic field, but do not move as no driving force is generated b) particles move randomly c) constant movement which is directed by external magnetic field.

4.3.4 Studies of micromotor motion

4.3.4.1 Particles vs. tubes in diluted peroxide solutions

In this first part the motion of catalytic motors in pure diluted peroxide is characterized and in the following those results are compared with surfactant containing solutions. Firstly microjets movement obtained at equal concentrations of peroxide are compared to the motion of catalytic Janus particles. Figure 4.3.6 displays the speed of tubes and particles as a function of H_2O_2 concentration without any surfactant considering both, absolute values and values relative to their catalytic area. Up to our knowledge, most previous publications on microjets use surfactant containing fuel solutions so those results can hardly be compared to any previous results. In figure 4.3.6 only tubes moving through a bubble propelled mechanism are considered, in a surfactant-free hydrogen peroxide solution the jets do not show any movement at concentrations lower than 5% H_2O_2 . Anyhow at 2 and 5% of peroxide some jets start producing bubbles (see table 4.3.1), but those bubbles do not have enough propulsion force to push tubes forward because they cannot detach from the exit of the tube, thus they are not generating jet force. When increasing the concentration of peroxide to 10% for the microjets a very interesting observation was made: about half of the observed microtubes move without bubbles, the rest move by bubble propulsion. The microjets that move without visible bubbles in 10 % H_2O_2 display a much lower average speed (60 $\mu\text{m/s}$) compared to bubble propelled jets (220 $\mu\text{m/s}$, data not shown). These results demonstrate that jets can move without surfactant, which made us suspect that two different mechanisms (phoretic and bubble propelled mechanism) may coexist depending on the fuel conditions, similar to what Wilson *et al.* described for artificial stomatocytes³⁰.

Table 4.3.1 Percentage of tubes producing bubbles, * marked items produced bubbles but did not move

H_2O_2 Concentration %	2	5	10	20	30
Percentage of bubbling tubes	25*	46*	50	100	100

It is accepted that in the absence of surfactants the bubbles tend to be larger than with surface tension decreasing agents and less frequent, which seems not to be the optimal case for motion at low Reynolds numbers^{24,31}. At higher hydrogen peroxide percentages the local concentration of O_2 is high enough to overcome surface tension and form bubbles that continuously propel the tubes, so that the speed value for bubbling tubes in pure peroxide solution is comparable to the speed obtained in most surfactant containing solutions (see figure 4.3.8), what might be seen as supporting information for the previously presented hypothesis. Janus particles also increase their speed with increasing fuel concentration, but only up to a threshold similar to the Michaelis Menten-like limit for enzymes⁷. The speed behaviour for particles is in quite good accordance with data published previously by Howse *et al.*⁷. Although the absolute values they reach are much lower than those of microjets (figure 4.3.7 a), the trend of relative speed per catalytic area totally changes: At low concentrations of H_2O_2 Janus particles present higher relative speed, whereas bubble propelled microtubes only start to self-propel at 10% peroxide, where coincidentally similar relative values are obtained for both types of micromotors. Figure 4.3.7 b indicates that specifically at low concentration surfactant-free conditions the underlying mechanism is more efficient for particle geometry per equal surface area.

As our particles do not produce any visible bubbles and the production of nano-sized bubbles is highly unlikely as a very high surface tension would have to be overcome, the mechanism for particle movement cannot be described as bubble propulsion. Currently, the most accepted theory to explain particle motion is the ratio of reactants to products (2:3), which produces a difference in entropy around the particle, leading to an osmotic pressure impelling the particle, i.e. diffusiophoresis^{12, 32, 33}. A related assumption is the occurrence of a driving force due to a localized gradient of oxygen molecules (leading equally to self-diffusiophoresis) and recent papers indicate that some electrokinetic mechanism may also be present^{8, 9}. In contrast to spherical particles, propulsion of Pt-tubes has been largely accepted to be due to bubble formation.

Mallouk *et al.* reported the evaluation of micromotor performances by comparing the mechanical power output of a given micromotor with its total chemical power input and identified some sources of energy loss, especially for electrophoretically moving nanorods³⁴. Their comparison with other motor types such as catalytic microtubes and helical magnetical motors lead to the conclusion that

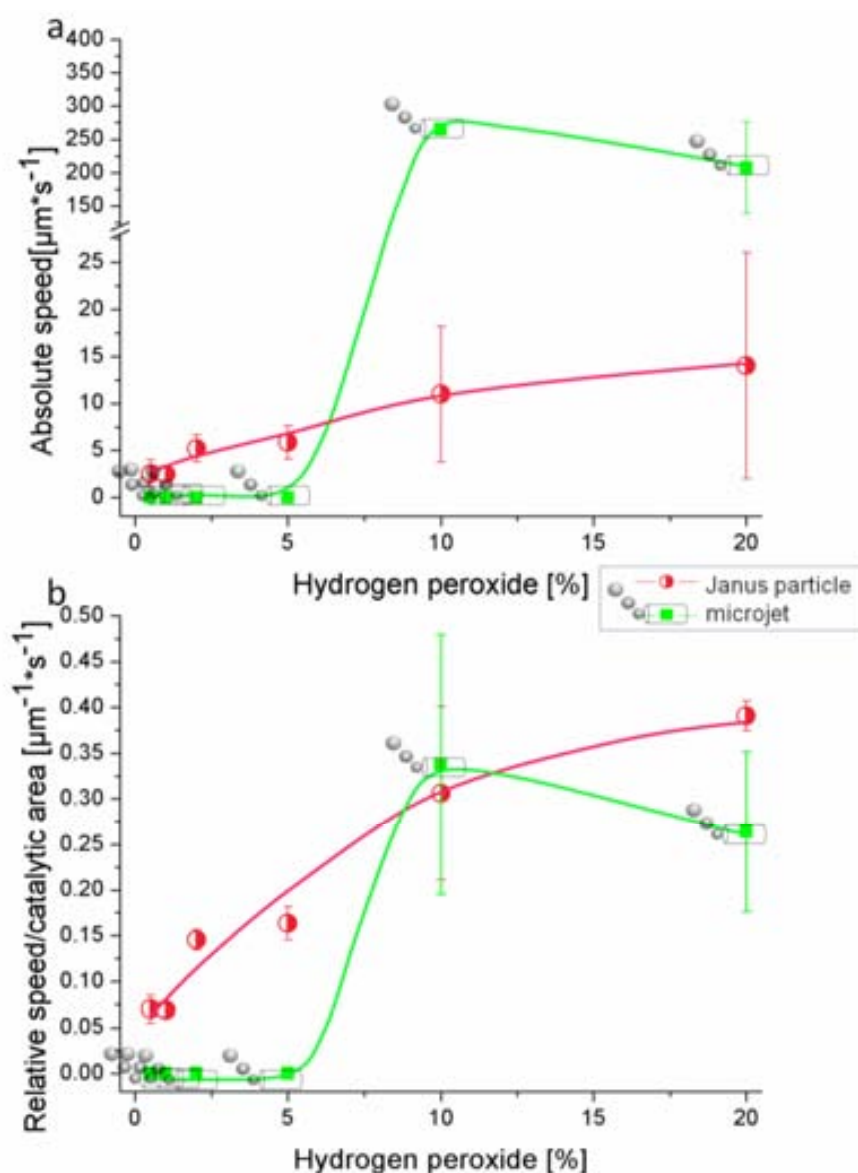


Fig. 4.3.6 Displays the speed of tubes and particles both in absolute values a) and relative to their catalytic area b) as a function of H_2O_2 concentration without any surfactant.

both are more efficient than self-electrophoretic motors. Considering relative speed values their affirmation that bubble propulsion is more efficient than phoresis-based mechanisms could not be confirmed in our comparative work when only H_2O_2 is employed as fuel component³⁴.

4.3.4.2 Particles vs. tubes in presence of surfactants

Four tensides were selected, representing different surfactant classes: Triton X as non-ionic, SDS as anionic and BACl as cationic surfactant, as well as FIT as an example of a commercially available mixture of anionic surfactants (dish soap). The surfactants were particularly selected in order to diminish specific interaction as metal-specific absorption. Even though we used a quarternary ammonium salt as positive surfactant, this group is sterically hindered by a long alkylic chain. At the same time we chose surfactants with relatively similar properties considering molecular mass and functional groups.

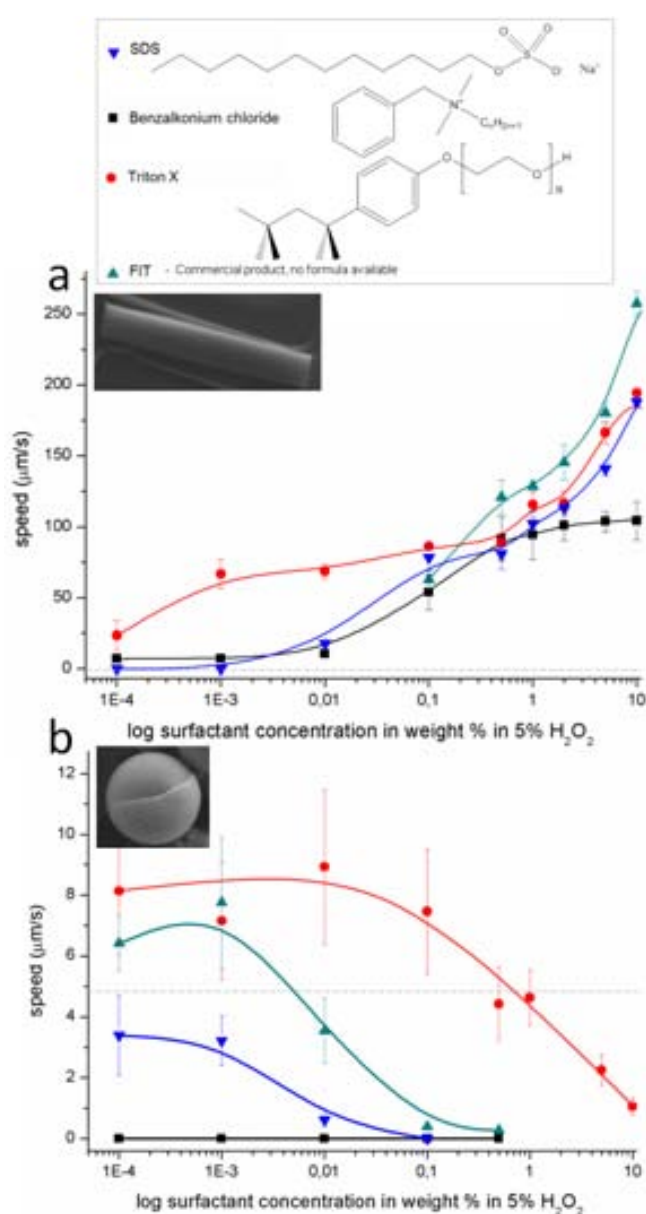


Fig. 4.3.7 Effect of surfactant concentration in 5% H_2O_2 solution on average speed of Pt-microtubes: a) and Pt covered microparticles b); dotted lines depict the maximum speed at surfactant free conditions Inset: chemical structures of Triton X (non-ionic), SDS (anionic), BACl (cationic), Fit (mixture of surfactants).

The experiments for figure 4.3.7 were performed in distilled water containing 5% H₂O₂ and surfactants in a concentration range between 0.0001 wt.% and 10 wt.%. Microjet speeds, as displayed in figure 4.3.7 a, increase with higher surfactant concentration following different increasing trends. This phenomenon can be explained by a tension-reducing effect by the surfactant which is necessary to enable bubble formation in tubular structures which rapidly leave the cavity of the tube. The addition of surfactant to the peroxide solution affects the speed of Pt-covered Janus particles in an entirely opposite fashion starting at very low concentrations: from surfactant concentrations of only 0.5 % the particle speed does not achieve as high values as without surfactant. First assumption was the passivation of Pt similar to the passivation by thiols²⁶ but the strong motion inhibiting effect of soap on particles might be only partially due to coverage of the catalytically active Pt. The critical micelle concentration of these surfactants (SDS: 0.23 wt.%, TritonX: 0.22 wt.%, BACl 0.205 wt.%³⁵) does not seem to have an important impact neither on the surface potential nor on the speed behaviour. This should be interpreted as a strong indication that a poisoning effect

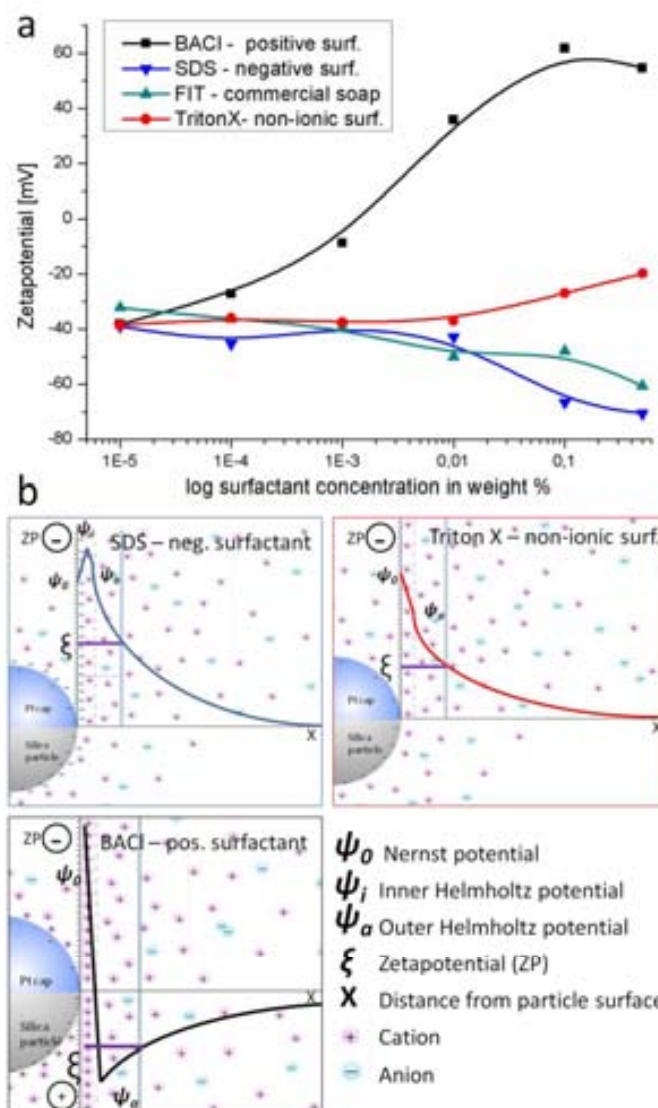


Fig. 4.3.8 Effect of surfactant concentration in water on Zetapotential of Pt covered Silica particles. b) Basic fundamentals on ZP theory are displayed to give an explication of changes in particle surroundings and Zetapotential, induced by a negatively charged surfactant SDS, non-ionic surfactant Triton-X and a positively charged surfactant BACl, (for more information see reference 36)

through the coverage of Pt with surfactant molecules only plays a partial role in the mechanism (compare with reference ²⁶). Another possible reason might lie in the mechanism of motion. The reason for particle movement excludes bubble propulsion since no bubbles are visible. In very recent papers self-electrophoretic mechanisms have been introduced into the discussion about the motion of Janus particles ^{8, 9}. All those results together with our data presented here might lead to the conclusion that more than one mechanism is overlaid and responsible for the motion. The propulsion has to be attributed to phoretic mechanism either caused by oxygen gradients or to ionic gradients caused by the reaction product ratio.

To estimate the impact of surfactant molecules on the ionic properties of the solution we measured the Zetapotential (ZP) of the Janus particles in different surfactant solutions. The measurements confirm that the surfactants have a strong influence on the particles' surface properties as displayed in figure 4.3.8. Diluted suspensions of Pt-covered particles in deionized water were placed in a disposable cell in an alternating electrical field, generated by the Zetasizer (Malvern Instruments). The electromagnetic field causes electrophoresis and through optical interaction with laser light the mobility of particles is determined, from which the ZP can be calculated ³⁶.

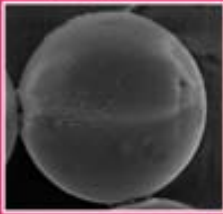
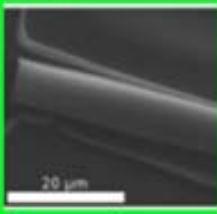







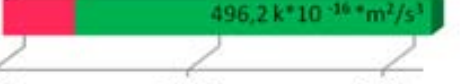
The initial value of the ZP at extremely low surfactant concentration coincides with the ZP value measured in pure water at around -40 mV, which is mainly due to the silanol groups on the particle surface. This value was compared to non covered Silica particle, which shows a slightly more negative potential (data not shown). The effects of the four tensides were very different from each other:

The non-ionic Triton X did hardly induce any changes in the Zetapotential until added concentrations reached 0.01 wt.% when the value shifts towards more neutral values (an expected behaviour at high concentrated solutions caused by compression of the double layer). The motion was almost unaffected at low concentrations and then speed slowly decays. At very high concentrations (1-10 wt.% Triton X) the reduction of speed might be due to viscosity changes. SDS constantly increases the negative ZP down to -70 mV. Strong inhibition of motion is found using SDS as anionic surfactant, concentrations as low as 0.5 wt.% completely stalled particle motion. FIT also causes higher absolute ZP values up to -65 mV. FIT slows particles down at concentrations higher than 0.001 wt.%. This behaviour is due to the inclusion of the anionic species into the electrochemical double layer (see figure 4.3.8 b). The strongest changes can be observed in presence of the cationic surfactant BACl. A concentration of 0.01 wt.% of that surfactant not only neutralized but inversed the negative Zetapotential of the half-covered Pt-particles. At the same time addition of this cationic surfactant Benzalkonium chloride inhibited any movement even at a concentration of only 0.0001 wt.%. Due to the negative surface charge of the silica particles additional electrostatic interactions increase the impact of positive surfactants on the double layer (inner and outer Helmholtz-layer, see figure 4.3.8 b) compared to neutral (Triton X) or anionic molecules (SDS) since they strongly alter the total charge of the particle surface area. As previously described, the results of the ZP measurements fit well with the speed changes of the motors, i.e. those surfactants that strongly affected the speed also provoked significant changes in the absolute Zetapotential values and vice versa. For an explanation we might assume that the particle movement is provoked at least partially by an ion gradient (ionic diffusiophoresis) created by the multistage decomposition of hydrogen peroxide in presence of Pt which involves the formation and decomposition of negative peroxide radicals ^{6,5}. This means that the gradient has to be built up in a highly charged medium in case of SDS, FIT and BACl, lowering the relative intensity of the gradient and therefore probably the propulsion force for microparticle movement. Those experiments may help to elucidate this current discussion in the literature about the mechanism of movement of catalytic Janus particles.

4.3.4.3 Comparisons particles vs. tubes

As we could observe, the optimal working conditions for both systems differ. While in microtubular jets the presence of a surfactant is essential to reduce surface tension and allow liberation of bubbles, in a spherical particle system the same molecules slow down the movement or even stop it completely. We compared the performance of both motor classes at “optimal” conditions: optimal particle velocities are extracted from experiments in a 5% H₂O₂ solution in pure water.

Table 4.3.2 Comparison of speed, object length, volume, weight and engine power of Pt Janus particles and Pt microtubular jets

Parameter		Janus particles	Microjets
SEM image			
Motor weight	[*10 ⁻¹⁰ mg]	1.64	2.98
Catalytic surface	[μm ²]	39.27	785.39
weight/catalytic surface	[10 ⁻¹³ mg/μm ²]	41.81	3.79
5% H₂O₂ without surfactant			
speed	[μm/s]		
speed/body length	[bl/s]		
speed/catalytic area	[1/(μm*s)]		
Engine power	[k*10 ⁻¹⁶ *m ² /s ³]		
5% H₂O₂, 5% Triton X			
speed	[μm/s]		
speed/body length	[bl/s]		
speed/catalytic area	[1/(μm*s)]		
Engine power	[k*10 ⁻¹⁶ *m ² /s ³]		

”engine power” = (Force*way)/ time = speed*weight*const in m/s²
 const corresponds to acceleration

Comparing maximum average speeds (data from figure 4.3.6 and 4.3.7) the used microtubes were almost 20 times faster than particles of comparable diameter. We decided to use the concept of "engine output"³⁷ or power as the probably most comparable parameter, evaluating the approximate work the microscale objects perform for their displacement per time unit. As "optimal" tube conditions, we analyzed experiments performed at 5% H₂O₂ solution, containing 5% surfactant. Those values reveal that in presence of surfactants the microtubular jet is more powerful than particles, using the same catalyst and fuel, while in surfactant free conditions particles perform better. The bubble-propulsion mechanism seems to yield in a more efficient drive than propulsion through gradient differences. Evaluating velocity/aspect ratios Howse et al.⁷ reached the conclusion that spherical geometry is better than rod like micromotors, but as geometries and hydrodynamic effects are not comparable at all, we see "engine power" as a probably more meaningful parameter. This is supported by Mallouk's group's latest work - the evaluation of the motor's "power conversion efficiency" and comparison of this Comparing maximum average speeds (data from figure 4.3.6 a and 4.3.7) the used microtubes are almost 20 times faster than particles of a comparable diameter. parameter for several kinds of motors³⁴. Their publication concludes that bubble driven motors have very low efficiencies, as most of the existing motors do today. To improve the performance of motors, Mallouk and co-workers expose several stages where energy is lost to other phenomena than movement. Assuming that bubble formation is one of those critical points adding surfactant helps the bubble formation and reduces the surface tension assisting the release of bubbles freely from the tubes. As the motion is based on bubble release the higher the frequency of bubbles the higher the speed of motion¹⁶. As can be seen in the data shown in Table 4.3.2 (green data) the speed and the engine power of tubes increases drastically after surfactant addition. The opposite conclusion can be drawn for particles. In this case the mechanism is highly probable to be ionic self-diffusiophoresis. Following Mallouk's argumentation it might be said that surfactant addition leads to less efficient creation of gradients, resulting in a lower power conversion, that is reflected in slower movement and worse "engine power" of microparticles.

4.3.5 Movement of thiol modified particles vs. tubes

After several days of storage the catalytic activity in both, microjets as well as Janus particles, decreased until almost complete stopping of any observed motion. This can be associated to passivation of Pt, probably by carbon monoxide or organic components that might deposit on the Pt surface. Pt is considered a noble metal in the chemical way, but the physical definition only considers materials that have all their d-bands completely filled as noble metals. In Pt two d-bands cross the Fermi level, therefore Pt does not fulfil this condition, which affects the chemical behaviour and may lead to a quick coverage of Pt by CO. To reactivate the particles' catalytic ability it was found sufficient to apply two minutes of O₂-plasma cleaning to remove all deposited material. Those findings led to the assumption that Pt might be passivated by different solutes in the media and further passivation experiments were initiated. The surface of Pt-covered particles was modified with 11-Mercaptoundecanoic acid (MUA). The mercapto-group of this molecule self-assembles on platinum, inhibiting so the availability of Pt as a catalyst and reducing/stopping the speed of the particle movement in H₂O₂.

Very similar results could be obtained functionalizing Pt covered tubes with MUA. As synthesized the tubes started producing bubbles, creating a force to detach from the cover slide and move around freely in the solution (see figure 4.3.10 b). After functionalization with MUA we observed a complete inhibition of bubble production and much less movement or detachment of the microtubes from their substrate. In figure 4.3.10 b (top) we see time lapse pictures of a detached tube, moving through impulses from bubble creation. Figure 4.3.10 (bottom) shows an array of MUA functionalized tubes in a solution 5% H₂O₂, 5% SDS. Neither bubble formation nor detachment of the tubes can be observed.

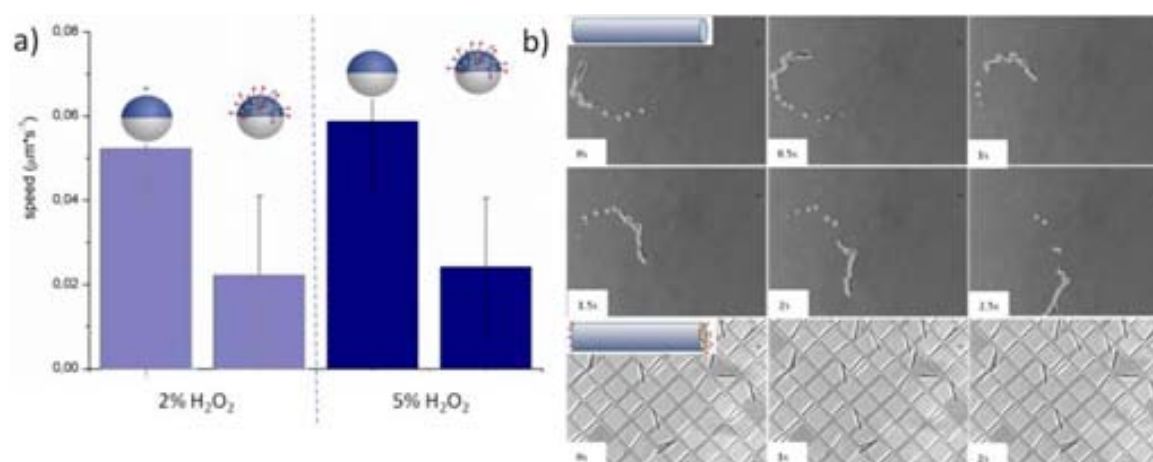


Fig. 4.3.10 Effects of MUA functionalization on average velocity of a) microparticles and b) Pt-microtubes (5% H₂O₂, 5% SDS). Janus particles show reduced speeds whereas tubes are completely stalled.

Apparently the passivation effect seems to be stronger in tubes, which might be due to the labile nature of the sulfo-bonding on a Pt surface. This bonding is susceptible to oxidation by higher quantities of H₂O₂, leading to a partial degradation of the MUA-layer on the particle surface. However, in the cavity of the microtube those bonds might be protected from oxidation and maintain so a higher covering with MUA. Mercapto groups tend to have a very high affinity to gold and Pt-surfaces.

4.3.6 Summary

In this chapter we presented the outcomes of a collaboration with the Sanchez' group, that was started to introduce directionality to our micromotors. The provided material enabled us to successfully direct the motion. Commercial 5 μm Silica particles were covered by a multilayer stack of [Co/Pt]₅ conferred defined "out-of-plane" magnetic properties to those Janus particles. In experiments with a combination of peroxide and an external magnetic field it could be shown that the motion can be directed by changing the orientation of a homogeneous magnetic field. This new kind of micromotors does not rely on enzyme catalysis any more, but the enzyme is replaced by Platinum as an inorganic catalyst for peroxide degradation. The found movement is more uniform and predictable, properties that enable us to properly characterize the movement and compare it with microjets as another type of micromotors. Even if the catalytic mechanism that is found on Pt surfaces is always the same the geometry and character of the motor have great impact. If the Pt is deposited on a conducting material electrophoretic mechanism causes movement, in case of

catalysis in a confined space as a microtube bubble formation is favoured, whereas the same material deposited on particles leads to gradient based movement. To contribute to the pool of micromotor knowledge the movement of spherical and tubular micromotors in surfactant free H₂O₂ solutions was characterized and compared. To improve their performance the surfactant free motion was compared to analogous experiments performed in different surfactant containing fuel solutions. Pt-microjet velocity benefits strongly from the addition of surface tension reducing agents such as SDS, Triton X or BACI to enhance bubble formation in order to propel the tubes, an effect that can be obtained as well by increasing the peroxide percentage. Observation on self-propelled non-bubbling tubes in pure diluted peroxide solutions may indicate that various mechanisms could contribute to motion. However to completely clarify this issue further investigations are needed.

In case of Janus particles the motion and the Zetapotentials were shown to be strongly influenced by the different kinds of surfactants. Therefore this study can be seen as evidence of ionic self-diffusiophoresis or as one motion mechanism in microparticles. The here presented results show however that the assumption of one single mechanism for particle propulsion should be revised. To explain the observed phenomena bubble-free tube movement and inhibition of particle movement by surfactants overlaid mechanisms are more adequate. Nonetheless, theoretical studies are needed to fully understand those observations.

The presence of thiol groups was found to have passivating effects on both, particles and tubes as previously found by Pumera's group²⁶. The effect on tubes was stronger than the effect on particles as the same concentration led to complete tube passivation while particles only slowed down. This was tentatively associated to partial oxidation of thiol groups by peroxide that is expected to be less pronounced in tubes as the surface is less accessible.

4.3.6 Literature

1. Smoukov, S. K.; Gangwal, S.; Marquez, M.; Velev, O. D. *Soft Matter* **2009**, 5, (6), 1285-1292.
2. Ren, B.; Ruditskiy, A.; Song, J. H.; Kretschmar, I. *Langmuir* **2011**, 28, (2), 1149-1156.
3. Marakov, D. CoPt and FePt magnetic alloys grown on van der Waals WSe₂(0001) surfaces and on arrays of SiO₂ spherical particles. doctoral, Universität Koblenz, Koblenz, 2008.
4. Albrecht, M.; Hu, G.; Guhr, I. L.; Ulbrich, T. C.; Boneberg, J.; Leiderer, P.; Schatz, G. *Nat Mater* **2005**, 4, (3), 203-206.
5. Fenton, H. J. H. *Journal of the Chemical Society, Transactions* **1894**, 65, (0), 899-910.
6. Baraban, L. Capped Colloids as Model Systems for Condensed Matter. University of Konstanz, Konstanz, 2008.
7. Howse, J. R.; Jones, R. A. L.; Ryan, A. J.; Gough, T.; Vafabakhsh, R.; Golestanian, R. *Physical Review Letters* **2007**, 99, (4), 048102.
8. Brown, A. T.; Poon, W. C. K. *cond-mat. soft* **2013**, arXiv:1312.4130.
9. Ebbens, S.; Gregory, D. A.; Dunderdale, G.; Howse, J. R.; Ibrahim, Y.; Liverpool, T. B.; Golestanian, R. *cond-mat. soft* **2013**, arXiv:1312.6250.
10. Ebbens, S. J.; Howse, J. R. *Langmuir* **2011**, 27, (20), 12293-12296.
11. Ebbens, S.; Tu, M.-H.; Howse, J. R.; Golestanian, R. *Physical Review E* **2012**, 85, (2), 020401.
12. Golestanian, R.; Liverpool, T. B.; Ajdari, A. *New Journal of Physics* **2007**, 9, (5), 126.
13. Gibbs, J. G.; Zhao, Y.-P. *Applied Physics Letters* **2009**, 94, (16), 163104.
14. Manjare, M.; Yang, B.; Zhao, Y. P. *Physical Review Letters* **2012**, 109, (12), 128305.
15. Mei, Y.; Huang, G.; Solovev, A. A.; Ureña, E. B.; Mönch, I.; Ding, F.; Reindl, T.; Fu, R. K. Y.; Chu, P. K.; Schmidt, O. G. *Advanced Materials* **2008**, 20, (21), 4085-4090.

16. Solovev, A. A.; Mei, Y.; Bermúdez Ureña, E.; Huang, G.; Schmidt, O. G. *Small* **2009**, 5, (14), 1688-1692.
17. Sanchez, S.; Solovev, A. A.; Mei, Y.; Schmidt, O. G. *Journal of the American Chemical Society* **2010**, 132, (38), 13144-13145.
18. Manesh, K. M.; Cardona, M.; Yuan, R.; Clark, M.; Kagan, D.; Balasubramanian, S.; Wang, J. *ACS Nano* **2010**, 4, (4), 1799-1804.
19. Yao, K.; Manjare, M.; Barrett, C. A.; Yang, B.; Salguero, T. T.; Zhao, Y. *The Journal of Physical Chemistry Letters* **2012**, 3, (16), 2204-2208.
20. Kagan, D.; Campuzano, S.; Balasubramanian, S.; Kuralay, F.; Flechsig, G.-U.; Wang, J. *Nano Letters* **2011**, 11, (5), 2083-2087.
21. Sanchez, S.; Solovev, A. A.; Schulze, S.; Schmidt, O. G. *Chemical Communications* **2011**, 47, (2), 698-700.
22. Manjare, M.; Yang, B.; Zhao, Y. P. *The Journal of Physical Chemistry C* **2013**, 117, (9), 4657-4665.
23. Zhao, G.; Sanchez, S.; Schmidt, O. G.; Pumera, M. *Chemical Communications* **2012**, 48, (81), 10090-10092.
24. Sanchez, S.; Ananth, A. N.; Fomin, V. M.; Viehrig, M.; Schmidt, O. G. *JACS* **2011**, 133, (38), 14860-14863.
25. Garcia, M.; Orozco, J.; Guix, M.; Gao, W.; Sattayasamitsathit, S.; Escarpa, A.; Merkoci, A.; Wang, J. *Nanoscale* **2013**, 5, (4), 1325-1331.
26. Zhao, G.; Sanchez, S.; Schmidt, O. G.; Pumera, M. *Nanoscale* **2013**, 5, (7), 2909-2914.
27. Gao, W.; Pei, A.; Wang, J. *ACS Nano* **2012**, 6, (9), 8432-8438.
28. Wang, H.; Zhao, G.; Pumera, M. *The Journal of Physical Chemistry C* **2014**, 118, 5268-5274.
29. Solovev, A. A.; Sanchez, S.; Pumera, M.; Mei, Y. F.; Schmidt, O. G. *Advanced Functional Materials* **2010**, 20, (15), 2430-2435.
30. Wilson, D. A.; de Nijs, B.; van Blaaderen, A.; Nolte, R. J. M.; van Hest, J. C. M. *Nanoscale* **2013**, 5, (4), 1315-1318.
31. Purcell, E. M. *American Journal of Physics* **1977**, 45, (1), 3-11.
32. Anderson, J. L. *Annu. Rev. Fluid Mech* **1989**, 21, (1), 61-99.
33. de Buyl, P.; Kapral, R. *Nanoscale* **2013**, 5, (4), 1337-1344.
34. Wang, W.; Chiang, T.-Y.; Velegol, D.; Mallouk, T. E. *JACS* **2013**, 135, (28), 10557-10565.
35. Aldrich, S., Product sheets SDS, Benzalkonium chloride, Triton X. 2013; pp Product sheets SDS, Benzalkonium chloride, Triton X.
36. Mueller, R. H., *Zetapotential und Partikelladung in der Laborpraxis – Einführung in die Theorie, praktische Meßdurchführung, Dateninterpretation* Wissenschaftliche Verlagsgesellschaft Stuttgart, 1966; p 254.
37. Becker, F.-M.; Boortz, G.; Dietrich, V.; Engelmann, L.; Ernst, C.; Fanghängel, G.; Höhne, H.; Lenertal, R.; Liesenberg, G.; Meyer, L.; Pews-Hooke, C.; Schmidt, G.-D.; Stamm, A.; Weber, K., *Formeln und Tabellen für die Sekundarstufe I und II*. 6th ed.; PAETEC Gesellschaft für Bildung und Technik mbH: Berlin, 1996.

4.4 Light driven micromotors

In the field of micromotors many efforts are taken to find a substitute for peroxide as fuel. Most approaches turn towards other high energy chemicals as hydrazine etc. but here we want to introduce an energy source that is widely used in nature: light. Light is an ideal source of energy and some materials are able to harvest this energy directly by undergoing chemical changes. Unfortunately silicon dioxide that until now was an ideal base for catalytically driven micromotors does not present any photosensitivity. Therefore we switched to silver chloride, a material that is known for its photochemical transitions that form the base of many of its applications. One observed process after light exposure is surface modification. Here we present endeavours to use those processes to create motion at the microscale.



4.4.1 State of the art - light driven micromotor

Light is considered to be a very attractive fuel for micromotors as it originates from a renewable source as the sun, does not generate any waste and it is very precisely controllable and easy to manipulate. One of the earliest works that generate motion from light was published in 1984 when Shinkai *et al.* used the photoisomerization of azobenzene to create molecular motion ¹. In the following decades several more systems based on molecular switches or light sensitive materials have been developed. A good overview is given in a recent review ² but those works shall not be discussed in detail as the dimensions and mechanisms do not coincide with those used in this thesis. Only in 2009 Ibele *et al.* found that AgCl particles move autonomously in deionized water when exposed to UV-light. The authors attribute this movement to asymmetric photodecomposition of the particles that creates a localized electrolyte gradient around the particle, resulting in self-diffusiophoresis. Furthermore they characterized collective behaviour and interactions of the AgCl with silica beads that are added as tracing particles ³. This work was continued and resulted in an additional publication on collective oscillations of those particles that rise from a multistep decomposition of AgCl, leading to a silver plated surface of the particles ⁴. Silver is known to oxidize in the presence of peroxide, so that both overlaid reactions result in two countervailing reactions:



To gain further insights into the mechanisms of those oscillations the reaction of silver disks lithographically patterned onto SiO₂ were exposed to similar conditions and oscillations of tracer particles could be observed ⁴. A later work classifies the silver chloride particles after their proximity between them as isolated, coupled or schooled particles to analyze their motion patterns ⁵. They realized that even though the particles' density is much higher than water, particles did not settle directly on the glass slide but few microns above. While isolated particles show behaviour similar to Brownian motion in both, absence and presence of UV light, coupled particles show significantly higher diffusion constants. This article showed clearly that the neighbouring particles have an important influence on the active diffusion of AgCl particles. The same group has used a similar formula to show the micromotor behaviour in response to stimuli as NH₃ addition or removal ⁶. The addition of NH₃ provokes exclusion zones, while evaporation of NH₃ seems to induce collective behaviour. UV light also induces clustering, both phenomena originate from partial solution and therefore gradient formation that causes phoretic motion.

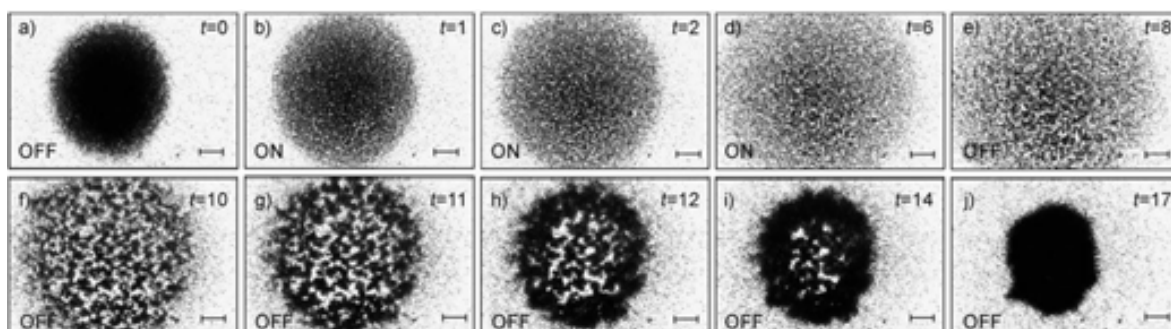


Fig. 4.4.1: a) AgCl particles previously exposed to UV light are observed under visible light. b-d) the UV light is turned back on and the interparticle spacing expands. e- j) the UV light is turned off again and the interparticle spacing diminishes again. Times are given in the upper right corner(t; seconds), the status of the UV light is given in the lower left corner. Scale bars: 20 mm, from reference 3.

Due to serendipity in a sideproject we discovered a novel synthesis for micrometer sized homogeneous AgCl particles and in this chapter we want to describe and characterize them and establish their use as AgCl micromotors.

4.4.2 State of the art - environmental applications of micromotors

Lately micromotors started gaining new applications in environmentally important fields, as monitoring, oil removal or pollutant degradation. To monitor pollutants, e.g. heavy metals or sodium azide Orozco *et al.* investigated the direct correlation of their concentration to bubble frequency and motility changes of artificial microfish ⁷. This work was followed by an article of Pumera's group, that reported the passivation of micromotors depending on the additive (thiols, amines) in solution ⁸ and in a later work they analyzed the effect of selected surfactants on tubes ⁹ which enables scientists to use micromotors for analysis of waste water quality. A further environmentally important approach was presented by Guix *et al.* who used microtubes covered by an organic self-assembled monolayer of different alkanethiols to remove oil from water samples ¹⁰. Also Janus particles based on magnesium decomposition in sea water were functionalized with alkanethiols and used to capture oil droplets. This last example is able to use the seawater itself as fuel, causing oxidation of magnesium that produces oxygen bubbles ¹¹. With the same scope Pumera *et al.* employed polysulfone capsules as a different kind of micromotors to shepherd oil droplets in the swimming medium ¹². The on board carrying of catalytically active substances introduces the possibility to use micromotors for waste water cleaning as shown by Soler *et al.* benefitting from the Fenton effect of a catalytic iron layer on the outside of microtubes ¹³. The importance of this new applications for micromotors as "smart devices" able to reach small pipes or cavities in waste water systems is reflected in recent reviews ^{14, 15}.

4.4.3 Properties of AgCl

Silver chloride (AgCl) structures have found widespread applications in many areas of our daily life, from photographic paper and photochromic lenses to medical materials, antiseptic catheters, bone cements and others ¹⁶⁻¹⁹. As this material is known to be light sensitive many traditional applications are based on that, with photography being its best-known example.

4.4.3.1 Degradation of pollutants

AgCl is known as an excellent photocatalyst for degradation of organic molecules ²⁰⁻²³ and therefore we want to show that the use of light driven AgCl micromotors bears advantages for the simultaneous decomposition of organic compounds. Non-biodegradable organic compounds are one of the major problems in waste water treatment, for example in a study published in 2005 in Oregon the authors found several indicators of human interference in the analyzed water. Amongst the detected substances were pharmaceuticals, cosmetic compounds, plasticizer and detergents ²⁴, whereas manifold organic pollutants are also found in industrial wastewaters ²⁵. Several methods are employed today to treat those residues, where the most common are probably coagulation and oxidation techniques ²⁵. Additionally in waste water treatment the most widespread practices are based on chlorine gas or sodium hypochlorite but they are more and more replaced by UV treatment to disinfect sewage water, considering that the UV light causes less possible side effects and no remaining toxic side products.

4.4.3.2 Antibacterial properties

Silver and its compounds have been known for centuries to inhibit antibacterial properties which implied that food containers and goblets were often made from silver. Lately scientists got interested in the interactions of AgNP and cell membranes that probably cause toxicity. However the mechanism for toxicity in silver macro objects is different: both, AgCl and Ag release small quantities of Ag^+ that inhibit bacterial growth; in AgCl there is a high probability that even Cl^- contributes to the effect. In AgNP it is believed that the higher surface might increase the quantity of released silver ions.

4.4.4 Branched AgCl superstructures

4.4.4.1 Synthesis

Bulk fabrication methods of AgCl have been described since centuries. More recently new approaches are being explored by fabricating assemblies at the micro- or nanoscopic level²⁶⁻²⁹, i.e. synthetic methods such as template directed, ionic liquid-assisted hydrothermal and capping agent methods enable scientists to synthesize AgCl micro-/nanocrystals with different morphologies, from nanowires or nanotubes to near spheres and cubes³⁰⁻³³. Recently tuning kinetic factors of crystal growth by modification of the concentration of Cl^- ions in solution or by absorption on the surface of AgCl preferential growth of cubic seeds on edges and corners led to the formation of branched superstructures³⁴. In this thesis a simple approach to control the concentration of the Cl^- ions is developed. To do so we engineer the formation of hierarchically branched superstructures. This new methodology is based on a source of silver ions in solution, a dimeric metal complex containing bridging chloride ions strongly stabilized in DMSO and its reaction with a heterocyclic ligand (either

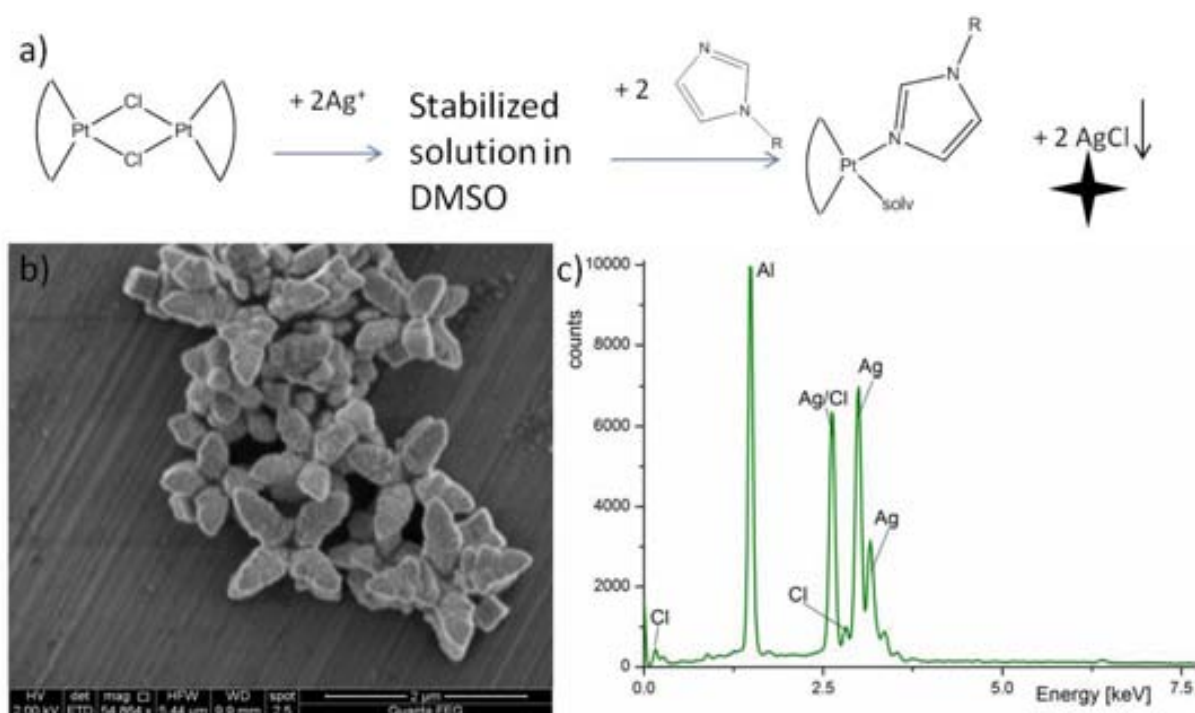


Fig. 4.4.2 a) Scheme of synthesis for AgCl microstars through delayed precipitation of AgCl from a dimeric complex bearing μ -chlorine ligands b) SEM image of several microstars resulting from the reaction displayed above c) EDX analysis shows that the sample contains only silver and chloride ions, Al comes from the aluminium sample holder.

1,4-bis(imidazol-1-ylmethyl)benzene) **1** or imidazole **2**). In a typical experiment a solution of AgPF_6 **4** is added to a solution of the bridged platinum complex $(2\mu\text{-Cl})\text{dmmba}(\text{Pt})$ **3** in DMSO and no precipitate is observed. At this stage no reaction seems to take place, therefore to subsequently shift the equilibrium towards the formation of the desired AgCl structures, we added the pyrazol ligand. Upon reaction with the dimer, it induces the controlled release of the Cl^- ions and the subsequent precipitation with Ag^+ present in solution (see scheme in figure 4.4.2 a). The structures **1-5** are displayed in the experimental part 3.4.4. The resulting precipitate is removed, washed and dried in air while avoiding the presence of light, all other compounds of the reaction remain in solution in DMSO and are removed during the washing process. EDX analysis of the different samples confirmed the expected AgCl composition (see figure 4.4.2 c).

4.4.2.2 Tuning experimental parameters

The nature of the Cl^- ions source was found to be crucial to AgCl microstars; replacing the dimeric complex in DMSO by other metal salts bearing chloride ions (as a related single-core Pt-dmmba complex **5**, CdCl_2 , CuCl_2) results in the formation of near-spherical or amorphous microstructures. Other salts such as NaCl did not lead to any precipitations at all. The solvent plays a crucial role on stabilizing the dimeric complex. In fact, when the reaction is repeated in a solvent different from DMSO such as acetone, acetonitrile, chloroform, ethanol or tetrahydrofuran, the immediate formation of a precipitate with the characteristic cube-like or amorphous particle shapes takes place (see figure 4.4.3). These results indicate that it should be possible to replace this dimeric Pt complex by other dimeric complexes with bridging Cl ligands in combination with suitable solvents. The solvent needs to guarantee the solubility and stability of the silver containing and the chlorine containing species next to each other, without inducing precipitation.

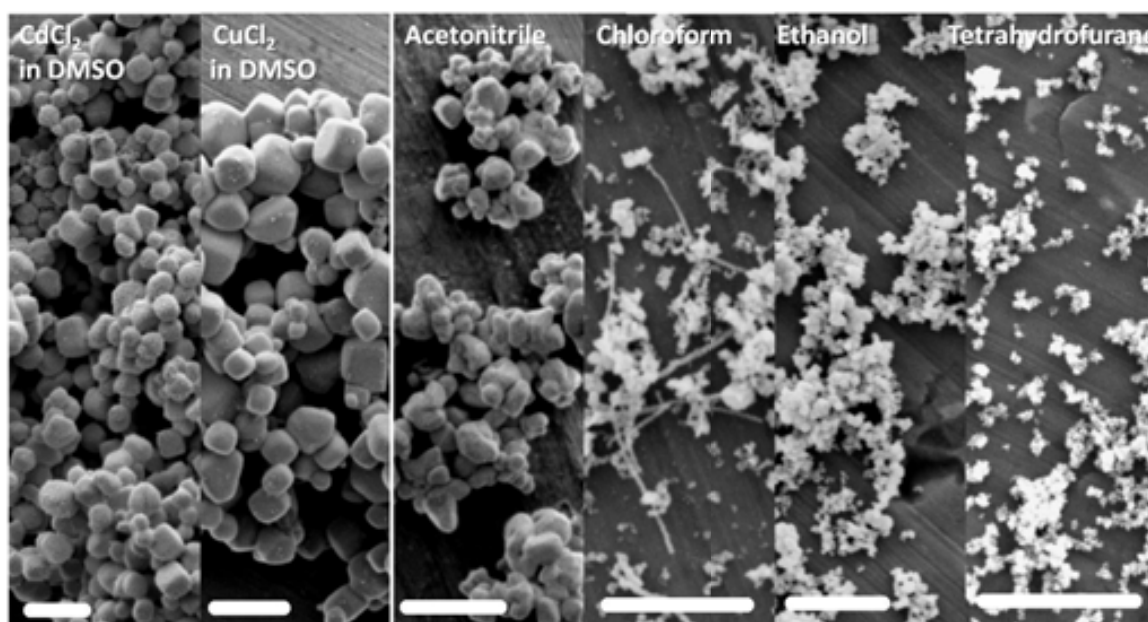


Fig. 4.4.3 AgCl crystals directly precipitated from CdCl_2 or CuCl_2 and **4** in DMSO to show how changing the Cl source affects the synthesis, and from **3** and **4** dissolved in different solvents (from left to right: acetonitrile, chloroform, ethanol and THF), scale bar: 1 μm .

4.4.2.2 Characterization of the chemical composition

XRD-analysis showed that the diffraction pattern and intensity peaks are in agreement with the specific formation of the chlorargyrite cubic phase (standard diffraction data JCPDS Card No. 00-031-1238) with no other detectable impurity. It has been found, that structures are sensible to light or radiation, which is a characteristic behaviour of AgCl^{21, 27, 30, 35}. The most obvious evidence is the darkening of aged samples. The XRD measurements after exposure to sunlight show typical 2 θ -signals at 38 and at 44 degrees that can be assigned to certain crystal plains in Ag crystals. They are described by the Miller indices of silver Ag [111] and Ag [200], while fresh samples give pure AgCl patterns (see figure 4.4.4 a).

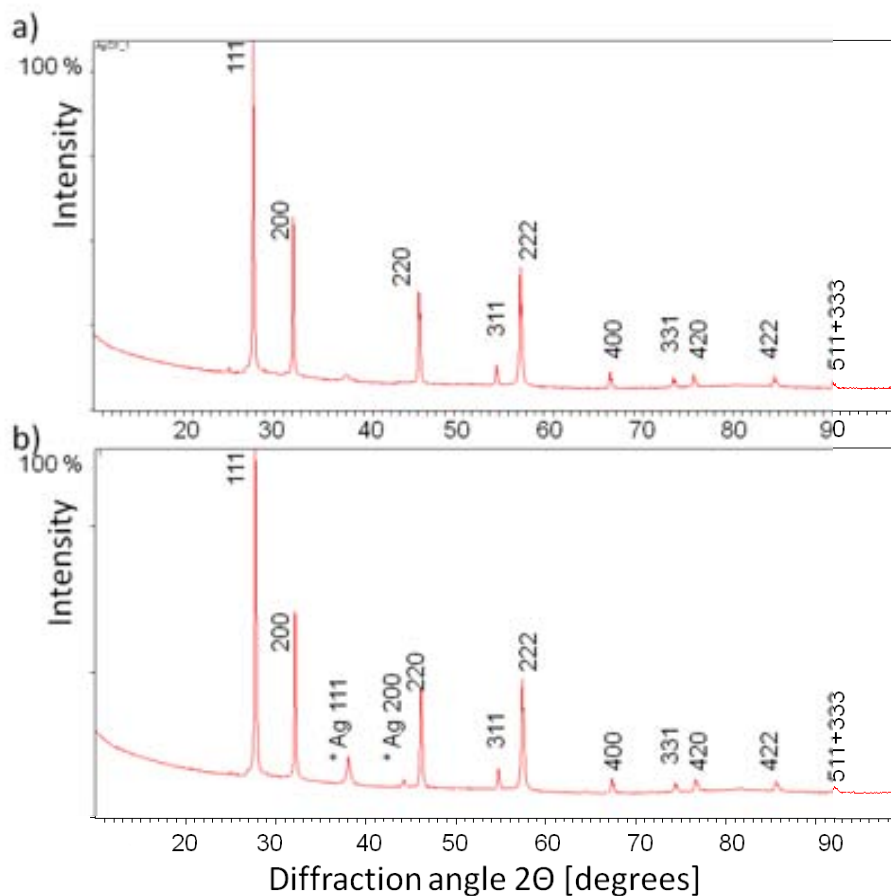


Fig. 4.4.4 Results from XRD analysis of a) freshly prepared AgCl microstars vs. b) aged AgCl/Ag compounds with Miller indices, that indicate the crystal plane that causes the signal. In aged AgCl samples one can find two important signals at 38 and 44 degrees that are attributed to silver.

Formation of such patterns was also induced upon irradiation by the electron beam of a SEM microscope and higher energetic radiation from a TEM microscope enhances this conversion. The crystalline structure of the modifications after beam exposure was checked on a transmission electron microscope working at 200 kV. Crystal structure analysis of the nanograins confirmed a lattice distance of 2,374 Å characteristic for Ag structures (see figure 4.4.5).

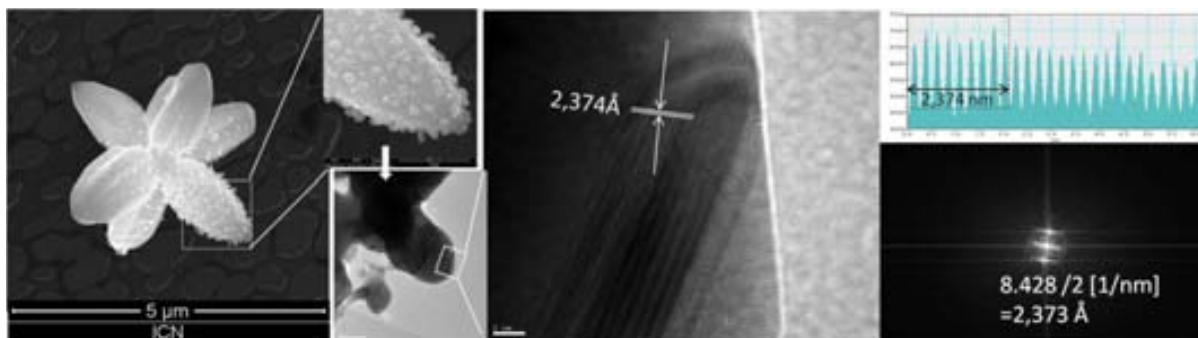


Fig 4.4.5 From left to right: SEM image of AgCl-microstar where only one extreme had been exposed to the electron beam. Inset macro view of the irradiated zone. TEM images and analysis of Ag nanograins on AgCl crystals that have been produced by irradiation, crystal lattice of Ag determined by TEM @ 200 kV.

4.4.4.4 Hexapod formation

Unexpectedly in some reactions we observed the formation of hexapod shaped structures with average dimensions of 2.5-3.0 μm , even though this is unusual for AgCl. The mechanism for the formation of these new challenging morphologies was followed with selected SEM images obtained at different growth steps (see figure 4.4.6). The key step is the initial formation of octahedral seeds, instead of typical AgCl cubes; subsequent preferential growth along the -111 - directions in the presence of Cl^- ions leads to the formation of the homogeneous hexapod structures. The question that arises then is: *What does cause the formation of initial octahedral seeds instead of the well-known cubic forms?* This fact has been tentatively attributed to the initial formation of AgBr

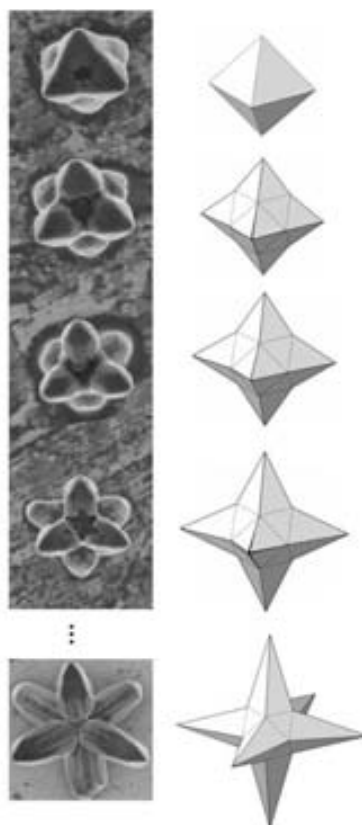


Fig. 4.4.6 SEM images of hexapod structures at different growth stages resulting from initial octahedral seeds, (images are not at scale).

structures due to the faster reaction of bromide impurities originating probably from the synthesis of the pyrazol ligand. AgBr seeds, which have already been shown to exhibit octahedral shapes in certain circumstances³⁶⁻³⁸, can then subsequently serve for the epitaxial crystal growth of AgCl, considering that both are very similar structures³⁶. The influence of other parameters such as an excess of water content coming from the solvent and/or the hygroscopic AgPF₆ was discarded by obtaining reproducible structures working both, under strict anhydrous and non-anhydrous conditions. Further work is currently ongoing to fully understand this mechanism.

4.4.5 Tuning octapod morphology

SEM images reveal the formation of morphologies strongly dependent on the stoichiometries of heterocyclus added (while keeping constant the 1:1 Ag/Cl ratio). At low amounts of heterocyclus shapes with rounded edges are observed, from knobbed cubes to tubby octapods. Increasing the ratio further (molar amounts of ranging from 0.6 to 1.0 equivalents of bix, see figure) the shapes get more defined and grow into concave cubes with overgrown corners up to the formation of octapod structures. Figure 4.4.7 shows the formation of homogeneous octapod microstructures at such ratios with average end-to-end dimensions of 2 μm. A further increase above 1.0 equivalents results in the formation of more irregular cube-like AgCl microstructures. These results can be tentatively explained considering the two different stages that involve the obtaining of crystals: nucleation and growth.

At low Cl⁻ concentrations, the cubic seeds precipitate showing already an incipient preferential growth through the cube edges. This preferential growth increases upon increasing the Cl⁻ concentration up to the formation of the octapod structures. Finally, at higher concentrations, the availability of Cl⁻ is too high so that fewer selective “docking” occurs and the energy differences of the different crystal facets loose importance.

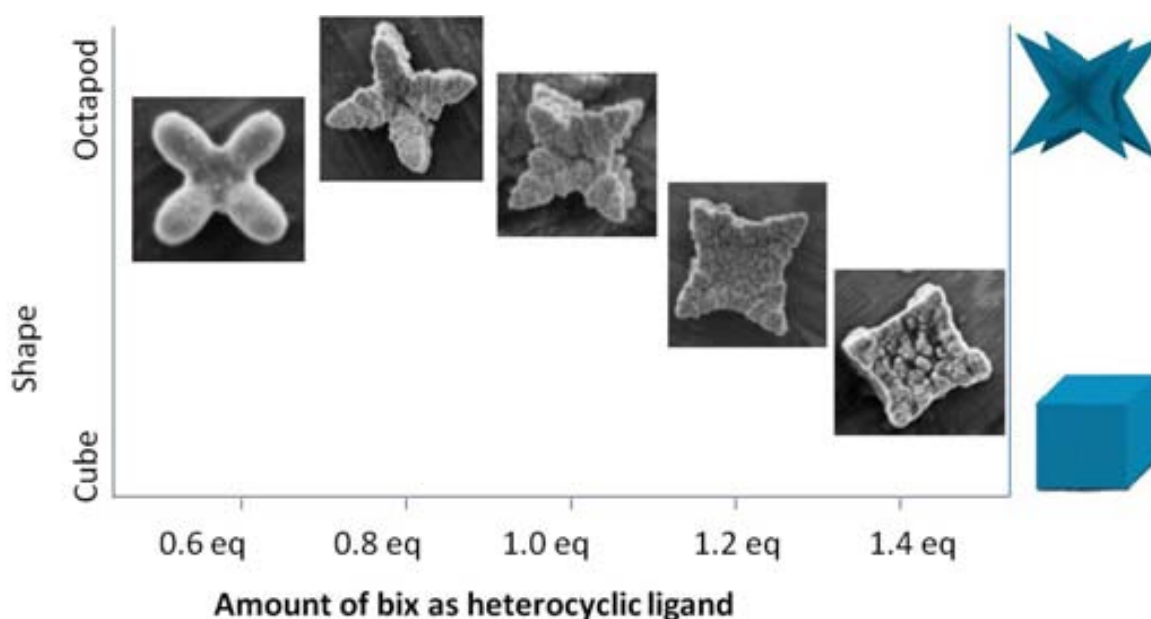


Fig. 4.4.7 SEM images of precipitated crystals at different conditions: dependence of shape on the molecular ratio of added heterocyclic compound

4.4.6 Light induced movement

Inspired by the work of Sen *et al.* we tried to construct a novel type of shaped micromotors. In comparison to previously reported work we did not observe significant Brownian motion, due to the larger size of the microstars compared to Sen's used amorphous particles⁵. As the surface transformation of AgCl occurs also at visible light initially we tried to obtain visible light induced movement. Particles were irradiated with white light of different intensities, but the experiments demonstrated that visible light does not cause significant motion. Most likely the conversion rate of

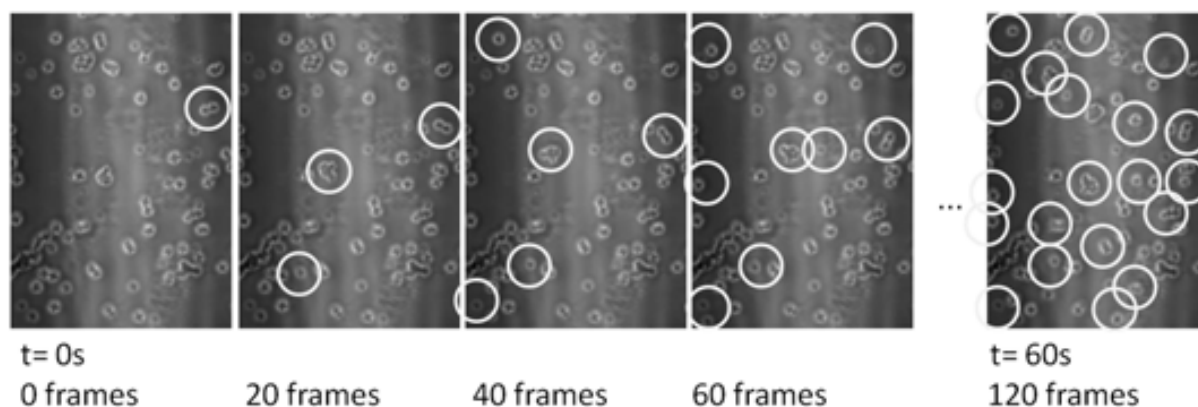


Fig. 4.4.8 Particle movement at onset of UV light. UV light induces the transformation from AgCl to Ag nanograins on the surface that creates a gradient of chlorine ions leading to particle motion through diffusiophoresis. Moving particles are labelled by a white circle.

AgCl to Ag nanograins on the surface is slower and no relevant gradient can be build up.

However at onset of focused UV light from a mercury arc lamp at maximum intensity (120 W, DAPI excitation 340-380 nm) the particles start moving one by one as displayed in figure 4.4.8 (motile particles are marked with a white circle). Those active particles undergo changes on their surface that discharge chloride ions, which probably lead to gradient creation and propel the particle motion. Gradient driven motion has been discussed for motile particles mostly in context of oxygen gradients that lead to propulsion, but other forms as ion gradients have also been proposed³⁹⁻⁴¹. Here the gradient is probably caused by released chloride ions, a thesis that is underpinned by the observation that in high concentrations of chloride ions (as 0.1 molar KCl) UV light caused no motion. In most cases the observed motion is random, with a high degree of rotations and changes of directions. Real directed motion in one constant direction is rarely witnessed. Some particles tilt and also rocking has been documented, two different positions are displayed in figure 4.4.9 a) in optical and electron microscope images. In part b) and c) of the same figure the movement of a single particles during approximately 30 s is tracked and some of its position prior to a change of direction are depicted.

To determine the life time of AgCl motors the experiment was placed in the inverted microscope, illuminated by UV-light and covered by a flat petri-dish to inhibit evaporation of solvent. At certain intervals of time (up to three hours) videos of particle movement were taken and evaluated.

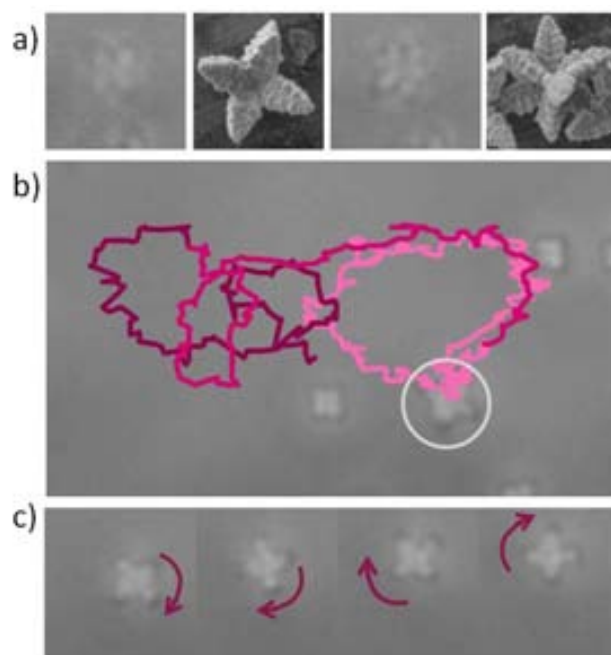


Fig. 4.4.9 a) Rotation of particles is confirmed through the observation of different particle orientations in the optical microscope and then comparison of the same orientation as observed by SEM b) tracking of a motile AgCl microstar performing circular movement (for better visibility the track is divided into 3 parts that are signalled by different tones) c) different alignments of the particle in tracked in b).

It was found that after UV light irradiation particles gain motility, what is probably caused by increasing gradients in the medium. Within 3 hours of experimental time no significant decay in particle movement was found. However microstars were found to lose their specific shape. Initially well-defined star shapes can be observed, but through surface reaction from AgCl to silver they lose their characteristic shape, resulting in the observation of mainly stubs at advanced time. However even after 3h microstar - stubs show considerable motion, as can be seen in figure 4.4.10. In absence of light, particles can be stored in water for a few days without morphology lost, in a dry state storage was possible over weeks, apart from nanograin formation on the surface without losing shape.

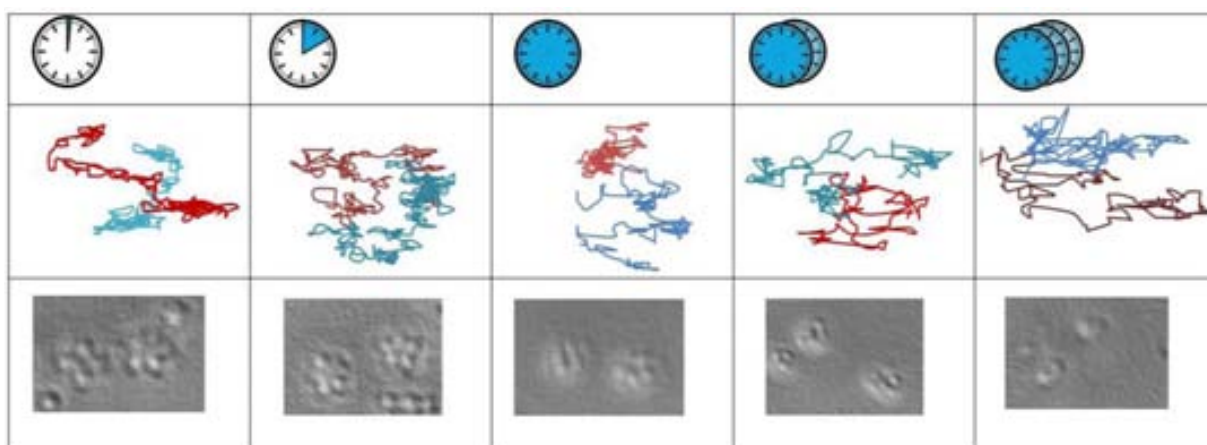


Fig. 4.4.10 Shape and trajectory of two random microstars, each track corresponds to 7.4 s of particle motion, registered after 1 min, 10 min, 1h, 2h and 3h. The images show the subsequent degradation of the microstar structures due to surface modification.

4.4.7 Decomposition of organic pollutants

We tested the photocatalytic activity of AgCl octapods by evaluation of the photocatalytic degradation: methyl orange (MO), methyl blue (MB) and rhodamine 6G (Rh) in aqueous solution were degraded. These three different organic dyes were chosen to prove versatility of the catalytic decomposition on different chemical structures. Our AgCl micromotors were evaluated in different light situations: one batch of microstars was divided and for each organic dye a sample containing microstars and a blank solutions were prepared. One pair of (sample and blank) was kept in absence of any light source and was then compared to a pair exposed to Barcelona sunlight in July. The sun is the most important source of visible and UV radiation on earth and the fluence rate of solar radiation is estimated to be around 1360 W/m^2 . It is proven that at sea level about 6% of sunlight is UV light (with UVA as the most abundant type with wavelength from 320 to 400 nm equates to the range of the DAPI filter).

After 30 min the solutions still showed some remaining colour, but after 3h of irradiation the solutions exposed to sun were almost completely colourless. The reference samples help evaluating the stability exposed to light but in absence of AgCl. Results of UV spectra to evaluate the quantity of degraded colorants are displayed in figure 4.4.11, showing clearly MO and Rh are completely stable to light exposure, while MB slightly decomposes. However a clearly increased degradation in presence of AgCl is observable. All the samples were stable when stored in darkness, in presence and absence of AgCl, only MB shows again some decomposition. In figure 4.4.11 can be seen that

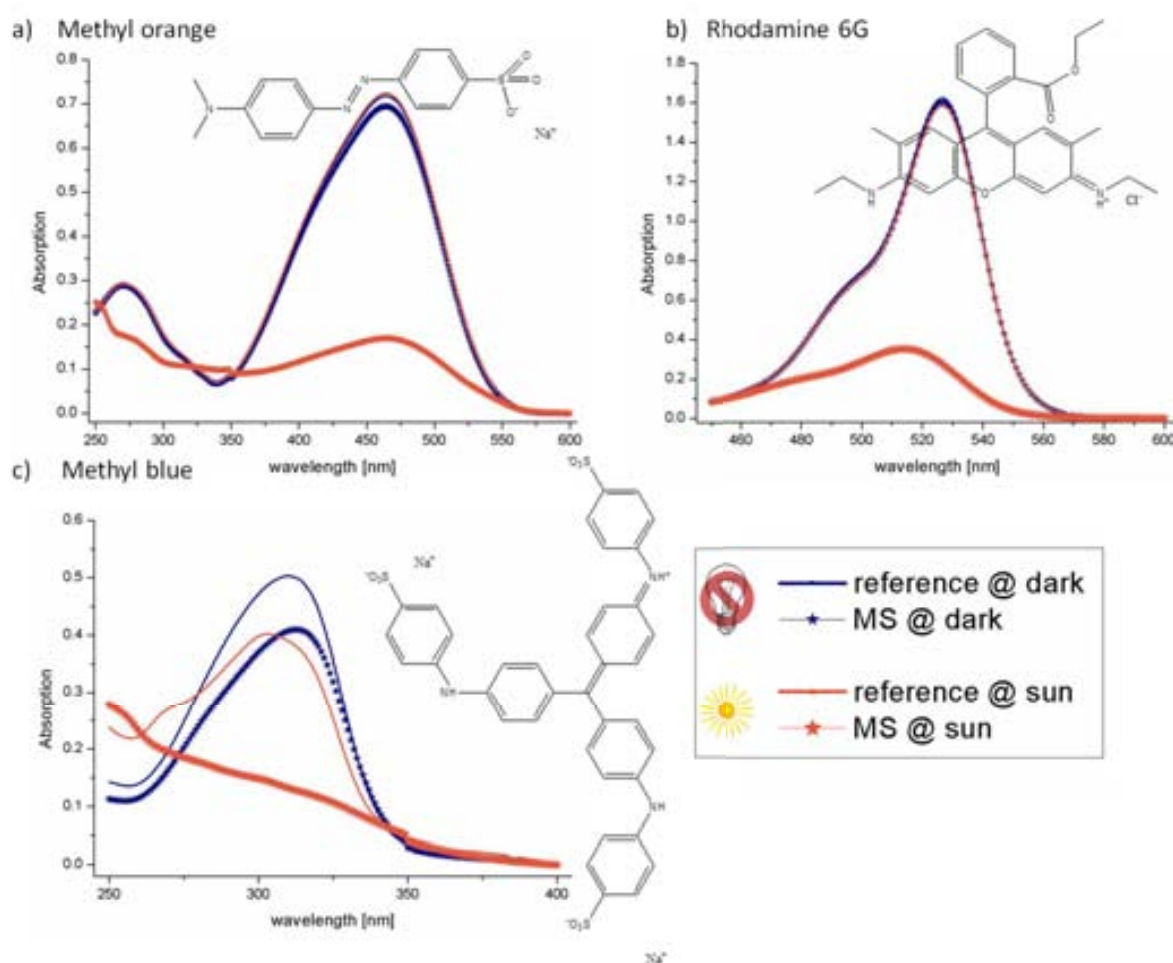


Fig. 4.4.11 Photocatalytic degradation of methyl orange, rhodamine 6G and methyl blue by AgCl octapod particles.

AgCl microstars were able to efficiently degrade all three organic colorants in sunlight. Samples exposed to low intensity UV light (ultraviolet TLC revelation lamp, 254 nm, 8 W), showed a lower degree of decomposition than after exposure to sunlight (results not shown).

Previously it was shown that UV light has enough energy to cause particle motion, and here we showed that microstars in sunlight (containing approx. 6% of UV light) are able to efficiently degrade organic molecules. Therefore we suggest our AgCl micromotors for waste water treatment. The fact that none of the three dyes were degraded by silver chloride particles at darkness shows that the catalytic activity is due to a photocatalytic process that involves the surface modification of AgCl to Ag nanograins.

4.4.8 Antibacterial activity

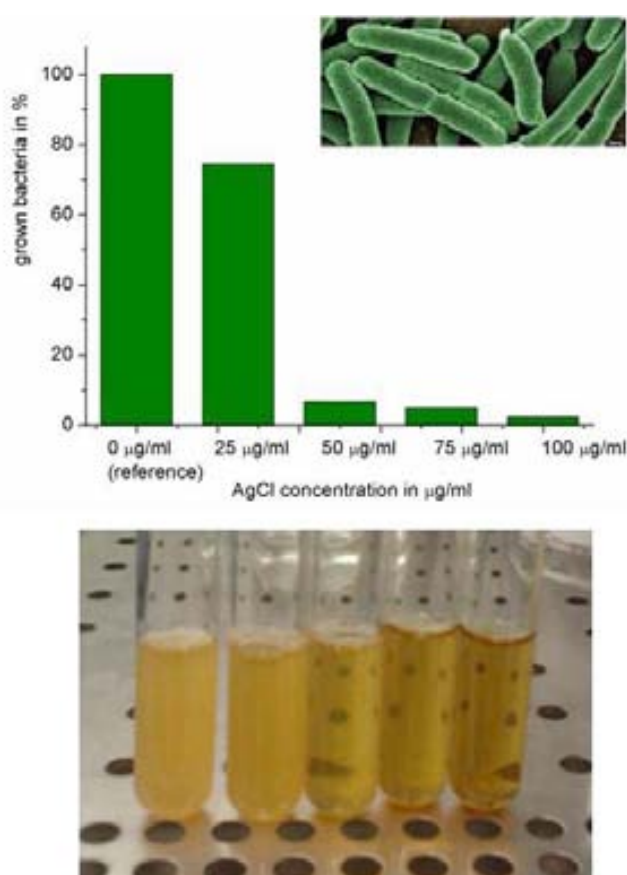


Fig. 4.4.12 Inhibition of bacterial growth tested on E. coli. It seems that at 50 $\mu\text{g/ml}$ exists some kind of threshold concentration that inhibits bacterial growth.

The degradation of organic molecules is an important branch of waste water treatment, however the disinfection of sewage waters holds equal impact. Therefore we designed a series of experiments to test the antibacterial properties of microstars in order to evaluate their suitability for environmental applications. As can be seen from figure 4.4.12 after addition of 25 $\mu\text{g/ml}$ microstars the bacteria growth dropped by approximately 25%. Further increase to 50 $\mu\text{g/ml}$ inhibited the growth of E.coli drastically, so that the overall growth rate only added up to 6.6% of the growth found in the reference sample. The addition of 75 and 100 $\mu\text{g/ml}$ hardly lowered the growth rate any further as values of 4.9 and 2.3 % are obtained. The values obtained with densimetry and counting of colonies gave coinciding results as can be seen in table 4.4.1. This results led to the conclusion that there is

probably a maximum ion concentration soluble in the Todd Hewitt Broth medium (THB, more information can be found in the experimental section), which is reached around 50 $\mu\text{g/ml}$. Therefore the concentration of Ag^+ -ions in THB was measured by ICP-MS and compared to an inorganic buffer with equal composition (without the organic components). As can be seen from figure 4.4.13 and table 4.4.2 both result differ strongly. It seems that some of the organic components of THB (dehydrated heart infusion, yeast enriched peptone and dextrose) increase the solubility of silver drastically. This might be due to complexation phenomena.

Table 4.4.1 Results of *E. coli* growth experiments in presence of different concentrations of AgCl microstar particles, measured by densimetry and colony counting.

	0 $\mu\text{g/ml}$	25 $\mu\text{g/ml}$	50 $\mu\text{g/ml}$	75 $\mu\text{g/ml}$	100 $\mu\text{g/ml}$
Optical density solution	1.859	1.505	0.29	0.413 [#]	0.41 [#]
# opt density of AgCl containing broth	Blank	0.123	0.167	0.321	0.367
Corrected opt dens	1.859	1.382	0.123	0.092	0.043
CFU					
10^{-2}	Densely grown colonies	Densely grown colonies	Densely grown colonies	Densely grown colonies	325
10^{-4}	Densely grown colonies	Densely grown colonies	18	12	14
Surviving CFU/ml	indeterminate	indeterminate	$9 \cdot 10^6$	$6 \cdot 10^6$	$7 \cdot 10^6$

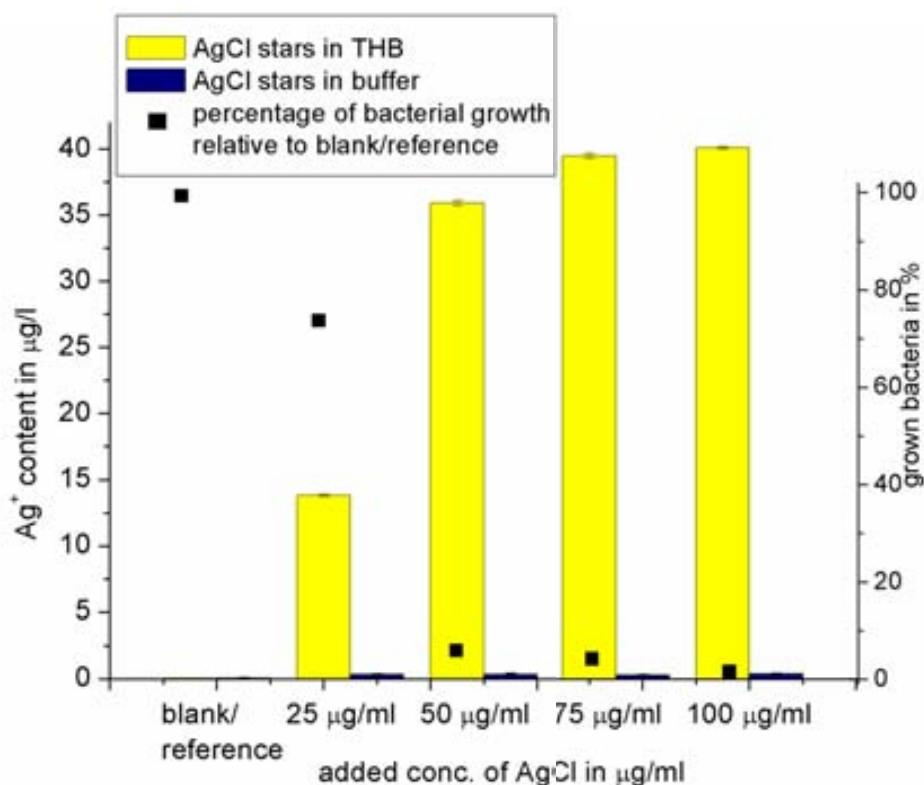


Fig. 4.4.13 Concentrations of silver ions were determined for THB and an analogous inorganic buffer and subsequently compared. It becomes obvious that in THB some complexation or similar processes have to be overlaid, influencing the solvation of Ag^+ ions strongly.

Table 4.4.2: Concentration of silver ions obtained by ICP ES

THB	Average content in $\mu\text{g/l}$	Stdv.
0 $\mu\text{g/ml}$	0.04	-
25 $\mu\text{g/ml}$	13.8	0.08
50 $\mu\text{g/ml}$	35.9	0.2
75 $\mu\text{g/ml}$	39.5	0.2
100 $\mu\text{g/ml}$	40.12	0.1
Buffer	Average content in $\mu\text{g/l}$	Stdv.
0 $\mu\text{g/ml}$	0.026	0.003
25 $\mu\text{g/ml}$	0.29	0.005
50 $\mu\text{g/ml}$	0.29	0.01
75 $\mu\text{g/ml}$	0.28	0.005
100 $\mu\text{g/ml}$	0.372	0.005

Having found this very interesting result the E.coli growth test was repeated at 25 and 50 $\mu\text{g/ml}$ that seemed to be the concentrations where the critical concentration lies to see whether only the dissolved Ag^+ is responsible for bactericidal effect. We compared particles that had been freshly synthesized and stored at darkness until their use to particles that were exposed to light during 12h. It was found that both fresh and aged particles show bactericide effects in the same range. In dilution experiments similar results have been obtained, so that we can conclude that the main factor is probably the concentration of silver ions and the formation of nanograins plays only a minor part. This result points towards a second life cycle for AgCl stars in waste water treatment. Once they lose their catalytic properties due to photoactive surface properties they are still able to inhibit bacterial growth, as the bars for aged microstars in figure 4.4.14 indicate.

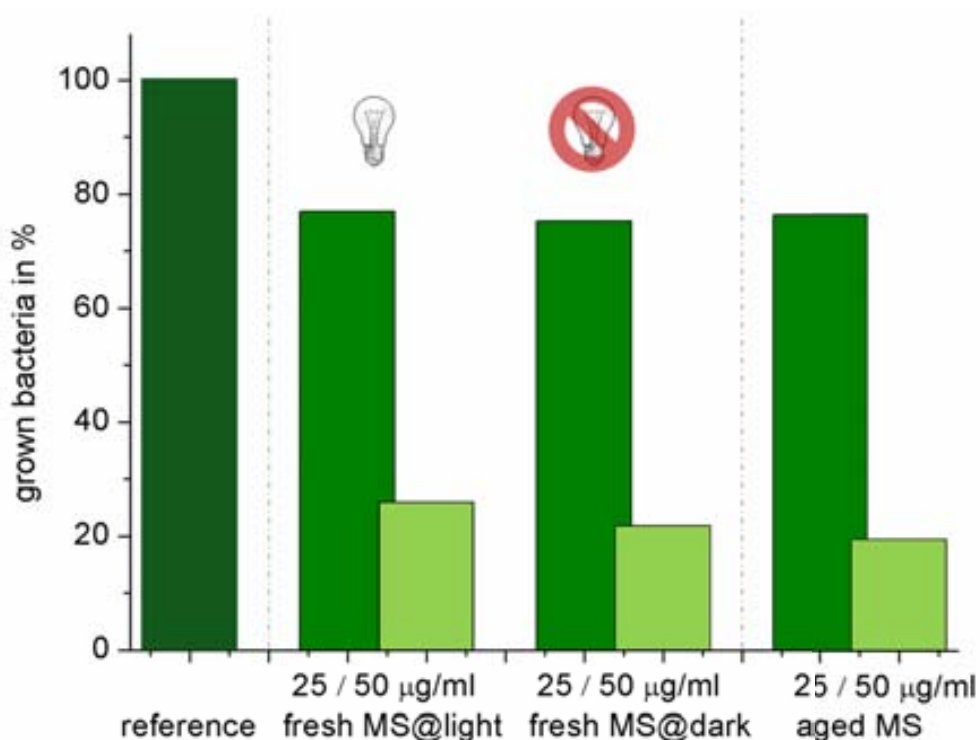


Fig. 4.4.14 Influence of light exposure of AgCl previous to or during bacterial growth.

4.4.9 Conclusions

After the pioneering works of Sen *et al.* on the use of AgCl as micromotors we are the first to introduce shaped AgCl particles as micromotors. Star shaped particles were obtained by overgrowth of corners, a modification that seems to lead to less agglomerations, compared to Sen's results. Their size of approx. 2 μm , as well as their homogeneous shapes facilitate the observation in optical microscopy and the characterization of motion. Furthermore those novel micromotors were used for environmental remediation benefitting from photocatalytic properties of silver chloride. It was proven that our microstars could move in pure water after UV irradiation and that the movement lasts for minimum 3h. Even though the surface modifications that occur in UV light destroy the defined shape of the microstars they keep moving. The AgCl microstars show the potential to be applied in waste water treatment due to their photocatalytic activity that was proven on three different organic molecules. However further efforts are needed to bring this new kind of motors at the level of control that can be reached currently with other types of micromotors, as directionality and speed control that have been achieved in Janus particles and in microjets are desirable. Due to their promising application in waste water treatment and the well known antibacterial properties of many kind of silver devices and silver containing compounds we tested them against *E. coli*. The microstars showed to diminish the bacterial growth from concentrations of only 25 $\mu\text{g/ml}$ and inhibited the growth completely from only 50 $\mu\text{g/ml}$ upwards. To elucidate the mechanism of this antibacterial properties solubility experiments were performed and it could be concluded that the growth inhibition is proportional to the amount of dissolved silver ions, at least for *E. coli*.

4.4.7 Literature

1. S. Shinkai and O. Manabe, in *Host Guest Complex Chemistry III*, eds. F. Vögtle and E. Weber, Springer Berlin Heidelberg, 1984, vol. 121, ch. 3, pp. 67-104.
2. M. Guix, C. C. Mayorga-Martinez and A. Merkoçi, *Chemical Reviews*, 2014, DOI: 10.1021/cr400273r.
3. M. Ibele, T. E. Mallouk and A. Sen, *Angewandte Chemie International Edition*, 2009, 48, 3308-3312.
4. M. E. Ibele, P. E. Lammert, V. H. Crespi and A. Sen, *ACS Nano*, 2010, 4, 4845-4851.
5. W. Duan, M. Ibele, R. Liu and A. Sen, *Eur. Phys. J. E*, 2012, 35, 1-8.
6. W. Duan, R. Liu and A. Sen, *Journal of the American Chemical Society*, 2013, 135, 1280-1283.
7. J. Orozco, V. García-Gradilla, M. D'Agostino, W. Gao, A. Cortés and J. Wang, *ACS Nano*, 2012, 7, 818-824.
8. G. Zhao, S. Sanchez, O. G. Schmidt and M. Pumera, *Nanoscale*, 2013, 5, 2909-2914.
9. H. Wang, G. Zhao and M. Pumera, *The Journal of Physical Chemistry C*, 2014, 118, 5268-5274.
10. M. Guix, J. Orozco, M. García, W. Gao, S. Sattayasamitsathit, A. Merkoçi, A. Escarpa and J. Wang, *ACS Nano*, 2012, 6, 4445-4451.
11. W. Gao, X. Feng, A. Pei, Y. Gu, J. Li and J. Wang, *Nanoscale*, 2013, 5, 4696-4700.
12. G. Zhao, T. H. Seah and M. Pumera, *Chemistry – A European Journal*, 2011, 17, 12020-12026.
13. L. Soler, V. Magdanz, V. M. Fomin, S. Sanchez and O. G. Schmidt, *ACS Nano*, 2013.
14. W. Gao and J. Wang, *ACS Nano*, 2014, DOI: 10.1021/nn500077a.
15. L. Soler and S. Sanchez, *Nanoscale*, 2014, DOI: 10.1039/C4NR01321B.
16. M. Lanz, D. Schürch and G. Calzaferri, *Journal of Photochemistry and Photobiology A: Chemistry*, 1999, 120, 105-117.
17. V. R. Reddy, A. Currao and G. Calzaferri, *Journal of Materials Chemistry*, 2007, 17, 3603-3609.

18. J. F. Hamilton, *Advances in Physics*, 1988, 37, 359-441.
19. R. J. Araujo, *Contemporary Physics*, 1980, 21, 77-84.
20. Y. Yamashita, N. Aoyama, N. Takezawa and K. Yoshida, *Environmental Science & Technology*, 2000, 34, 5211-5214.
21. P. Wang, B. Huang, Z. Lou, X. Zhang, X. Qin, Y. Dai, Z. Zheng and X. Wang, *Chemistry – A European Journal*, 2010, 16, 538-544.
22. M. Zhu, P. Chen and M. Liu, *Langmuir*, 2013, 29, 9259-9268.
23. M. Zhu, P. Chen, W. Ma, B. Lei and M. Liu, *ACS Applied Materials & Interfaces*, 2012, 4, 6386-6392.
24. U. S. I. Reports, *Organic Wastewater Compounds, Pharmaceuticals, and Coliphage in Ground Water Receiving Discharge from Onsite Wastewater Treatment Systems near La Pine, Oregon: Occurrence and Implications for Transport.*, 2009.
25. E. Commission, *Organic Pollutants: sources, pathways, and fate through urban wastewater treatment systems*, http://ec.europa.eu/environment/waste/sludge/pdf/sludge_pollutants_3.pdf, Accessed 27/04, 2014.
26. S.-W. Kim, H.-E. Chung, J.-H. Kwon, H.-G. Yoon and W. Kim, *Bulletin of the Korean Chemical Society*, 2010, 31, 2918-2922.
27. M. Choi, K.-H. Shin and J. Jang, *Journal of Colloid and Interface Science*, 2010, 341, 83.
28. L.-Y. Hao, C.-L. Zhu, W.-Q. Jiang, C.-N. Chen, Y. Hu and Z.-Y. Chen, *Journal of Materials Chemistry*, 2004, 14, 2929-2934.
29. A. Abbasi and A. Morsali, *J Inorg Organomet Polym*, 2013, 23, 286-292.
30. Y. Tang, Z. Jiang, G. Xing, A. Li, P. D. Kanhere, Y. Zhang, T. C. Sum, S. Li, X. Chen, Z. Dong and Z. Chen, *Advanced Functional Materials*, 2013, 23, 2932-2940.
31. P. Wang, B. Huang, X. Qin, X. Zhang, Y. Dai, J. Wei and M.-H. Whangbo, *Angewandte Chemie International Edition*, 2008, 47, 7931-7933.
32. S. Peng and Y. Sun, *Journal of Materials Chemistry*, 2011, 21, 11644-11650.
33. W. M. Schuette and W. E. Buhro, *ACS Nano*, 2013, 7, 3844-3853.
34. Z. Lou, B. Huang, X. Qin, X. Zhang, H. Cheng, Y. Liu, S. Wang, J. Wang and Y. Dai, *Chemical Communications*, 2012, 48, 3488-3490.
35. C. An, R. Wang, S. Wang and X. Zhang, *Journal of Materials Chemistry*, 2011, 21, 11532-11536.
36. Q. Liang, Y. Shi, W. Ma, Z. Li and X. Yang, *Applied Catalysis A: General*, 2013, 455, 199-205.
37. I. H. Leubner, *The Journal of Physical Chemistry*, 1987, 91, 6069-6073.
38. Z. Yan, G. Compagnini and D. B. Chrisey, *The Journal of Physical Chemistry C*, 2010, 115, 5058-5062.
39. J. L. Anderson, *Annu. Rev. Fluid Mech*, 1989, 21, 61-99.
40. S. Ebbens, D. A. Gregory, G. Dunderdale, J. R. Howse, Y. Ibrahim, T. B. Liverpool and R. Golestanian, *cond-mat. soft*, 2013, arXiv:1312.6250.
41. A. T. Brown and W. C. K. Poon, *cond-mat. soft* 2013, arXiv:1312.4130.

Conclusions and future
perspectives

5

5.1 Conclusions

This thesis deals with the synthesis and characterization of micromotors and the search for first applications.

- In **Chapter 4.1** for the first time a particle tandem was propelled enzymatically.
- The methodology for synthesis, asymmetrization, functionalization and grafting methods for two biologic molecules (catalase and DNA) were developed. This knowledge had not yet been applied to the field of micromotors.
- We obtained a novel method for motion based DNA detection and showed in a proof of concept experiment its feasibility.

- In **Chapter 4.2** the endurance of enzyme based micromotors could be enhanced by an encapsulation strategy.
- Despite the chemical anchoring on the silica surface the enzyme becomes more resistant to environmental damage as oxidizing media, high temperature and proteolytic enzymes. This enables the micromotors to "drive" in more hostile environments.
- The here presented method was broadened to the use with Glucose oxidase and despite the fact that no glucose fuelled motion was obtained we envision that encapsulation is the way to go.

- In **Chapter 4.3** magnetic guidance was introduced to our micromotors by embracing an approach recently presented by another group^{1,2}.
- In order to characterize the particle motion the enzymes were replaced by Pt which enabled us to study the fuel dependence of the Janus motors in presence and absence of surfactants.
- Microtubes are used to compare the behaviour between different motor classes. To the best of our knowledge this was still missing in research articles.
- The behaviour of Pt driven Janus particles in presence of thiols was evaluated for the first time and was compared to microtubes.

- In **Chapter 4.4** a light based micromotor was developed, based on the precipitation of star silver chloride particles and UV propelled movement could be documented.
- The first application of light driven micromotors has been developed, based on the catalytic properties of AgCl. We showed the degradation of organic pollutants using three different dyes.
- Furthermore the AgCl material itself antibacterial properties, so that we obtained a hybrid motor for environmentally friendly water cleaning.

- Additionally in **Chapter 3** a detailed list of all performed experiments and all kinds of used chemicals, materials, methods etc. is given in order to facilitate the reproduction and continuation of this work.

5.2 future perspectives

The integration of functional biomolecules in inorganic micromotors can open doors for new fuels and less expensive, biodegradable drives. Further experiments based on the results of this thesis will hopefully provide a more solid approach to create enzyme driven micromotors. If the use and grafting of enzymes is more standardized and reliable, the introduction of other enzymes as GOx will be enormously facilitated and that will probably lead to the unlocking of new fuels. A related strategy that has only been tangent in this work is the use of enzyme mimics as for example Feringa et al. used a Mn-complex mimicking catalase³. We envision that this strategy will be a promising alternative for the use of sensitive enzymes. However both methods, the enzyme mimics and the encapsulation for stability improvement hold important advantages and should be developed in parallel. That would enable us to perform more extended comparisons between organic and inorganic systems that might further elucidate the mechanism of motion.

Everybody agrees that the engineering of micromotors aspects as precise control of motor speed, on/off switches and the implementation of "intelligent motors" sensing gradients, so called "taxi-driven" movement will be challenges that have to be approached in the near future. For this scope it would be beneficial to fully characterize and compare different types of motors in comparable circumstances. That will help to increase the transferability of knowledge from one motor type to another. Despite those handicaps first applications for micromotors have been presented and once advances in the control will be achieved more and more applications will be realized. To reach the ultimate goal, the drug delivery device for use in the human body several obstacles have to be eliminated, apart from the fuelling mainly further miniaturization has to be achieved.

1. Baraban, L.; Makarov, D.; Streubel, R.; Mönch, I.; Grimm, D.; Sanchez, S.; Schmidt, O. G. *ACS Nano* **2012**, 6, (4), 3383-3389.
2. Baraban, L.; Tasinkevych, M.; Popescu, M. N.; Sanchez, S.; Dietrich, S.; Schmidt, O. G. *Soft Matter* **2012**, 8, (1), 48-52.
3. Vicario, J.; Eelkema, R.; Browne, W. R.; Meetsma, A.; La Crois, R. M.; Feringa, B. L. *Chemical Communications* **2005**, (31), 3936-3938.